IMPROVED RECEIVER CHARACTERIZATION AND SOURCE SELECTION TECHNIQUE FOR MICROWAVE-FREQUENCY NOISE MEASUREMENT

IMPROVED RECEIVER CHARACTERIZATION AND SOURCE SELECTION TECHNIQUE FOR MICROWAVE-FREQUENCY NOISE MEASUREMENT

by

YING LIEN WANG

Bachelor of Applied Science

University of Waterloo

2005

A thesis

Submitted to the School of Graduate Studies

in Partial Fulfillment of the Requirements

for the degree of

Master of Applied Science

McMaster University

Hamilton, Ontario, Canada

MASTER OF APPLIED SCIENCE (2008) McMaster University

(Electrical and Computer Engineering) Hamilton, Ontario

TITLE: Improved Receiver Characterization and Source Selection Technique for Microwave-Frequency Noise Measurement

AUTHOR: Ying Lien Wang, BASc. (University of Waterloo)

SUPERVISORS: Dr. Chih-Hung James Chen and
Dr. Mohamed Bakr

NUMBER OF PAGES: x, 123

Abstract

An accurate noise measurement is essential to a proper characterization of a noisy device. In the 1950s, the IRE first proposed the classical noise parameters for characterizing a noisy linear two-port network, and subsequently a measurement and extraction procedure. Since then, the task of accurately characterizing the parameters has always been challenging due to the sensitive nature of the noise parameters. This is especially so for an on-wafer device noise measurement, as opposed to that of a packaged device, due to various factors such as the lower noise level and losses in the signal path. Combined with the downscaling of the MOSFET technology in recent decades, which also improved the device's noise performance, they make noise measurement and characterization become even more difficult.

A typical noise measurement starts with the calibration or characterization of the measurement system. This step is as important as the measurement itself in terms of the ultimate accuracy of the results. This thesis presents a noise receiver characterization method which improves upon existing methods by accurately taking into account the different reflection coefficient of the noise source between its hot and cold states. The improvement allows more precise determination of the receiver characteristics.

Numerous studies have investigated the effect of the choice of the source terminations on the noise measurement results. These studies often provided contradicting suggestions on the selection techniques. In the thesis, a selection technique is proposed that allows quick determination of desirable terminations. Analyses using real measurement data on a 65 nm n-type MOSFET show that the proposed technique is able to provide terminations that yield noise parameters with smaller uncertainties relative to other terminations.

Acknowledgements

First of all, I would like to express my appreciation to Professor Chih-Hung James Chen for giving me the opportunity to work on the research project. As my supervisor, Professor Chen has always been immensely supportive. He was always there whenever I had questions and would answer them with the utmost patience. Without his concrete guidance and generous encouragement, this project would have been impossible.

Also, I would like to thank my co-supervisor, Professor Mohamed Bakr, for his support. Professor Bakr provided me with valuable suggestions and comments which I would not have obtained elsewhere. The mathematical knowledge I learned from him helped me establish a solid foundation on which the research was built.

In addition, Dr. Ognian Marinov's broad understandings of both the theoretical and practical aspects of instrumentation have benefited me greatly throughout the research. He unselfishly spent countless hours helping my work and shared his insights on the project. I am grateful of his help and the valuable knowledge he passed to me.

I also owe gratitude to the ECE department's staff. In particular, I would like to thank Cheryl Gies for always being able to answer any question of mine since before I started my study here. Cosmin Coroiu and Terry Greenlay, too, have helped me resolve the technical issue I came across. Without their knowledge, my experience here would not have been smooth.

Finally, I want to say thanks to my family as their support is the one constant in my life.

Table of Contents

List of Figures

List of Tables

Chapter 1: INTRODUCTION

The discovery of the phenomenon of noise is accredited to Brown as he first observed random fluctuations of microscopic particles within pollens floating in water [1]. Decades later in 1906, Einstein [3] and Smoluchowski [4] published their independent studies that provided a statistical analysis of Brownian motion. Based on their studies, engineers were able to extend the concept of noise to areas in communications and electronics.

Noise in electronic circuits is defined as unwanted fluctuations in current and voltage. There are several types of noise present in electronic circuits. These various types of noise arise due to the quantized nature of electrical charge. In the following section, the physical mechanisms of electronic noise are reviewed.

1.1 Types of Electronic Noise

The types of electronic noise reviewed in this section include shot noise, thermal noise, flicker noise, burst noise, and avalanche noise.

1.1.1 Shot Noise

Shot noise was first investigated by Schottky [5] in vacuum tubes. It is a phenomenon that can only be observed in direct-current flow. Due to the discrete nature of electrical charge, a current flow is neither continuous nor smooth. It is the result of all the individual charges that cross a plane. At one instant, the number of charges crossing the plane of observation could be different than that of the next instant. The fluctuation of the overall current flow is the noise. In order to illustrate the mechanism that causes shot noise, one can examine the operation of a diode. Figure 1-1 a) is a schematic of a diode in forward bias where V is the bias voltage. Figure 1-1 b) shows the carrier concentrations across the diode in forward bias. In this region, holes from the p region and electrons from the n region cross the junction if they possess enough energy. The combination of these charges forms the forward current I. Specifically, shot noise can be calculated, according to Campbell's theorem, as [6]

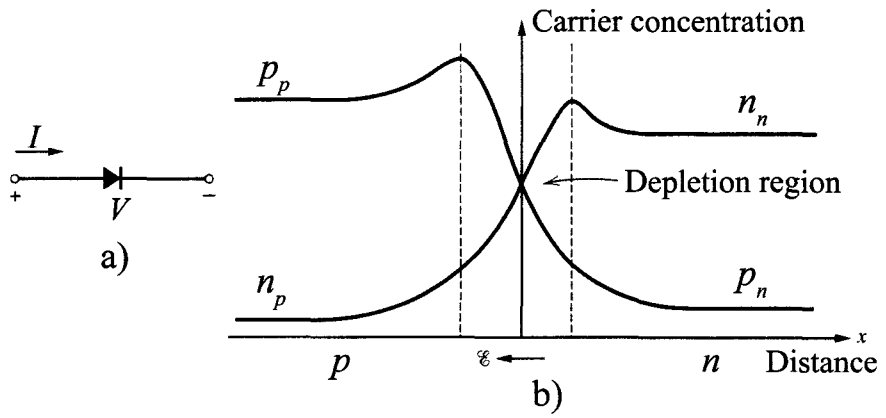

Figure 1-1 - a) A forward-biased pn junction diode and b) the carrier concentrations in the diode [1].

$$\overline{i^2} = \overline{(I(t) - I_D)^2} = \lim_{T\to\infty} \frac{1}{T} \int_0^T (I(t) - I_D)^2 \, dt, \tag{1.1}$$

where I_D is the average value of the current. Since the event of a carrier crossing the junction is random and thus independent of the other carriers, it can be approximated as a Poisson process. Therefore, the mean-square value of the noise current can be written as

$$\overline{i^2} = 2qI_D \Delta f, \tag{1.2}$$

where q is the elementary charge and Δf is the operating bandwidth. Since shot noise is directly proportional to the bandwidth, as shown in the equation, its spectral density is constant over the entire frequency range. Such characteristic suggests shot noise is a white noise.

When there are a large number of charges crossing a junction, the Poisson distribution of the number of crossing charges approaches a Gaussian distribution. Therefore, shot noise is also said to be approximated by a Gaussian distribution.

1.1.2 Thermal Noise

Thermal noise is present in all conductors. Unlike shot noise, its generation does not require the presence of a net current. It was first described by Johnson as spontaneous movements of charges in a conductor due to thermal agitation [7]. Nyquist then did a quantitative analysis of thermal noise [8].

Since thermal noise is generated by thermal motion of charges, it is directly proportional to temperature. Its presence in a resistor can be modeled by a voltage generator or a current generator calculated as

$$\overline{v^2} = 4kTR\Delta f \text{, and} \tag{1.3}$$

$$\overline{i^2} = 4kT(1/R)\Delta f \text{,} \tag{1.4}$$

where k is the Boltzmann's constant, and R is the resistance of the resistor. Figure 1-2 illustrates the two models for a resistor.

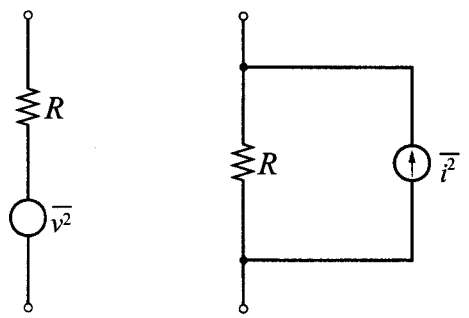

Figure 1-2 - Representations of thermal noise using a) a voltage source and b) a current source [1].

Like shot noise, thermal noise's spectral density is also constant and its distribution also Gaussian. Thus when present together in a circuit, the two kinds of noise would be indistinguishable. Although they are generated by difference mechanisms, some authors support a unified view of the two [9].

1.1.3 Flicker Noise

Flicker noise, also called 1/f noise, was first measured by Johnson [10]. Later, Schottky provided an explanation using vacuum tubes. Like shot noise, it is related to direct current. It is generated as impurities and defects trap charge carriers. The random trapping produces fluctuation in the signal in the following form

$$\overline{i^2} = K\frac{I^a}{f^b}\Delta f \text{,} \tag{1.5}$$

where K is a constant depending on the device's level of impurities, a is a constant between 0.5 and 2, b is a constant around 1, and Δf is a small bandwidth at frequency f. Since flicker noise has a spectral density with frequency in the denominator, it is not a white noise and is more dominant at low frequencies as illustrated in Figure 1-3.

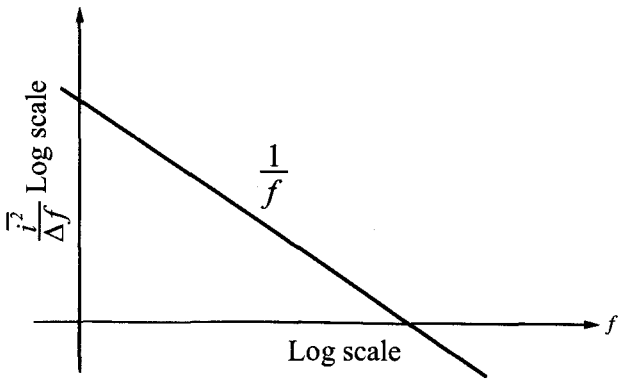

Figure 1-3 - Flicker noise's spectral density over frequency [1].

It should be noted that its amplitude does not exhibit a Gaussian distribution.

1.1.4 Burst Noise

Burst noise was first described by Tan [12]. The origin of burst noise is not well understood. It manifests itself as random bursts in the signal at discrete levels for short durations as shown in Figure 1-4 a). It is also called popcorn noise because the bursts make popping sounds through speakers.

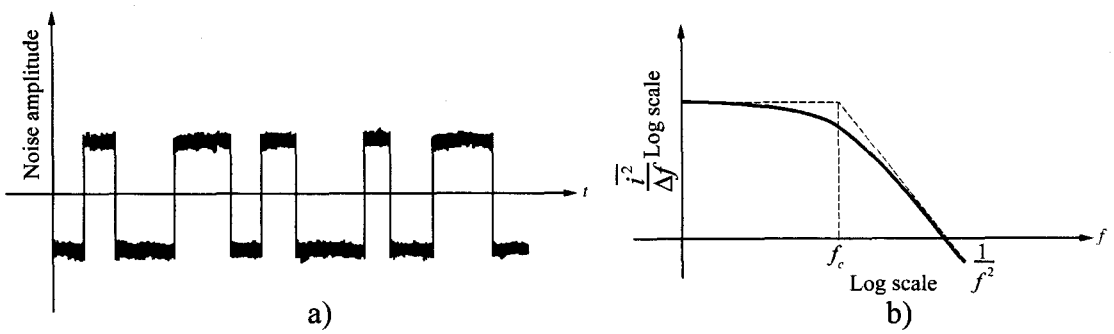

Figure 1-4 - Burst noise's a) typical waveform and b) spectral density over frequency [1].

Burst noise can be modeled as

$$\overline{i^2} = K\frac{I^a}{1+\left(\frac{f}{f_a}\right)^2}\Delta f, \tag{1.6}$$

where K is a constant for the device, a is a constant between 0.5 and 2, I is direct current, and f_a is the particular frequency for a noise process. Since the spectral density of burst noise has f^2 in the denominator, it is also non-white and a low-frequency phenomenon as shown in Figure 1-1 b).

1.1.5 Avalanche Noise

Avalanche noise is created when a reverse-bias breakdown happens at a pn junction. When a breakdown occurs, the large electric field accelerates free electrons which in turn bump into silicon atoms in the depletion regions to create more carriers. The random nature of this mechanism results in unpredictable and large fluctuations in the current.

1.2 High-Frequency Noise of MOSFETs

Several important figures of merit for RF applications are the unity gain frequency, f_t, the maximum oscillation frequency, f_{max}, and the noise figure. f_t is defined as the frequency at which the current gain of the amplifier becomes unity. f_{max} is defined as the frequency the power gain becomes unity. The noise figure, which is reviewed in greater detail in Chapter 2, describes the noise performance of the device. As f_t and f_{max} limit the maximum operating frequency of a device, it is desirable for them to be high while for the noise figure to be low. Traditionally, BJTs are preferable to MOSFETs for RF applications because of the technology's higher f_t and f_{max}. Such advantages are attributed to the BJT's higher transconductance, g_m, of which its f_t and f_{max} are functions as

$$f_t = \frac{g_m}{2\pi(C_\pi + C_\mu)}, \text{ and} \tag{1.7}$$

$$f_{\max} = \sqrt{\frac{f_t}{2\pi R_B C_\mu}}, \tag{1.8}$$

where C_π is the emitter-base capacitance, C_μ is the collector-base capacitance, and R_B is the total base resistance.

For the past few decades, the semiconductor industry has thrived on the fact that the downscaling of devices brings about improved functionality along with reduced cost. This translates to a decreasing cost-per-function ratio with each generation of technology. For the CMOS technology in particular, downscaling provides benefits in digital as well as RF applications. Figures of merits described above have been shown to improve with downscaling [13], [14]. Table 1.1 is the International Technology Roadmap for Semiocnductors' prediction on RF and analog mixed-mixed signal requirements for CMOS and bipolar technologies. As shown in the table, f_t of the RF CMOS technology would surpass that of the bipolar technology in 2014. Also, the minimum noise figure, NF_{min}, is also to improve.

Table 1.1 - ITRC's predictions on RF and analog mixed-signal requirements for CMOS and bipolar technologies (2007)

Year of Production	2007	2008	2009	2010	2011	2012	2013	2014	2015
Performance RF/Analog CMOS									
Gate Length (nm)	53	45	37	32	28	25	22	20	18
Peak f_t (GHz)	170	200	240	280	320	360	400	440	490
Peak f_{max} (GHz)	200	240	290	340	390	440	510	560	630
NF_{min} (dB) at 5 GHz	0.25	0.22	0.2	<0.2	<0.2	<0.2	<0.2	<0.2	<0.2
General Analog NPN									
Peak f_t (GHz) [V_{cb} = 1V]	250	275	300	320	340	360	380	395	415
Peak f_{max} (GHz)	280	305	330	350	370	390	410	425	445
NF_{min} (dB) at 60 GHz	3	2.5	2.2	1.9	1.7	1.5	1.4	1.3	1.2

Aside from the benefits of downscaling, as the device feature size becomes smaller, new sources of noise also emerge. As it is crucial to have reliable noise models for RF applications, the major noise sources present in the MOSFET's output current and the impacts of downscaling on them are briefly reviewed in the following sub-sections.

1.2.1 Channel Thermal Noise

It has been known for some time that as the channel length decreases, the channel thermal noise model for long-channel device would fail as the actual thermal noise becomes greater than the prediction, as shown in Figure 1-5 [20]. In the figure, the solid lines indicate the channel thermal noise's spectral densities for short-channel devices while the dashed lines are for long-channel devices. It can be see that at 0.18 μm channel length, the difference can be as large one decade. Also shown in the figure is that the enhancement of the noise is rapid as the device shrinks down. In fact, thermal noise is the most dominant component in the drain-current noise as shown in Figure 1-6.

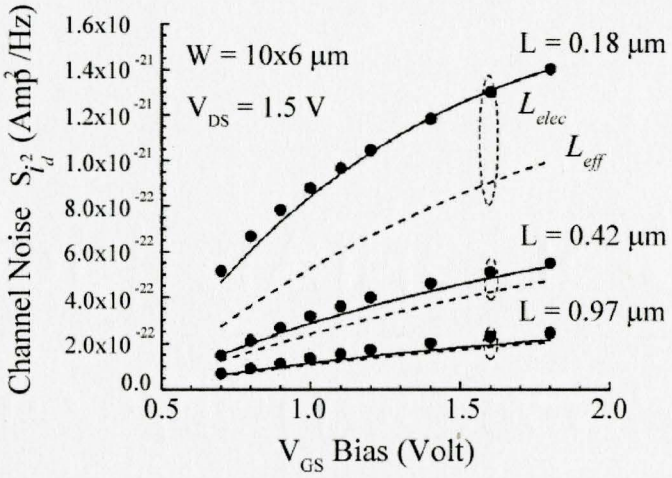

Figure 1-5 - Extracted (circle) and simulated (lines) power spectral density of the channel thermal noise of nMOSTFET [19], [18].

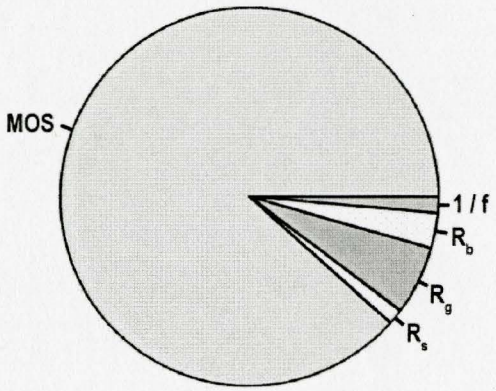

Figure 1-6 - Components of the drain-current noise at high frequencies in a short-channel MOSFET in saturation [18].

1.2.2 Induced Gate Noise

The induced gate noise arises from the capacitive coupling between the channel thermal noise and the gate [15]-[17]. This noise is correlated to the channel thermal noise and increases as the frequency increases. However, the correlation coefficient, C, becomes smaller as the device shrinks and so does the noise itself as shown in Figure 1-7 and Figure 1-8, respectively. As the result, the effect of the induced gate noise is small compared to those of the channel thermal noise and the gate resistance noise.

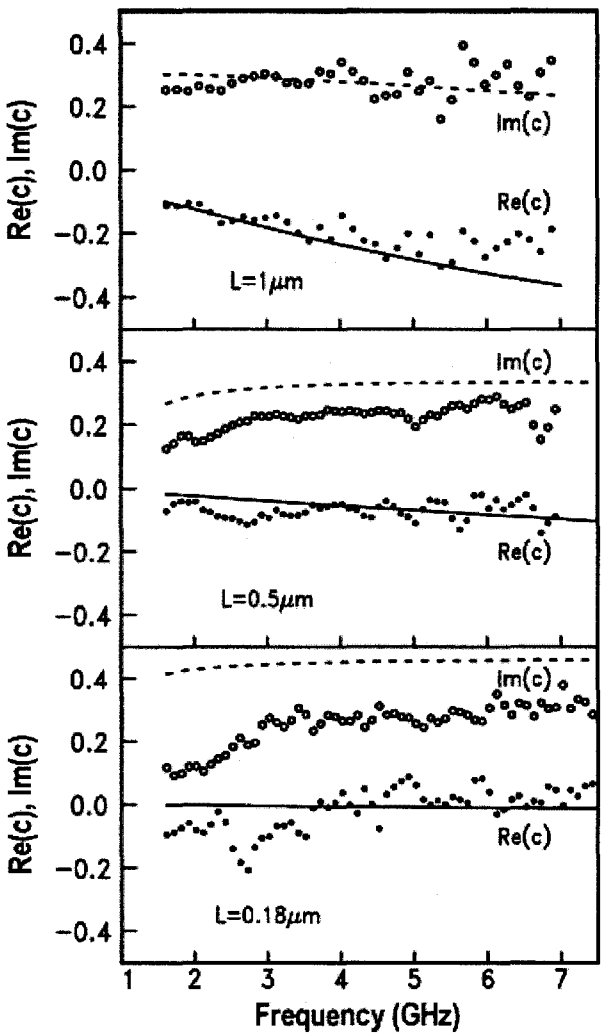

Figure 1-7 - The correlation between the induced gate noise and the channel thermal noise of devices with different channel lengths [18].

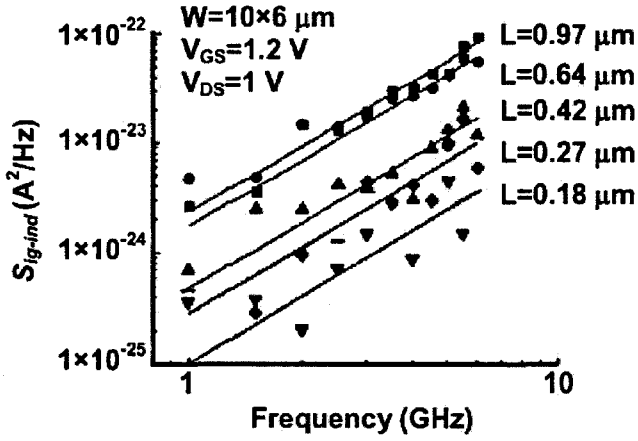

Figure 1-8 - Induced gate noise of n-type MOSFET of various channel lengths and a width of 10×6 μm [19].

1.2.3 Gate Resistance Noise

The gate resistance noise is a thermal noise generated in the gate resistance, R_g, which is a function of the MOSFET's geometry and the sheet resistance of the gate material. The expression for R_g in submicron MOSFETs is

$$R_g = \frac{R_{gsh}W}{12n_f^2L} + \frac{\rho_{con}}{WL}, \tag{1.9}$$

where R_{gsh} is the gate polysilicon's sheet resistance, W, L, and N_f are the width, channel length, and the number of fingers of the MOSFET. ρ_{con} is the contact resistivity between the silicide and the polysilicon the gate composes of. As shown in the expression, as L decreases with scaling, the gate resistance increases.

1.3 Motivation for the Research and Thesis Outline

The use of RF CMOS technology has become common thanks to the benefits such as higher f_t, and f_{max}, and lower noise figure provided by the aggressive downscaling. In the area of wireless communications, the technology has a crucial role especially in applications such as Wideband Code Division Multiple Access, wireless LAN, and ultra-wideband technology. While the technology enjoys the improved noise

performance, the decreasing noise level also makes the measurement and the characterization processes more difficult. Issues such as accuracy and uncertainty thus become more pronounced. Therefore, it is the purpose of this thesis to investigate the challenges in the high-frequency noise measurement and characterization of modern MOSFETs and provide improvements upon existing techniques. To that purpose, an novel noise receiver characterization technique is developed to more accurately determine the receiver gain of the measurement system. Also, a new source termination selection criterion is described and analyzed to provide a practical way of choosing what terminations to use for a noise measurement.

The rest of this thesis is organized as follows. Chapter 2 introduces the concept of noise parameters. The background of the conventional noise parameter is covered and the various parameter extraction methods are reviewed. In Chapter 3, the uncertainty issues associated with noise characterization are discussed. The various sources of uncertainties are also described in the chapter. In particular, existing source termination selection techniques aimed at minimizing uncertainties are reviewed. In Chapter 4 and 5, an improved noise receiver characterization technique and a novel source termination selection technique are introduced. The proposed techniques are applied to the measurement data obtained through an on-wafer measurement of a 65 nm n-type MOSFET. The results are presented and analyzed to support the proposed techniques. Finally, Chapter 6 summarizes the study and provides suggestions on future improvements on this work.

Chapter 2: THE NOISE PARAMETERS

To determine the noise performance of a MOSFET, the device is commonly modeled as a noisy linear two-port. This two-port is defined by a set of noise parameters whose values are extracted from measurement results. Thus the general process of characterizing a device's noise performance involves a measurement stage and an extraction stage.

Based on these noise parameters, various measurement and extraction techniques were developed over the years. It is the purpose of this chapter to provide a review on the concept of noise parameters and their extraction techniques.

2.1 The Conventional Noise Parameters

The noise of a device is described by its noise factor. Noise factor was first suggested by Friis [23]. It is defined for any two-port as the signal-to-noise power ratio at the input of the two-port divided by the signal-to-noise power ratio at the output at 290 degrees Kelvin. It is written as

$$F = \frac{P_{Si} / P_{Ni}}{P_{So} / P_{No}}, \tag{2.1}$$

where

P_{Si} = the available signal power at the input,

P_{So} = the available signal power at the output,

P_{Ni} = the available noise power at the input,

P_{No} = the available noise power at the output.

The available power is defined as the power transmitted to a load presenting an impedance that is a conjugate match of that of the source. Thus this definition of noise factor is independent of whatever the two-port might be connected to. The fixed temperature of 290 degrees Kelvin is required since thermal noise is temperature dependent.

Later in 1956, Rothe modeled a noisy two-port with theoretical voltage and current sources defined with certain parameters [24]. He then related these parameters to the noise factor of the two-port and provided a complete model with which the noise

performance of a two-port can be calculated for any matching conditions at its ports. In 1960, the Institute of Radio Engineers (IRE) provided a similar analysis with a set of noise parameters that become the classical representation of a noisy two-port today [25]. In this representation, the intrinsic noise of the two-port is modeled by a voltage and a current source as shown in Figure 2-1.

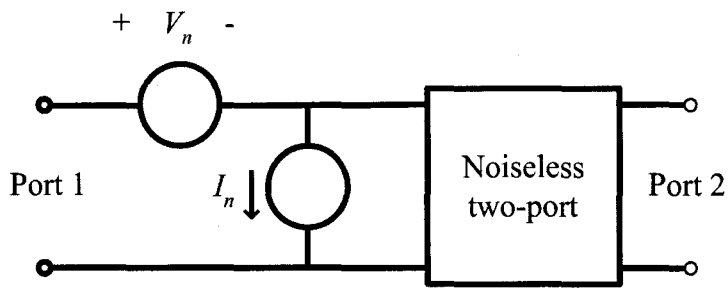

Figure 2-1 - Representaion of a noisy two-port.

In the figure, the two noise sources are assumed to be correlated with the voltage source expressed by the Nyquist formula as

$$\overline{V_n^2} = 4kT_oR_n\Delta f, \tag{2.2}$$

where

k = the Boltzmann constant,

T_o = the standard temperature of 290 degrees Kelvin,

R_n = the equivalent noise resistance of the source (not an actual resistance),

Δf = the bandwidth.

As the two sources are correlated, the current source can be expressed as the sum of a correlated part, i_{nc}, and an uncorrelated part, i_{nu}. The correlation between i_{nc} and V_n is defined by a correlation admittance Y_c, that is, $i_{nc} = Y_cV_n$. With this two-port model, the IRE derived the noise factor of the device based on these parameters as

$$F = F_o + \frac{R_n}{G_s}\left[(G_s - G_o)^2 + (B_s - B_o)^2\right], \tag{2.3}$$

where

F_o = the minimum noise factor of the noisy two-port,

G_s = the real part of the source admittance Y_s,

B_s = the imaginary part of the source admittance Y_s,

G_o = the real part of the optimum source admittance Y_o that yields F_o,

B_o = the imaginary part of the optimum source admittance Y_o that yields F_o.

This equation shows that as long as the four noise parameters F_o, R_n, G_s, and B_s are given, the linear two-port's noise factor can be calculated for any source impedance Y_s.

Based on this representation of a linear noisy two-port, many noise parameters extraction techniques have been developed over the years. These techniques can be roughly divided into two groups depending on their measurement procedures. The first group applies variations of a noise parameter extraction called the Y-factor method [26]-[42]. This method requires a known noise source placed at the input of the device under test (DUT), which is the noisy two-port, during the measurement. The output noise power must be measured both for the noise source's ON and OFF states. The second group uses the cold-only approach [43]-[46]. This approach differs from the previous in that the noise source only has to be ON during the system calibration stage but not the measurement stage.

2.2 Conventional Noise Parameter Extraction Techniques

Ideally, in order to solve equation (2.3), it would require four measurements of the noise power at four different Y_s, which would provide four values of F with four equations. However, inevitable errors from various sources associated with the measurement process render that impossible. Therefore, various techniques have been developed to solve the problem and these techniques are reviewed in the rest of this section.

2.2.1 Lane's Method

As experimental errors are inevitably present in the measurement result, more than four measurements of noise power is needed to determine the four unknowns in equation (2.3) for a statistical smoothing. Lane's method provides a simple way to solve this equation by using four new parameters to linearize the equation into the form [26]

$$F = A + BG_s + \frac{C + BB_s^2 + DB_s}{G_s}, \tag{2.4}$$

where

$$F_o = A + \sqrt{4BC - D^2}, \tag{2.5}$$

$$R_n = B, \tag{2.6}$$

$$G_o = \frac{\sqrt{4BC - D^2}}{2B}, \tag{2.7}$$

$$B_o = \frac{-D}{2B}. \tag{2.8}$$

Lane suggested that a least-squares fitting can be applied to the measurement results with the error criterion as

$$\varepsilon \equiv \frac{1}{2}\sum_{i=1}^{n} W_i \left[A + B\left(G_i + \frac{B_i^2}{G_i} \right) + \frac{C}{G_i} + \frac{DB_i}{G_i} - F_i \right]^2, \tag{2.9}$$

where

n = the number of source admittances used,

W_i = a weighting factor to differentiate the effects of the source admittances,

G_i = the real part of the source admittance Y_i,

B_i = the imaginary part of the source admittance Y_i,

ε = the error between the fitted F_i and F_i given by measurements.

In order to find the A, B, C, and D that minimize ε, equation (2.9) is differentiated by A, B, C, and D and equate to 0 as

$$\frac{\partial \varepsilon}{\partial A} = \sum_{i=1}^{n} W_i P = 0, \tag{2.10}$$

$$\frac{\partial \varepsilon}{\partial B} = \sum_{i=1}^{n} W_i \left(G_i + \frac{B_i^2}{G_i} \right) P = 0, \tag{2.11}$$

$$\frac{\partial \varepsilon}{\partial C} = \sum_{i=1}^{n} W_i \frac{P}{G_i} = 0, \tag{2.12}$$

$$\frac{\partial \varepsilon}{\partial D} = \sum_{i=1}^{n} W_i \frac{B_i}{G_i} P = 0, \tag{2.13}$$

where

$$P = \left[A + B\left(G_i + \frac{B_i^2}{G_i} \right) + \frac{C}{G_i} + \frac{DB_i}{G_i} - F_i \right]. \tag{2.14}$$

Equations (2.10) to (2.13) then can be solved for A, B, C, and D.

Although the method is simple, a shortcoming is that the presence of B (R_n) in the denominators of (2.7) and (2.8) makes the result sensitive to measurement errors for devices with large R_n. Another trade-off for the simplicity is that the error criterion assumes the errors come from only the measured noise factors but not from other measured values such as the source admittances. Nevertheless, Lane's method became the basis of many other more sophisticated noise parameter extraction techniques.

2.2.2 Adamian and Uhlir's Method

Different from Lane's approach of using the noise factor equation (2.3), Adamian and Uhlir directly related the noise parameters to the measured noise power [43]. In this method, the noise receiver is modeled also by a voltage source and a current source that are correlated.

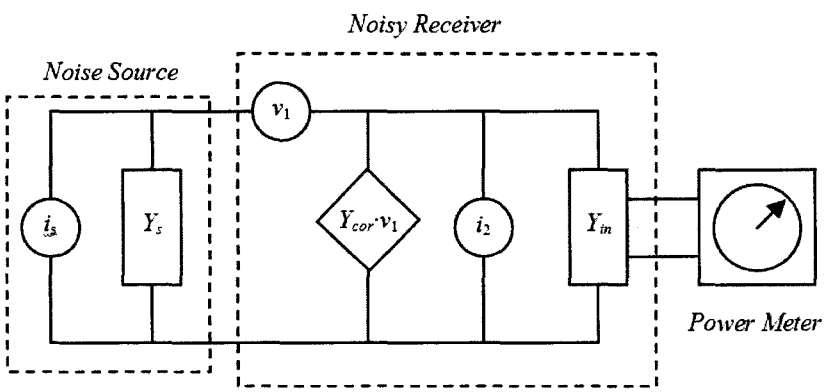

Figure 2-2 - Adamian and Uhlir's noise receiver model [43].

In Figure 2-2, the noise source is modeled by a current source, i_s, and its source admittance, Y_s. The noisy receiver is modeled by two uncorrelated sources, v_1 and i_2. The correlated part of the noise sources is represented by $Y_{cor} \cdot v_1$. Y_{in} is the output admittance of the receiver to the power meter. The noise parameters are related to the noise generators by

$$R_n = \frac{\overline{|v_1|^2}}{4kT_o\Delta f}, \tag{2.15}$$

$$G_n = \frac{\overline{|i_2|^2}}{4kT_o\Delta f}. \tag{2.16}$$

Finally, the measured receiver noise power is linked to these parameters by

$$P_s = \frac{4kT_oKG_{in}}{|Y_s + Y_{in}|^2}\left(|Y_s + Y_{cor}|^2 \cdot R_n + G_n + t_sG_s\right), \tag{2.17}$$

where t_s is the noise temperature of the source normalized by the standard temperature T_o, K is an unknown, G_{in} is the real part of Y_{in}. The noise parameters that characterize the noisy receiver are R_n, G_n, and the complex $Y_{cor} = G_{cor} + B_{cor}$ in this case. In order to solve for K, Adamian proposed that the measurements are taken at two different levels of noise source powers, namely t_{sc} and t_{sh}. The two noise levels give rise to P_{sc} and P_{sh}, with which K can be found by

$$K = \frac{(P_{sh} - P_{sc})|Y_{in} + Y_s|^2}{4kT_o\Delta fG_{in}(t_{sh} - t_{sc})}, \tag{2.18}$$

assuming Y_s stays constant at the two source noise levels.

Once K is found, the noise parameters can be calculated by first linearizing (2.17) into

$$\lambda P_s|Y_s + Y_{in}|^2 - t_sG_s = |Y_s|^2 \cdot A + B + 2G_s \cdot C + 2B_s \cdot D, \tag{2.19}$$

where

$$\lambda = \frac{1}{4kT_o\Delta fKG_{in}}, \tag{2.20}$$

$$A = R_n, \tag{2.21}$$

$$B = G_n + |Y_{cor}|^2 R_n, \tag{2.22}$$

$$C = G_{cor} \cdot R_n, \tag{2.23}$$

$$D = B_{cor} \cdot R_n. \tag{2.24}$$

Equation (2.17) then can be solved with a fitting using the P_s and Y_s values obtained from at least four measurements. Once A, B, C, and D are obtained from the fitting, the convention noise parameters can be found by

$$F_o = 1 + 2R_n G_{cor} + 2\sqrt{R_n G_n + (R_n G_{cor})^2}\,, \tag{2.25}$$

$$G_o = \sqrt{\frac{G_n}{R_n} + G_{cor}^2}\,, \tag{2.26}$$

$$B_o = -B_{cor}\,. \tag{2.27}$$

The important assumption made in this method is that Y_s is constant for different noise source levels and, consequently, K is not dependent on the source admittance. This assumption, however, is not true as will be shown later.

2.2.3 Caruso and Sannino's Method

In Caruso and Sannino's method, they related the noise parameters to the effective noise temperatures, T_e and $T_{\min}$ [28], which are defined as

$$T_e = T_o(F-1), \tag{2.28}$$

$$T_{\min} = T_o(F_0 - 1). \tag{2.29}$$

Using (2.28) and (2.29) and the modified version of the noise factor equation [29],

$$F = F_o + R_n G_o \cdot \frac{|Y_s - Y_o|^2}{G_o G_s}\,, \tag{2.30}$$

it can be derived that

$$T_e = T_{\min} + 4T_o N \frac{|\Gamma_s - \Gamma_o|^2}{(1-|\Gamma_s|^2)(1-|\Gamma_o|^2)}, \tag{2.31}$$

where

$$N = R_n G_o\,, \tag{2.32}$$

and Γ_s and Γ_o are the corresponding reflection coefficients of Y_s and Y_o. Replacing Γ_s with $\rho_s \exp(j\theta_s)$ and Γ_o with $\rho_o \exp(j\theta_o)$, it can be shown that

$$T_e = A + \frac{1}{1-\rho_s^2}\cdot B + \frac{\rho_s \cos(\theta_s)}{1-\rho_s^2}\cdot C + \frac{\rho_s \sin(\theta_s)}{1-\rho_s^2}\cdot D\,, \tag{2.33}$$

where

$$T_{\min} = A + \frac{B + \Delta}{2}\,, \tag{2.34}$$

$$N = \frac{\Delta}{4T_o}, \tag{2.35}$$

$$\rho_o = \sqrt{\frac{B-\Delta}{B+\Delta}}, \tag{2.36}$$

$$\theta_o = \tan^{-1}\left(\frac{D}{C}\right), \tag{2.37}$$

$$\Delta = \sqrt{B^2 - C^2 + D^2}\,. \tag{2.38}$$

The linear equation (2.33) again can be solved with a fitting of the results of more than four measurements.

Mathematically, Caruso and Sannino's method is very similar to Lane's method. However, a source admittance selection criterion was proposed for selecting particular points for the measurement. This criterion identifies certain "singular loci" among all possible source admittances. If source admittances chosen lie close to a certain singular locus, they would not be sufficient to define a surface for the fitting. Such points would result in an ill-conditioned coefficient matrix for the fitting and, consequently, large errors in the final results.

2.2.4 O'Callaghan and Mondal's Method

This method introduces the vector concept of conducting the least-squares fitting calculation [32]. For the fitting, the common noise factor equation is first rearranged into the following form

$$F = \left(F_o - 2R_nG_o\right) + R_n\left(\frac{G_s^2 + B_s^2}{G_s}\right) - 2R_nB_o\left(\frac{B_s}{G_s}\right) + R_n\left(G_o^2 + B_o^2\right)\left(\frac{1}{G_s}\right). \tag{2.39}$$

With the fitting of the multiple measurement results in mind, the following vectors are defined.

$$\overline{F_n^m} = \left(F_1^m, F_2^m, ..., F_i^m, ..., F_n^m\right)^T, \tag{2.40}$$

$$\overline{V_1} = \left(1,1,...,1,...,1\right)^T, \tag{2.41}$$

$$\overline{V_2} = \left(\frac{G_{s1}^2 + B_{s1}^2}{G_{s1}}, \frac{G_{s2}^2 + B_{s2}^2}{G_{s2}}, ..., \frac{G_{si}^2 + B_{si}^2}{G_{si}}, ..., \frac{G_{sn}^2 + B_{sn}^2}{G_{sn}}\right), \tag{2.42}$$

$$\overline{V_3} = \left(\frac{B_{s1}}{G_{s1}}, \frac{B_{s2}}{G_{s2}}, \ldots, \frac{B_{si}}{G_{si}}, \ldots, \frac{B_{sn}}{G_{sn}} \right), \tag{2.43}$$

$$\overline{V_4} = \left(\frac{1}{G_{s1}}, \frac{1}{G_{s2}}, \ldots, \frac{1}{G_{si}}, \ldots, \frac{1}{G_{sn}} \right), \tag{2.44}$$

where F_i^m, B_{si}, and G_{si} are measured noise figure and its corresponding source conductance and susceptance of the ith measurement. Replacing the source-independent terms of equation (2.39) using

$$C_1 = F_o - 2R_n G_o, \tag{2.45}$$

$$C_2 = R_n, \tag{2.46}$$

$$C_3 = -2R_n B_o, \tag{2.47}$$

$$C_4 = R_n \left(G_o^2 + B_o^2 \right), \tag{2.48}$$

and get

$$\overline{F_n^m} = C_1 \overline{V_1} + C_2 \overline{V_2} + C_3 \overline{V_3} + C_4 \overline{V_4}. \tag{2.49}$$

A fitting is then applied to (2.49) to find C_1, C_2, C_3, and C_4 with the error vector being

$$\varepsilon = \left[\sum_{i=1}^{n} \left(\overline{F_i^m} - \sum_{j=1}^{4} C_j V_{ji} \right) \right]^{\frac{1}{2}}. \tag{2.50}$$

As the magnitude of the error vector is minimized when it is orthogonal to all $\overline{V_i}$ according to Hilbert's project theorem, a system of four linear equations can be obtained by applying the inner products to get

$$\sum_{j=1}^{4} \left\langle \overline{V_i}, \overline{V_j} \right\rangle C_j = \left\langle \overline{F_n^m}, \overline{V_j} \right\rangle. \tag{2.51}$$

Once this system of equations is solved using fitting or Cholesky's method, the conventional noise parameters can be found through

$$R_n = C_2, \tag{2.52}$$

$$B_o = -C_3 / 2R_n, \tag{2.53}$$

$$G_o = \sqrt{\frac{C_4}{R_n} - B_o^2}, \tag{2.54}$$

$$F_o = C_1 + 2R_n G_o. \tag{2.55}$$

The use of the Cholesky's method has the advantage of higher efficiency over the traditional least-squares technique. Another more important advantage of this method is that it can prevent the error caused by points of the same singular locus.

2.2.5 Vasilescu's Method

The noise parameter extraction methods discussed so far in this chapter have all based on the Lane's technique, which involves applying a fitting procedure to a linearized version of the noise factor equation. Vasilescu et al., however, developed a method that directly solves a system of four non-linear equations for the noise parameters [33].

The first step of the procedure is to write out the noise factor equation for each set of the measurement data as

$$F_i = F_o + \frac{R_n}{G_{si}}\left[(G_{si} - G_o)^2 + (B_{si} - B_o)^2\right], \tag{2.56}$$

where i = 1, 2, 3, and 4. The next step is to subtract each equation from its previous equation to eliminate F_o. This operation eventually yields

$$a_i\left(G_o^2 + B_o^2\right) + 2bB_o - \frac{c_i}{R_n} = -d_i \quad (i = 1,2,3), \tag{2.57}$$

where

$$a_i = \frac{1}{G_{si}} - \frac{1}{G_{si+1}}, \tag{2.58}$$

$$b_i = \frac{B_{si+1}}{G_{si+1}} - \frac{B_{si}}{G_{si}}, \tag{2.59}$$

$$c_i = F_i - F_{i+1}, \tag{2.60}$$

$$d_i = G_{si} - G_{si+1} + \frac{B_{si+1}^2}{G_{si+1}} - \frac{B_{si}^2}{G_{si}}. \tag{2.61}$$

Subtracting each equation from its previous equation again after making each equation have identical $\left(G_o^2 + B_o^2\right)$ term can further eliminate the G_o and B_o terms and yield

$$e_i B_o + \frac{f_i}{R_n} = g_i \quad (i = 1,2), \tag{2.62}$$

where

$$e_i = 2(b_i a_{i+1} - b_{i+1} a_i), \tag{2.63}$$

$$f_i = c_{i+1} a_i - c_i a_{i+1}, \tag{2.64}$$

$$g_i = d_{i+1} a_i - d_i a_{i+1}. \tag{2.65}$$

Finally, solving the system of equations yields

$$R_n = \frac{e_2 f_1 - e_1 f_2}{g_1 e_2 - g_2 e_1}, \tag{2.66}$$

$$B_o = \frac{g_1 - f_1 / R_n}{e_1}, \tag{2.67}$$

$$G_o = \sqrt{\frac{c_1 / R_n - d_1 - 2 d_1 B_o}{a_1} - B_o^2}, \tag{2.68}$$

$$F_o = F_1 - \frac{R_n}{G_{s1}} \left[(G_{s1} - G_o)^2 + (B_{s1} - B_o)^2 \right]. \tag{2.69}$$

Ideally, equation (2.66) to (2.69) would provide the exact solutions of the device's noise parameters. However, there would inevitably be errors in the measurement values thus the quantification of errors is necessary. For this purpose, Vasilescu introduced the error terms ΔF_1, ΔG_{s1}, and ΔB_{s1} into (2.69). Rearranging the expression gives

$$\Delta F_1 \cong R_n \left[R_{s1} (1 - P)(A + B) - S_1 P \right], \tag{2.70}$$

where

$$P = \frac{\Delta G_{s1}}{G_{s1}} = \frac{\Delta B_{s1}}{B_{s1}}, \tag{2.71}$$

$$A = \Delta G_{s1} (G_{s1} - G_o) + \Delta B_{s1} (B_{s1} - B_o), \tag{2.72}$$

$$B = \Delta G_{s1}^2 + \Delta B_{s1}^2, \tag{2.73}$$

$$S_1 = R_{s1} \left[(G_{s1} - G_o)^2 + (B_{s1} - B_o)^2 \right]. \tag{2.74}$$

Equation (2.70) provides an estimate on the variation in the measured noise figure assuming the errors in G_{s1} and B_{s1} are equal.

In Vasilescu's experimental verification, nine measurements were made. The above procedure was repeated for all possible combination of four sets of data. Each combination provides a set of extracted noise parameters F_o, R_n, G_o, and B_o along with the source admittances used. Using these values, the noise figure was computed for each

set, and the error between the calculated noise figure and the measured noise figure was recorded. To evaluate these sets of data, the sum of the modulus of all nine errors was calculated for each combination. The combination that resulted in the least error was then regarded as the best set of measurement data.

Although Vasilescu's technique seems to be simple in execution, there are two issues regarding its accuracy. First, if this procedure is applied to only four points, the result would be the same as that obtained from Lane's method. In other words, solving the system of four non-linear equations does not affect the overall accuracy in the extracted noise parameters. Secondly, applying this technique to multiple combinations of measurement data and then evaluating each set of data as described above does not guarantee that the extracted noise parameters are actually more accurate. Also, as more source admittances are used for the measurement, the computation would become expensive very fast.

2.2.6 Mitama and Katoh's Method

So far the methods based on Lane's approach all defined the error criterion for the fitting to be the difference between the measured noise figure and the fitted noise figure. Such definition implies that the source admittances values are free of errors, which is untrue in reality. For this reason, Mitama and Katoh proposed a different error criterion for the fitting procedure [34]. This new error term is defined as

$$\varepsilon_{ni} = \sqrt{w_{gi}\left(G_{si} - G_{si}^{m}\right)^2 + w_{bi}\left(B_{si} - B_{si}^{m}\right)^2 + w_{fi}\left(F_i - F_i^{m}\right)^2}\,, \tag{2.75}$$

where w_{gi}, w_{bi}, and w_{fi} are weighting factors, the subscript i indicates the ith measurement, and the overscript m indicates measured value. Equation (2.75) shows that the error not only takes into account of the inaccuracy in the F measurement but also that in the source admittance measurement. Graphically, the conventional error term and this current error term are illustrated in Figure 2-3.

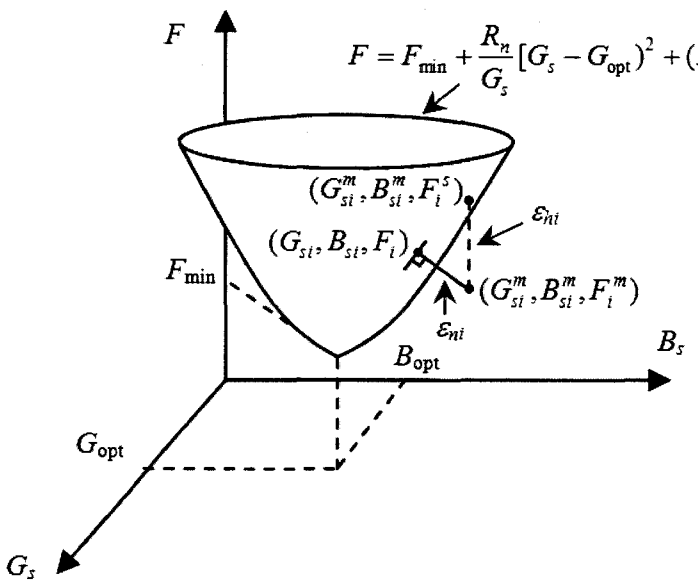

Figure 2-3 - The conventional fitting error term and Mitama and Katoh's error term [34].

As shown in Figure 2-3, the conventional error, labelled ε_{hi}, is the vertical distance between the measured noise figure, F_i^m, to the fitted noise figure, F_i^s, while G_{si}^m and B_{si}^m are treated as if they are true values. The minimum noise figure is labelled as $F_{\min}$. The new error term proposed by Mitama and Katoh is labelled as ε_{ni}, which is the distance between the measured point to the fitted surface. The error criterion for the fitting is the sum of all the error terms and is written as

$$S = \min\left(\sum_{i=1}^{n} \varepsilon_{ni,\min}^2\right), \tag{2.76}$$

where n is the number of measurements. Before the least-squares method or any other kind of fitting can be applied, the analytical expression of $\varepsilon_{ni,\min}$ needs to be determined. For that purpose, an error function is defined as

$$\hat{G}(G_s, B_s, F^m, R_n, G_o, B_o) = F_{\min} + \frac{R_n}{G_s}\left[(G_s - G_o)^2 + (B_s - B_o)^2\right] - F_m, \tag{2.77}$$

where the subscript m indicates measurement value. Assuming that the error is small, that is

$$G(G_s, B_s, F^m, R_n, G_o, B_o) \approx 0, \tag{2.78}$$

Taylor series expansion can be applied to the equation for the ith measurement data and yields

$$\begin{aligned}&\hat{G}_i^k + \hat{G}_{Gsi}^{k\,'}\left(G_{si} - G_{si}^m\right) + \hat{G}_{Bsi}^{k\,'}\left(B_{si} - B_{si}^m\right) + \hat{G}_{Fmi}^{k\,'}\left(F_i - F_{mi}\right) + \\ &\hat{G}_{F\min i}^{k\,'}\left(F_{\min} - F_{\min}^k\right) + \hat{G}_{Rni}^{k\,'}\left(R_n - R_n^k\right) + \hat{G}_{Goi}^{k\,'}\left(G_o - G_o^k\right) + \hat{G}_{Boi}^{k\,'}\left(B_o - B_o^k\right),\end{aligned} \tag{2.79}$$

where $\hat{G}_V^{k\,'}$ is defined as the partial derivative of the error function with respect to V, and V could be G_s, B_s, F^m, $F_{\min}$, R_n, G_{opt}, and B_{opt} of the kth iteration. Substituting (2.79) into (2.75) then gives

$$\varepsilon_{ni,\min}^k = \sqrt{w_i^k} \cdot \left| d_i^k \right|, \tag{2.80}$$

where

$$w_i^k = \frac{1}{\left(\hat{F}_{Gi}^{k\,'} / w_{gi}\right) + \left(\hat{F}_{Bi}^{k\,'} / w_{bi}\right) + \left(\hat{F}_{Fmi}^{k\,'} / w_{fi}\right)}, \tag{2.81}$$

$$d_i^k = -\begin{bmatrix}\hat{F}_i^k + \hat{F}_{F\min i}^{k\,'}\left(F_{\min} - F_{\min}^k\right) + \hat{F}_{Rni}^{k\,'}\left(R_n - R_n^k\right) + \\ \hat{F}_{Goi}^{k\,'}\left(G_o - G_o^k\right) + \hat{F}_{Boi}^{k\,'}\left(B_o - B_o^k\right)\end{bmatrix}. \tag{2.82}$$

Applying the least-squares method to (2.76), a system of four linear equations is obtained as

$$\frac{\partial S}{\partial F_{\min}} = 2\sum_{i=1}^{n} w_i \hat{F}_{F\min i}^{k\,'} d_i^k = 0, \tag{2.83}$$

$$\frac{\partial S}{\partial R_n} = 2\sum_{i=1}^{n} w_i \hat{F}_{Rni}^{k\,'} d_i^k = 0, \tag{2.84}$$

$$\frac{\partial S}{\partial G_o} = 2\sum_{i=1}^{n} w_i \hat{F}_{Goi}^{k\,'} d_i^k = 0, \tag{2.85}$$

$$\frac{\partial S}{\partial B_o} = 2\sum_{i=1}^{n} w_i \hat{F}_{Boi}^{k\,'} d_i^k = 0. \tag{2.86}$$

To solve the system of equations, the initial values of the noise parameters, $F_{\min}^0$, R_n^0, G_o^0, and B_o^0 are first calculated using the conventional Lane's method. Iteratively, (2.83) to (2.86) can then be solved.

Mitama and Katoh's method brings up the important point that the measured noise figure is not the only source of errors. In fact, apart from the sources of errors

taken into account in this method, there are other origins of errors that ultimately affect the accuracy of the extracted noise parameters. Later on, other authors built upon this method and provided more sophisticated techniques. For example, Boudiaf and Laporte developed a noise parameter extraction procedure that takes the advantage of known measurement uncertainties and use them to calculate the weighting factors [35].

2.3 Wave-based Noise Parameters and Extraction Techniques

Beside the conventional noise parameters of F_o, R_n, G_o, and B_o, a linear two-port network's noise behaviour can also be described by several other different but equivalent sets of noise parameters. This representation of noise behaviour allows easy calculations of noise figures for a two-port network. The intuitive, impedance-based representation of noise also demonstrates the dependence of noise factors on the source admittances attached to the network.

Different from the noise parameters introduced by Rothe and Dahlke [24], the focus of this section is on the wave-based noise parameters. The concept was first introduced by the pioneering work of Penfield [47]. Instead of representing the internal noise of the two-port network by voltage or current sources, this method uses waves. Such wave-based representation allows the use of the scattering parameters which are widely used in the microwave frequency range. Unlike the conventional noise parameters, wave-based noise parameters represent the intrinsic noise behaviour of a two -port network. They do not necessarily depend on the reflection coefficient seen by the input of the two-port.

2.3.1 Derivation of Wave-based Noise Parameters

Unlike the conventional method which models a linear two-port's internal noise with voltage or current sources attached to the noise-less two-port as shown in Figure 2-1, now the noise is represented by two noise wave generators c_1 and c_2 at the input of a noiseless two-port as shown in Figure 2-4.

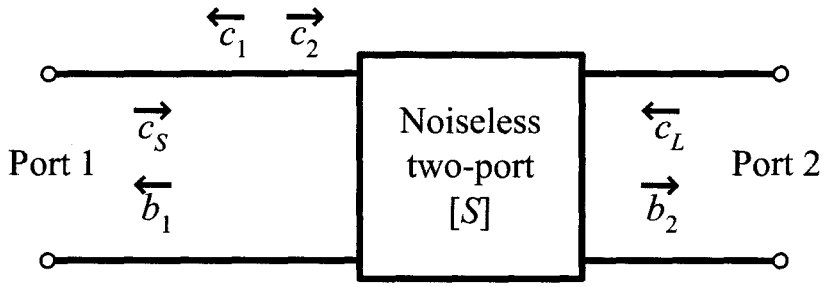

Figure 2-4 - Wave-based model of a linear noisy two-port [47].

In Figure 2-4, c_S and c_L represent the noise waves from the source and the load, respectively, incident on the two-port network while b_1 and b_2 are the total noise waves in directions leaving the two-port. Letting the two-port's scattering matrix be [*S*], these noise waves can be related as

$$\begin{bmatrix} b_1 - c_1 \\ b_2 \end{bmatrix} = \begin{bmatrix} S_{11} & S_{12} \\ S_{21} & S_{22} \end{bmatrix} \times \begin{bmatrix} c_S + c_2 \\ c_L \end{bmatrix}. \tag{2.87}$$

Comparing with the model in Figure 2-1, c_1 and c_2 can be written as

$$c_1 = \frac{v_n - Z_v^* i_n}{2\sqrt{\mathrm{Re}(Z_v)}}, \tag{2.88}$$

$$c_2 = -\frac{v_n + Z_v i_n}{2\sqrt{\mathrm{Re}(Z_v)}}, \tag{2.89}$$

where Z_v is a device-dependent impedance that is chosen to make c_1 and c_2 uncorrelated. The quantities c_1 and c_2 can also be represented by their noise temperatures T_1 and T_2. These noise temperatures, along with Z_v, are then used in deriving an expression for a two-port's noise factor for a given source impedance:

$$F = 1 + \frac{T_2}{T_0} + \frac{T_1 + T_2}{T_0} \times \frac{|Z_s - Z_v|^2}{4R_s \,\mathrm{Re}(Z_v)}, \tag{2.90}$$

where Z_s is the source impedance and R_S is the real part of Z_s.

Since a noisy two-port can also be represented by other combinations of voltage or current sources, Hillbrand provided a more general treatment that uses waves to replace these sources [48]. Letting these noise waves be c_i, where i indicates which of the two noise sources it replaces, a correlation matrix can be formed in the following general form

$$C = \begin{bmatrix} \overline{c_1 c_1^*} & \overline{c_1 c_2^*} \\ \overline{c_2 c_1^*} & \overline{c_2 c_2^*} \end{bmatrix}, \tag{2.91}$$

for any combination of voltage and current sources. The overbars in (2.91) indicate the values are the mean fluctuations. This correlation matrix's elements serve to characterize the noise behaviour of the two-port and, therefore, become the basis of the following work on two-port noise analysis using noise waves.

Using the wave-based noise analysis technique, Meys [49] developed a measurement method to characterize a linear two-port's noise properties. This method involves extending the two-port model by adding a noise source generating a known noise wave c_s to the input of the two-port. The total noise traveling toward the input of the device can be calculated as

$$c_t = \Gamma_s c_1 + c_2 + c_S, \tag{2.92}$$

where c_t is the total noise wave going toward the two-port's input, and Γ_s is the reflection coefficient of the noise source. Taking the mean-square value of (2.92) yields

$$\overline{|c_t|^2} = |\Gamma_s|^2 \overline{|c_1|^2} + 2\,\mathrm{Re}\left(\Gamma_S \overline{|c_2^* c_1|}\right) + \overline{|c_2|^2} + \overline{|c_S|^2}, \tag{2.93}$$

Equation (2.93) assumes that the noise source is uncorrelated with the two-port's internal noise. The overbar in this expression, again, represents time average. By applying the expression for thermal noise power to each term of this equation, it yields

$$\overline{|c_t|^2} = kT_t \Delta f,\ \overline{|c_1|^2} = kT_1 \Delta f,\ \overline{|c_2|^2} = kT_2 \Delta f,\ \overline{|c_2^* c_1|} = kT_3 \Delta f e^{j\phi_c},\ \text{and}$$

$$\Gamma_s = |\Gamma_s| e^{j\phi_s}, \tag{2.94}$$

where k is the Boltzmann's constant, Δf is the bandwidth, and T_t, T_1, and T_2 are noise temperatures. The four parameters T_1, T_2, T_3, and ϕ_c are the desired noise parameters that describe the intrinsic noise behaviour of the two-port.

To see how the new noise parameters relate to the conventional noise parameters, it is necessary to reintroduce the source reflection coefficient into the equations as the conventional noise parameters are dependent on the source impedance. To do that, the source noise wave is rewritten as

$$\overline{|c_s|^2} = \left(1 - |\Gamma_s|^2\right) kT_s \Delta f, \tag{2.95}$$

where T_s is the source noise temperature. Substituting (2.94) and (2.95) back into (2.93) yields, in terms of noise temperatures,

$$T_t = T_2 + |\Gamma_s|^2 T_1 + 2T_3|\Gamma_s|\cos(\phi_s + \phi_c) + T_s\left(1 - |\Gamma_s|^2\right). \tag{2.96}$$

By rearranging (2.96), the noise temperature of the two-port referred its input, T_n, can be written as

$$T_n = \frac{T_t}{1-|\Gamma_s|^2} - T_s = \frac{T_2 + |\Gamma_s|^2 T_1 + 2T_3|\Gamma_s|\cos(\phi_s + \phi_c)}{1-|\Gamma_s|^2}. \tag{2.97}$$

Comparing this result with the conventional noise figure equation (2.3) modified to be in terms of noise temperatures

$$T_n = T_{\min} + \frac{4T_o R_n}{Z_o \cdot |1+\Gamma_o|^2} \times \frac{|\Gamma_s - \Gamma_o|^2}{1-|\Gamma_s|^2}, \tag{2.98}$$

it then can be shown that,

$$T_2 = T_{\min} + \frac{4T_o R_n}{Z_o \cdot |1+\Gamma_o|^2} \times |\Gamma_o|^2, \tag{2.99}$$

$$T_1 = \frac{4T_o R_n}{Z_o \cdot |1+\Gamma_o|^2} - T_{\min}, \tag{2.100}$$

$$T_3 = \frac{4T_o R_n}{Z_o \cdot |1+\Gamma_o|^2} \times |\Gamma_o|, \text{ and} \tag{2.101}$$

$$\phi_c = \pi - \arg(\Gamma_o), \tag{2.102}$$

where Γ_o is the reflection coefficient of the optimal source impedance $Z_o = 1/Y_o$. Equations (2.99) to (2.102) show how to convert between the conventional source admittance- or impedance-based noise parameters and the wave-based noise parameters as defined here.

Once the noise parameters were properly defined, Meys proposed a simple measurement method. The measurement could be done by first connecting a noise source with various ϕ_s and a $|\Gamma_s| \approx 1$ to the DUT. Under these conditions, (2.96) can be approximated as

$$T_t = T_1 + T_2 + 2T_3\cos(\phi_s + \phi_c). \tag{2.103}$$

As ϕ_c is the only variable, the measured T_t for various ϕ_s can be plotted and (T_1+T_2), T_3, and ϕ_c can be determined.

To find T_1 and T_2, a matched noise source ($\Gamma_s = 0$) with a known T_s is connected to the input of the two-port. Equation (2.96) then can be written as

$$T_t = T_2 + T_s . \tag{2.104}$$

This allows T_2 and, subsequently, T_1 to be found.

Based on Meys' formulation of wave-based noise parameters, Valk *et al.* [50] developed a method for de-embedding two-port noise parameters from a cascaded two-port network. This work is worth noting because it applies to the practical situation in which a matching network is attached to the DUT's output. Using this de-embedding technique, the noise parameters of the DUT could be extracted assuming the noise parameters of the matching network are known.

2.4 Noise Parameter Extraction Techniques

Just like the conventional admittance-based noise parameters, there are variations in their definitions which require different measurement and extractions techniques. In this section, these techniques are reviewed and discussed.

2.4.1 Hecken's Method

Hecken [51] developed a different set of noise parameters using noise waves for noisy multi-ports. In this model, the internal noise is also represented by two noise wave generators at the input of the two-port as in Figure 2-4. The difference is that a lossless "matching network" is added between the noise source and the two-port, as shown in Figure 2-5.

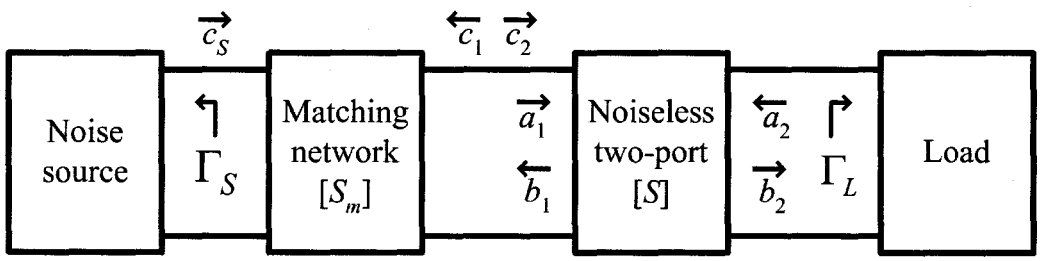

Figure 2-5 - Noise model of a linear noisy two-port by Hecken [51].

In Figure 2-5, c_S is the noise wave generated by the noise source. Γ_S and Γ_L are the reflection coefficients when looking at the outputs of the noise source and the load, respectively. The scattering matrix of the matching network is represented by $[S_m]$, and that of the noiseless two-port is represented by $[S]$.

Assuming Γ_S and Γ_L are both zero, the total outgoing noise wave of the two-port can be expressed as

$$b_2 = \frac{S_{21}}{1 - S_{m,22}S_{11}}\left(S_{m,22}c_1 + c_2 + S_{m,21}c_S\right). \tag{2.105}$$

Using the mean-square expression, the noise factor of the two-port becomes

$$F = 1 + \frac{\overline{|c_2|^2} + |S_{m,22}|^2\overline{|c_1|^2} + S_{m,22}\overline{\left(c_1 c_2^*\right)} + S_{m,22}^*\overline{\left(c_1^* c_2\right)}}{|S_{m,21}|^2\overline{|c_S|^2}}. \tag{2.106}$$

Using the following definitions

$$q_1 = \frac{\overline{|c_1|^2}}{\overline{|c_S|^2}},\ q_2 = \frac{\overline{|c_2|^2}}{\overline{|c_S|^2}},\ \text{and}\ \Gamma_{12} = \frac{\overline{|c_1 c_2^*|}}{\sqrt{\overline{|c_1|^2}\,\overline{|c_2|^2}}}, \tag{2.107}$$

(2.106) can be simplified to

$$F = 1 + \frac{|S_{m,22}|^2 q_1 + q_2 + \sqrt{q_1 q_2}\left(\Gamma_{12}S_{m,22} + \Gamma_{12}^* S_{m,22}^*\right)}{1 - |S_{m,22}|^2}. \tag{2.108}$$

where q_1, q_2, and Γ_{12} are the noise parameters of the two-port.

Since the initial assumption is $\Gamma_L = 0$, this condition needs to be enforced at the measurement stage. This condition is easily satisfied because the input impedance of a noise figure meter is likely equal to the characteristic impedance of the transmission line. By making the lossless matching network's $S_{m,22}$ equal zero, (2.108) becomes

$$F = 1 + q_2, \tag{2.109}$$

which q_2 can be determined.

Once q_2 is found, the next step is to vary $S_{m,22}$'s magnitude and phase angle until F_o is achieved, which is the absolute minimum value of F. The phase angle ϕ_{S0} of the $S_{m,22}$ obtained by this step allows one to find the phase angle ϕ_r of Γ_{12} given by $\phi_r = \pi$ -

ϕ_{S0}. Once q_2, the optimal $S_{m,22}$, and ϕ_r are known, they can be used in (2.108) to solve for q_1 and Γ_{12}.

Although the step involving manually adjusting the reflection coefficient of the matching network is theoretically possible, it is inconvenient for an on-wafer measurement. For an on-wafer measurement, the DUT usually has an input impedance not equal to the characteristic impedance. Manual adjustment of the source impedance in this case would be tedious. Also, adjusting the reflection coefficient manually may be time consuming. Further, this may generate an inconsistent source of uncertainty in the measurement results due to human errors.

2.4.2 Wedge's Method

Wedge [52],[53] developed a set of two-port noise parameters by modeling the intrinsic noise as noise waves leaving each port as shown in Figure 2-6.

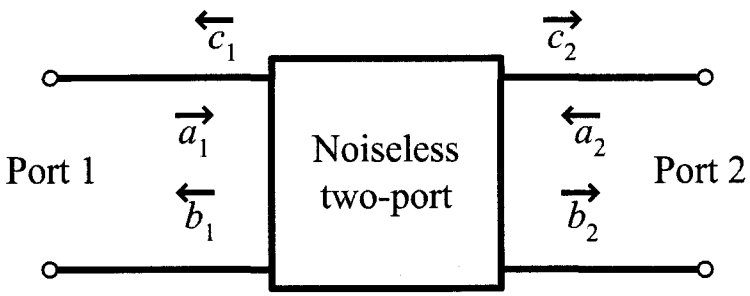

Figure 2-6 - Wedge's linear noisy two-port model [53].

In Figure 2-6, c_1 and c_2 are the intrinsic noise waves of the two-port. The incoming waves are modeled by a_1 and a_2, while b_1 and b_2 model the total noise leaving their respective port. These noise waves are related through the two-port's scattering parameters as

$$\begin{bmatrix} b_1 \\ b_2 \end{bmatrix} = \begin{bmatrix} S_{11} & S_{12} \\ S_{21} & S_{22} \end{bmatrix} \times \begin{bmatrix} a_1 \\ a_2 \end{bmatrix} + \begin{bmatrix} c_1 \\ c_2 \end{bmatrix}. \tag{2.110}$$

The intrinsic noise behaviour of the two-port can be described by the correlation matrix formed by c_1 and c_2 as

$$C_s = \begin{bmatrix} \overline{|c_1|^2} & \overline{c_1 c_2^*} \\ \overline{c_2 c_1^*} & \overline{|c_2|^2} \end{bmatrix}, \tag{2.111}$$

which is essentially the same as the general correlation matrix (2.91). Since the correlation matrix defines the intrinsic noise behaviour of the two-port, its components $\overline{|c_1|^2}$, $\overline{|c_2|^2}$, and the complex $\overline{c_1 c_2^*}$ are chosen to be the two-port's noise parameters. These parameters can be represented by the conventional noise parameters $T_{\min}$, R_n, and Γ_o as [53]

$$\overline{|c_1|^2} = kT_{\min}\left(|S_{11}|^2 - 1\right) + \frac{kt|1 - S_{11}\Gamma_o|^2}{|1+\Gamma_o|^2},$$

$$\overline{|c_2|^2} = |S_{21}|^2\left(kT_{\min} + \frac{kt|\Gamma_o|^2}{|1+\Gamma_o|^2}\right),$$

$$\overline{c_1 c_2^*} = \frac{-S_{21}^*\Gamma_o^* kt}{|1+\Gamma_o|^2} + \frac{S_{11}}{S_{21}}\overline{|c_2|^2}, \tag{2.112}$$

where

$$t = \frac{4T_0 R_n}{Z_0}. \tag{2.113}$$

and Z_0 is the normalization impedance.

The main components of the measurement system consist of two noise sources of known noise temperatures T_1 and T_2, and a noise power meter. The two noise sources are connected to port 1 and port 2 of the two-port, respectively, through two circulators. Therefore, the total noise powers, $\overline{|d_1|^2}$ and $\overline{|d_2|^2}$, leaving the two circulators for the power meter become

$$\overline{|d_1|^2} = \overline{|c_1|^2} + kT_1|S_{11}|^2 + kT_2|S_{12}|^2, \tag{2.114}$$

$$\overline{|d_2|^2} = \overline{|c_2|^2} + kT_1|S_{21}|^2 + kT_2|S_{22}|^2, \tag{2.115}$$

with a correlation product of

$$\overline{d_1 d_2^*} = \overline{c_1 c_2^*} + kT_1 S_{11} S_{21}^* + kT_2 S_{12} S_{22}^*. \tag{2.116}$$

Once the S parameters of the two-port are measured, $\overline{|c_1|^2}$ and $\overline{|c_2|^2}$ can easily be calculated by measuring $\overline{|d_1|^2}$ and $\overline{|d_2|^2}$ once. To find the correlation product, a 0°/180° hybrid coupler is used to take the noise waves d_1 and d_2 as the input and output to the power

meter. The 0°/180° coupler produces two output waves e_1 and e_2 whose powers are related as

$$\overline{|e_1|^2} - \overline{|e_2|^2} = 2\left[\mathrm{Re}\left(\overline{c_1 c_2^*}\right) + kT_1\,\mathrm{Re}\left(S_{11}S_{21}^*\right) + kT_2\,\mathrm{Re}\left(S_{12}S_{22}^*\right)\right]. \tag{2.117}$$

Using a 90° hybrid coupler, another relationship is resulted here as

$$\overline{|e_1|^2} - \overline{|e_2|^2} = 2\left[\mathrm{Im}\left(\overline{c_1 c_2^*}\right) + kT_1\,\mathrm{Im}\left(S_{11}S_{21}^*\right) + kT_2\,\mathrm{Im}\left(S_{12}S_{22}^*\right)\right]. \tag{2.118}$$

Equations (2.117) and (2.118) allow the correlation term $\overline{c_1 c_2^*}$ to be determined.

The measurement procedure described is theoretically sound. However, a source of uncertainty stems from the change of a part of the system. In the first step of the measurement where $\overline{|d_1|^2}$ and $\overline{|d_2|^2}$ in (2.114) and (2.115) are measured, a THRU is put in place between the circulator and the noise power meter. In the following step, the THRU is disconnected and replaced with a 0°/180° hybrid coupler followed by a 90° hybrid coupler. Such physical changes to the measurement system could cause uncertainties and undermine the system calibration. A similar measurement method based on the same principle by Withington [54] uses a different setup that uses an interferometer. In this work, the outputs of the two-port travel through separate routes before arriving at the interferometer. The use of the interferometer avoids the need to physically switching components, thus the particular source of uncertainty. However, as each arm of the interferometer has its own set of amplifiers, the calibration would require more effort.

2.4.3 Engen and Wait's Method

From a practical point of view, the purpose of a set of noise parameters is to help the designer decide how to terminate a two-port for optimal noise or power performance. With this in mind, Engen and Wait [55], [56] presented a set of noise parameters with physical meanings for the ease of application. The model they used is shown in Figure 2-7.

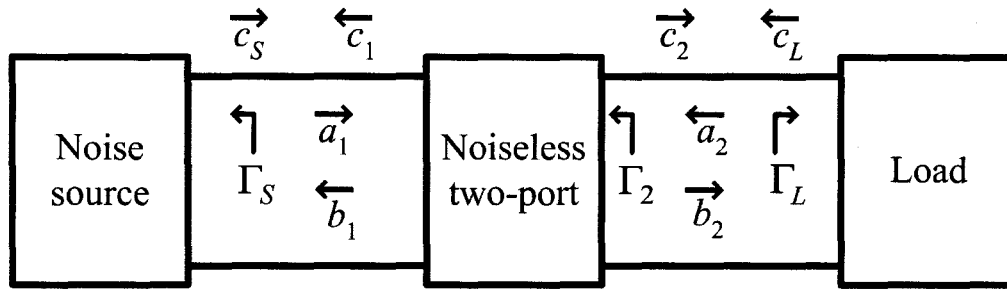

Figure 2-7 - Noise model of a linear two-port used by Engen and Wait [56].

The two-port's available noise waves are labelled as c_1 and c_2 leaving Port 1 and 2, respectively. A noise source with a reflection coefficient of Γ_S is connected to Port 1 and a load is connected to Port 2. The total incoming noise waves to the two-port are a_1 and a_2 and the total outgoing waves are b_1 and b_2. By inspecting Figure 2-7, the total incoming waves can be written as

$$a_1 = c_S + \Gamma_S b_1, \tag{2.119}$$

$$a_2 = c_L + \Gamma_L b_2. \tag{2.120}$$

Since c_1 and c_2 represent the internal noise of the two-port, they are likely to be correlated and can be related as

$$c_2 = \alpha \cdot c_1 + c_0. \tag{2.121}$$

where $\alpha \cdot c_1$ is the part of c_2 that is completely correlated with c_1, and c_0 is the uncorrelated part. The total outgoing waves b_1 and b_2 are related to the other noise waves through equation (2.110). Using (2.110), (2.120), and (2.121), b_2 becomes

$$b_2 = \frac{S_{21} c_s}{1 - S_{11}\Gamma_S} + \left(\frac{S_{21}\Gamma_S}{1 - S_{11}\Gamma_S} + \alpha \right) c_1 + c_0 + a_2\Gamma_2, \tag{2.122}$$

where Γ_2 is the reflection coefficient looking at port 2. Assuming that the load is noiseless ($c_L = 0$) and matched for zero reflection coefficient ($\Gamma_L = 0$), the total noise of the network consisting of the noise source and the two-port can be written as

$$\hat{b}_2 = \frac{S_{21} c_S}{1 - S_{11}\Gamma_S} + \left(\frac{S_{21}\Gamma_S}{1 - S_{11}\Gamma_S} + \alpha \right) c_1 + c_0. \tag{2.123}$$

The time average value of $\hat{b}_2$ is then used in the expression for the available power of the network of the noise source and the two-port to yield

$$P_{av,2}=\frac{\overline{\left|\hat{b}_2\right|^2}}{1-\left|\Gamma_2\right|^2}=\frac{1}{1-\left|\Gamma_2\right|^2}\left[\overline{\left|\frac{S_{21}c_S}{1-S_{11}\Gamma_S}\right|^2}+\left|\frac{S_{21}\Gamma_S}{1-S_{11}\Gamma_S}+\alpha\right|^2\overline{\left|c_1\right|^2}+\overline{\left|c_0\right|^2}\right]. \tag{2.124}$$

It should be noted that because (2.124) is derived from an expression for available power, it only works when the two-port's output also presents the real characteristic impedance of the transmission line. Therefore, if the output impedance of a two-port is not equal to the characteristic impedance, extra care must be taken when extracting the noise parameter. With a change of variable

$$\Gamma_S'=\frac{\Gamma_S-S_{11}^*}{1-S_{11}\Gamma_S}, \tag{2.125}$$

and using

$$\overline{\left|c_S\right|^2}=T_S\left(1-\left|\Gamma_S\right|^2\right), \tag{2.126}$$

(2.124) becomes

$$T_{out,2}=\frac{G}{1-\left|\Gamma_2\right|^2}\left[T_S\left(1-\left|\Gamma_S'\right|^2\right)+T_a+T_{rev}\left|\Gamma_S'-\beta\right|^2\right], \tag{2.127}$$

Where the Boltzmann's constant is factored out to yield the temperature expression,

$$G=\frac{\left|S_{21}\right|^2}{1-\left|S_{11}\right|^2},\ T_a=\frac{\overline{\left|c_0\right|^2}}{G},\ T_{rev}=\frac{\overline{\left|c_1\right|^2}}{1-\left|S_{11}\right|^2},\ \text{and}$$

$$\beta=-S_{11}^*-\frac{\alpha\left(1-\left|S_{11}\right|^2\right)}{S_{21}}. \tag{2.128}$$

In (2.124), T_a, T_{rev}, and β are the desired noise parameters. With the exception of β, these parameters have physical meanings and they are as follows:

G = the terminal-invariant power gain of the two-port

T_a = the minimum noise temperature of the two-port referred to its input

T_{rev} = the reverse available noise temperature from the input port of the two-port.

To relate these noise parameters to the conventional noise parameters, (2.127) needs to be cast into the form of (2.31), which is a modified version of the original noise factor equation. This means the right side of (2.127) needs to have a minimum T_S to match $T_{\min}$ of (2.31), plus a remainder term. To find the minimum $T_{out,2}$, the physical definition of T_e is applied to (2.127); that is, T_e is the effective noise temperature given to

a particular source impedance of a source-DUT network under the condition that the DUT is modeled as a noiseless amplifier and the output power is the same as in the case when the noisy DUT is connected to the noiseless version of the source impedance. Mathematically, this means the $T_{out,2}$ when $T_a = T_{rev} = 0$, should equal the $T_{out,2}$ when $T_S = 0$. Such condition yields the equation

$$T_S\left(\left|1-\Gamma_S'\right|^2\right) = T_a + T_{rev}\left|\Gamma_S' - \beta\right|, \tag{2.129}$$

and thus

$$T_S = \frac{T_a + T_{rev}\left|\Gamma_S' - \beta\right|}{\left|1-\Gamma_S'\right|^2}. \tag{2.130}$$

With (2.130), $T_{S,\min}$ can be found to be

$$T_{S,\min} = \frac{T_a(K+1) + T_{rev}\left(1-|\beta|^2\right)(K+1)}{2}, \tag{2.131}$$

where

$$K = \left\{1 + \frac{4T_aT_{rev}|\beta|^2}{\left[T_a + T_{rev}\left(1-|\beta|^2\right)\right]^2}\right\}^{\frac{1}{2}}. \tag{2.132}$$

At $T_{S,\min}$, the Γ_S' is defined as Γ_o' and is written as

$$\Gamma_o' = \frac{2T_{rev}|\beta|^2}{(T_a + T_{rev})(1+K) + T_{rev}|\beta|^2(1-K)}, \tag{2.133}$$

where

$$\Gamma_o = \frac{\Gamma_o' + S_{11}^*}{1 + S_{11}\Gamma_o'}. \tag{2.134}$$

Substituting Γ_o' back into (2.130) and subtracting the result from (2.131) yields

$$T_S = T_{S,\min} + \frac{K\left[T_a + T_{rev}\left(1-|\beta|^2\right)\right]\left|\Gamma_S' - \Gamma_o'\right|^2}{\left(1-\left|\Gamma_S'\right|^2\right)\left(1-\left|\Gamma_o'\right|^{2'}\right)}. \tag{2.135}$$

Converting Γ_S' and Γ_o' back to Γ_S and Γ_o using (2.125), (2.135) becomes

$$T_S = T_{S,\min} + \frac{K\left[T_a + T_{rev}\left(1-|\beta|^2\right)\right]|\Gamma_S - \Gamma_o|^2}{\left(1-|\Gamma_S|^2\right)\left(1-|\Gamma_o|^{2'}\right)}. \tag{2.136}$$

At this point, the effective noise temperature has been converted into the form similar to that of (2.31). By comparing the two equations, the conventional noise parameters in (2.31) then can be represented in terms of the wave-based noise parameters, T_{rev}, T_a, and β. First, $T_{\min}$, in terms of the wave-based parameters, has already been found in equation (2.131). To find the expression for Γ_o, (2.133) is substituted into (2.135) to yield

$$\Gamma_o^{'} = \left(\frac{T_{rev}}{T_{\min} + T_{rev}}\right)\cdot\beta. \tag{2.137}$$

Using the definition (2.125),

$$\Gamma_o = \frac{\Gamma_o^{'} + S_{11}^{*}}{S_{11}\Gamma_o^{*} + 1}. \tag{2.138}$$

Finally, comparing (2.31) and (2.136) shows that

$$K = \frac{4T_o R_n G_o}{T_a + T_{rev}\left(1-|\beta|^2\right)}. \tag{2.139}$$

Rewriting G_o in terms of Γ_o, R_n can be written as

$$R_n = \frac{KZ_o\left[T_a + T_{rev}\left(1-|\beta|^2\right)\right]|1+\Gamma_o|^2}{4T_o\left(1-|\Gamma_o|^2\right)}. \tag{2.140}$$

To extract the noise parameters of interest, the first step in the measurement procedure is to determine T_{rev}. The measurement is done by reversing the DUT's input port at Port 2 and its output port is now Port 1. Assuming that the reverse available power gain of the two-port is negligible, T_{rev} is simply the available noise temperature at Port 2 while the noise source is in the cold (OFF) state.

To find β, (2.127) is first rearranged to become

$$T_{rev}\left|\Gamma_S^{'} - \beta\right|^2 + T_a = \left(1-|\Gamma_2|^2\right)T_{out,2}/G - T_S\left(1-|\Gamma_S^{'}|^2\right). \tag{2.141}$$

By measuring $T_{out,2}$ with different Γ_S and taking the differences between the results using (2.141), β can be calculated by solving

$$\beta_r\left(x_1 - x_{ref}\right) + \beta_i\left(y_1 - y_{ref}\right) = \kappa_1,$$

$$\beta_r\left(x_2 - x_{ref}\right) + \beta_i\left(y_2 - y_{ref}\right) = \kappa_2, \tag{2.142}$$

where

$$\beta = \beta_r + j\beta_i,$$

$$\Gamma_S' = x + jy,$$

$$\kappa_x = \frac{\left(1 - \left|\Gamma_{2,ref}\right|^2\right)T_{out,2,ref} - \left(1 - \left|\Gamma_{2,x}\right|^2\right)T_{out,2,x}}{2GT_{rev}} + \left(1 - \frac{T_s}{T_{rev}}\right)\frac{\left|\Gamma_x'\right|^2 - \left|\Gamma_{ref}'\right|^2}{2}, \tag{2.143}$$

and the subscript i indicates the ith Γ_S.

Finally, a Y-factor measurement can be done using (2.127) for the cold and the hot states of the noise source as

$$Y = \frac{T_{S,hot}\left(1 - \left|\Gamma_{S,hot}'\right|^2\right) + T_a + T_{rev}\left|\Gamma_{S,hot}' - \beta\right|^2}{T_{S,cold}\left(1 - \left|\Gamma_{S,cold}'\right|^2\right) + T_a + T_{rev}\left|\Gamma_{S,cold}' - \beta\right|^2}. \tag{2.144}$$

Equation (2.144) then can be rearranged to find T_a.

The theory of Engen and Wait's method is straight forward. However, one disadvantage of this technique lies in the initial assumption that the output impedance of the two-port is the characteristic impedance of the transmission line. Such assumption is quite valid for a packaged device with well-matched input and output, but may not apply to the on-wafer measurement. Therefore, the measured noise powers or temperatures cannot be directly applied to the equations. Another issue is that doing both a forward and a reverse measurement of the two-port device requires physically changing the orientation of the two-port, thus creating uncertainty.

2.4.4 Randa's Method

Randa [57], [58] modified the noise parameters from [53] and created a similar set of parameters which are

$$X_1 = \frac{\overline{\left|c_1\right|^2}}{k},\ X_2 = \frac{1}{k}\overline{\left|\frac{c_2}{S_{21}}\right|^2},\ \text{and}\ X_{12} = \frac{1}{k}\overline{\left|c_1\left(\frac{c_2}{S_{21}}\right)^*\right|}. \tag{2.145}$$

Using an approach similar to that in [56], the same equation for $T_{out,2}$ in terms of the X parameters is derived and can be written as

$$T_{out,2} = \frac{|S_{21}|^2}{1-|\Gamma_2|^2}\left[\begin{array}{l}\dfrac{1-|\Gamma_S|^2}{|1-\Gamma_S S_{11}|^2}T_S + X_1\left|\dfrac{\Gamma_S}{1-\Gamma_S S_{11}}\right|^2 \\ +X_2 + 2\mathrm{Re}\left(\dfrac{\Gamma_S X_{12}}{1-\Gamma_S S_{11}}\right)\end{array}\right]. \tag{2.146}$$

Since (2.146) is identical to (2.127), the same restriction of having an output port presenting the real characteristic impedance of the transmission line also applies. A similar expression can be derived for the reverse configuration by letting the two-port's input port be Port 2 and the output port be Port 1. The resulted equation is

$$T_{out,1} = \frac{1}{1-|\Gamma_2|^2}\left[\begin{array}{l}\dfrac{|S_{12}|^2\left(1-|\Gamma_S|^2\right)}{|1-\Gamma_S S_{22}|^2}T_S + X_2\left|\dfrac{S_{12}S_{21}\Gamma_S}{1-\Gamma_S S_{22}}\right|^2 \\ +X_1 + 2\mathrm{Re}\left(\dfrac{S_{12}S_{21}\Gamma_S X_{12}^*}{1-\Gamma_S S_{22}}\right)\end{array}\right]. \tag{2.147}$$

In (2.147), Γ_2 is still the reflection coefficient looking at Port 2 except that now Port 2 is the input port of the DUT.

By letting Γ_S equal 0, (2.146) becomes

$$T_{out,2} = \frac{|S_{21}|^2}{1-|S_{22}|^2}[T_S + X_2]. \tag{2.148}$$

Experimentally, this means using a matched source impedance so that the source does not have any reflection back toward the DUT. Since the S parameters can be easily measured with a network analyzer and T_S is the known noise temperature of the noise source, X_2 can be determined from (2.148). Similarly, rewriting (2.147) by letting Γ_S equal zero gives

$$T_{out,1} = \frac{1}{1-|S_{11}|^2}\left[\frac{|S_{12}|^2}{|1-S_{22}|^2}T_S + X_1\right]. \tag{2.149}$$

Like the previous expression for $T_{out,2}$, (2.149) allows X_1 to be calculated with a reverse measurement while having a source matched to the output of the DUT. Once X_1 and X_2 are found, applying (2.146) to measurements using $|\Gamma_S| = 1$ with different phase angles can provide a system of equations to solve for X_{12}.

In reality, trying to achieve a matched output impedance throughout the measurements would be impractical for an on-wafer DUT as the device is unlikely to have a standard output impedance. Therefore, in the actual measurement setup, there exists a mismatch between the DUT's output and the noise power meter. This mismatch factor, M, is defined as the portion of the available noise power form the DUT that actually is delivered to the power meter. Letting the reflection coefficient of the DUT's output be Γ_{out} and that of the power meter's input be Γ_L, M can be written as

$$M = \frac{\left(1-|\Gamma_{out}|^2\right)\left(1-|\Gamma_L|^2\right)}{|1-\Gamma_{out}\Gamma_L|^2}, \tag{2.150}$$

And the actual power measured by the power meter, P_L, and the available noise power at the DUT's output, P_{out}, are related by

$$P_L = P_{out}M\ . \tag{2.151}$$

With this relation, the available noise power, and thus the noise temperature at the DUT's output, can be calculated from the measured noise power. The noise temperature then can be used in equations (2.148) and (2.149).

Chapter 3: UNCERTAINTY ISSUES

As shown in Table 1.1, the International Technology Roadmap for Semiconductor predicts that for the 37 nm RF CMOS, the minimum noise figure, F_{min}, will reach a value of 0.2 dB at 5 GHz. Meanwhile, an existing study comparing various noise parameter extraction methods concludes that the best uncertainty achieved has a value of 0.2 dB. This means the extracted F_{min} will have an uncertainty of 100%. Thus the uncertainty issue becomes more and more important, and obtaining accurate results turns into a major challenge.

Many sources of errors may be present in a measurement system. They are roughly categorized into raw errors and residual errors. Raw errors are the errors present in an uncalibrated system. Once a system is calibrated, the sources of errors that remain are residual. In general, the calibration of a measurement system involves the measurement of certain "standards," which are devices with known characteristics and behaviours. The characteristics of the measurement system then can be obtained by removing the effects of the standards from the measurement results.

In this chapter, the potential sources of errors present in a noise measurement system are reviewed followed by various works aimed at analyzing and dealing with uncertainty issues.

3.1 Sources of Measurement Errors

In a microwave noise measurement system, an important instrument is the vector network analyzer (VNA). A VNA measures the transmission and reflection of signals of a network. Three kinds of errors associated with a VNA measurement are the systematic error, the random error, and drift error. After the calibration, the systematic, or repeatable, errors can be removed to a certain degree. The system errors that cannot be removed due to the accuracy limitations of the calibration standards are the residual system errors. A calibration cannot eliminate random errors because their random effects to the measurement results are not repeatable among different measurements. Finally, drift errors are the results of varying temperatures and component aging. As these three

types of errors cannot not be removed through a system calibration, they all contribute to the measurement uncertainties of the VNA.

To develop a model that quantifies the effect of these errors on the final measurement result, each individual cause of error needs to be defined. The conventional method that a VNA uses in calibration to de-embed the DUT from the fixtures of the measurement system models the network with twelve error terms. The uncertain portions of these error terms after the calibration become the residual errors. These twelve error terms are listed below.

E_{DF} = forward residual directivity; due to signal leakage through the directional coupler on port 1.

E_{SF} = forward residual source match; due to the mismatch between the VNA's test port and the source impedance.

E_{RF} = forward residual reflection tracking; due to the path differences between the test and reference paths.

E_{XF} = forward crosstalk.

E_{LF} = forward load match.

E_{TF} = forward transmission tracking.

E_{DR} = reverse residual directivity.

E_{SR} = reverse residual source match.

E_{RR} = reverse residual reflection tracking.

E_{XR} = reverse crosstalk.

E_{LR} = reverse load match.

E_{TR} = reverse transmission tracking.

The first six residual error terms are for measurement in the forward direction and the second six terms are for the reverse direction. These terms are illustrated on a signal flow graph in Figure 3-1.

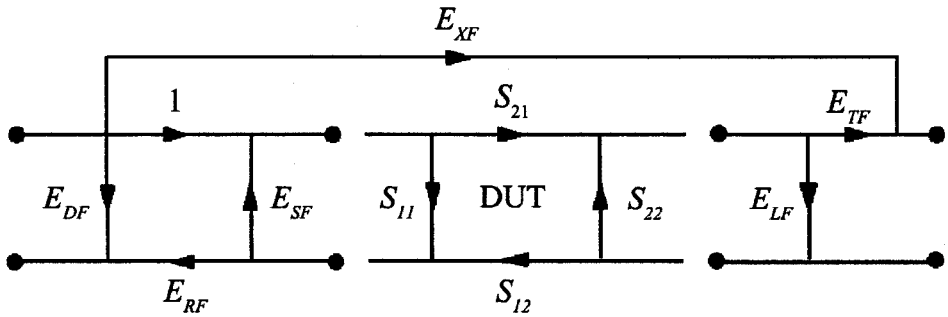

Figure 3-1 - Signal flow diagram of the forward two-port error terms [60].

The left block and the right block surrounding the DUT are the error adapter models in addition to the ideal measurement system. For the reverse direction, the model diagram would be the same except the reverse error terms are used. Other than the twelve residual error terms, there are two other sources of residual terms that contribute to the over systematic error. They are the dynamic accuracy's magnitude, A_M, and phase, A_P. The dynamic accuracy is due to a host of systematic errors originated in the VNA instead of the limitations of the calibration standards.

The three sources of random errors are noise, connector repeatability, and interconnecting cable stability. The two kinds of noises are noise floor N_F, and trace noise N_T. The uncertainty caused by the noise floor can be reduced through averaging repeated measurement results. The phase noise, on the other hand, could be caused by the noise floor, phase noise of the local oscillator in the test set, or reducing the IF bandwidth. It can be reduced by smoothing the trace. Connector repeatability and cable stability refer to the effect of changes in connections and cable forms that take place during the measurement stage.

All these uncertainties ultimately manifest in the measurement result as deviations in magnitude and phase of the real value. For the uncertainty in the reflection measurement, the forward reflection magnitude uncertainty can be written as

$$\Delta S_{11,mag} = \sqrt{(systematic + stability)^2 + noise^2}\ , \tag{3.1}$$

where

$$systematic = E_{DF} + E_{RF}S_{11} + E_{SF}S_{11}^2 + E_{LF}S_{21}S_{12} + A_M S_{11},$$

$$stability = \sqrt{C^2 + R^2}\ ,$$

$$C^2 = C_{RM1}^2\left(1+S_{11}^4\right)+4C_{TM1}^2S_{11}^2+C_{RM2}^2S_{21}^2S_{12}^2,$$

$$R^2 = \left(R_{R1}\left(1+S_{11}^2\right)+2R_{T1}S_{11}\right)^2+\left(R_{R2}S_{21}S_{12}\right)^2,$$

$$noise^2 = \left(N_TS_{11}\right)^2+N_F^2,$$

A_M = magnitude dynamic accuracy,

C_{RM1} = Port 1 cable magnitude reflection stability,

C_{TM1} = Port 1 cable magnitude transmission stability,

C_{RM2} = Port 2 cable magnitude reflection stability,

R_{R1} = Port 1 connector reflection repeatability,

R_{T1} = Port 1 connector transmission repeatability,

R_{R2} = Port 2 connector reflection repeatability.

The forward reflection phase uncertainty is

$$\Delta S_{11,pahse} = \sin^{-1}\left(\frac{\sqrt{\left(systematic+stability\right)^2+noise^2}}{S_{11}}\right)+2C_{TP1}, \tag{3.2}$$

where

$$systematic = E_{DF}+E_{RF}S_{11}+E_{SF}S_{11}^2+E_{LF}S_{21}S_{12}+\sin\left(A_P\right)S_{11},$$

$$stability = \sqrt{C^2+R^2},$$

$$C^2 = C_{RM1}^2\left(1+S_{11}^4\right)+4C_{TM1}^2S_{11}^2+C_{RM2}^2S_{21}^2S_{12}^2,$$

$$R^2 = \left(R_{R1}\left(1+S_{11}^2\right)+2R_{T1}S_{11}\right)^2+\left(R_{R2}S_{21}S_{12}\right)^2,$$

$$noise^2 = \left(N_TS_{11}\right)^2+N_F^2$$

A_P = phase dynamic accuracy,

The forward transmission uncertainty is written as

$$\Delta S_{21,mag} = \sqrt{\left(systematic+stability\right)^2+noise^2}, \tag{3.3}$$

where

$$systematic = E_{XF}+S_{21}\left(E_{TF}+E_{SF}S_{11}+E_{LF}S_{22}+E_{SF}E_{LF}S_{21}S_{12}+A_M\right),$$

$$stability = \sqrt{C^2+R^2},$$

$$C^2 = S_{21}^2\left(C_{TM1}^2+C_{TM2}^2+\left(C_{R1}S_{11}\right)^2+\left(C_{R2}S_{22}\right)^2\right),$$

$$R^2 = S_{21}^2\left(\left(R_{T1}+R_{R1}S_{11}\right)^2+\left(R_{T2}+R_{R2}S_{22}\right)^2\right),$$

$$noise^2 = (N_T S_{11})^2 + N_F^2.$$

The forward transmission phase uncertainty is

$$\Delta S_{21,mag} = \sin^{-1}\left(\frac{\sqrt{(systematic + stability)^2 + noise^2}}{S_{21}}\right) + C_{TP1} + C_{TP2}, \qquad (3.4)$$

where

$$systematic = E_{XF} + S_{21}(E_{TF} + E_{SF}S_{11} + E_{LF}S_{22} + E_{SF}E_{LF}S_{21}S_{12} + \sin(A_p)),$$

$$stability = \sqrt{C^2 + R^2},$$

$$C^2 = S_{21}^2\left(C_{TM1}^2 + C_{TM2}^2 + (C_{R1}S_{11})^2 + (C_{R2}S_{22})^2\right),$$

$$R^2 = S_{21}^2\left((R_{T1} + R_{R1}S_{11})^2 + (R_{T2} + R_{R2}S_{22})^2\right),$$

$$noise^2 = (N_T S_{11})^2 + N_F^2.$$

The uncertainties for reverse reflection and transmission measurement have the same forms except that the residual error terms are those for reverse measurements.

Another important instrument typically used in microwave noise measurement is the noise figure meter (NFM). The use of a NFM typically involves placing a known noise source at the input of the DUT or standards for measurement and calibration purposes. The three types of errors are also present in the noise figure measurement. Specifically, the overall measurement uncertainty can be attributed to the uncertainty in the noise source, δENR, the uncertainty in the DUT's gain, δG, the uncertainty in the measurement receiver's noise figure, δNF_2, the overall noise figure of the DUT and the receiver network, δNF_{12}, and the mismatch uncertainty, δM. Among these sources of uncertainties, the uncertainty due to the mismatch has relatively little effect on the overall noise figure uncertainty [61]. The individual effect of each of the first four sources of uncertainties on the overall noise figure uncertainty, δNF, can be derived from the equation

$$F_{12} = F_1 + \frac{F_2 - 1}{G}, \qquad (3.5)$$

where F_{12} is the noise factor of the DUT and the noise receiver, F_1 is the noise factor of the DUT, F_2 is the noise factor of the noise receiver, and G is the gain of the DUT. Application of Taylor's Theorem and some algebra yields

$$\delta F_1 = \delta F_{12} - \left(\frac{1}{G_1}\right)\delta F_2 + \left(\frac{F_2 - 1}{G_1^2}\right)\delta G_1 . \tag{3.6}$$

With a conversion from linear scale to logarithmic, it can be shown that

$$\delta NF_1 = \left(\frac{F_{12}}{F_1}\right)\delta NF_1 - \left(\frac{F_2}{F_1 G_1}\right)\delta NF_2 + \left(\frac{F_2 - 1}{F_1 G_1}\right)\delta G_{dB} . \tag{3.7}$$

The effect of the uncertainty in the *ENR* of the noise source is present on each term of (3.7). For a DUT that is an amplifier, however, the effect of δENR on the δG_1 in the third term of (3.7) will cancel out because F_2 and F_{12} are measured at the same frequency. As the result, the error term associated with the *ENR* can be written as

$$\left(\frac{F_{12}}{F_1} - \frac{F_2}{F_1 G_1}\right)\delta ENR . \tag{3.8}$$

Finally, the effects of each uncertainty on the overall noise figure measurement's uncertainty is [61]

$$\delta NF = \left\{ \begin{array}{l} \left[\left(\frac{F_{12}}{F_1}\right)\delta NF_{12}\right]^2 - \left[\left(\frac{F_2}{F_1 G_1}\right)\delta NF_2\right]^2 + \left[\left(\frac{F_2 - 1}{F_1 G_1}\right)\delta G_{dB}\right]^2 \\ + \left[\left(\frac{F_{12}}{F_1} - \frac{F_2}{F_1 - G_1}\right)\delta ENR\right]^2 \end{array} \right\}^{0.5} . \tag{3.9}$$

Equation (3.9) allows the overall uncertainty of δNF_2, δNF_{12}, δG, and δENR once their values are known. For a DUT that is an amplifier, δNF_2, δNF_{12}, and δG can be calculated as [61]

$$\delta NF_{12} = \left[(\delta_{NS-DUT})^2 + (\delta_{NFM})^2\right]^{0.5}, \tag{3.10}$$

$$\delta NF_2 = \left[(\delta_{NS-NFM})^2 + (\delta_{NFM})^2\right]^{0.5}, \tag{3.11}$$

$$\delta G_1 = \left[(\delta_{NS-DUT})^2 + (\delta_{NS-NFM})^2 + (\delta_{DUT-NFM})^2 + (\delta_{NFMGain})^2\right]^{0.5}, \tag{3.12}$$

where

$\delta_{NS\text{-}DUT}$ = the maximum mismatching uncertainty between the noise source and the DUT ,

δ_{NFM} = the noise figure meter's uncertainty,

$\delta_{NS\text{-}NFM}$ = the maximum mismatching uncertainty between the noise source and the noise figure meter,

$\delta_{DUT\text{-}NFM}$ = the maximum mismatching uncertainty between the *DUT* and the noise figure meter.

Among these parameters, δ_{NFM} is dependent on the frequency and the noise source's ENR. The uncertainties due to mismatching interfaces, on the other hand, depend on the source impedance as it is calculated as $-20\log(1-|\Gamma_x|\cdot|\Gamma_y|)$, where x and y indicate the two interfaces. It should be noted that this value is the absolute maximum mismatching uncertainty assuming the phases of the two reflection coefficients are unknown. This assumption is not true as these reflection coefficients can be easily calculated, to a certain degree of accuracy, using the *S* parameters measured by the VNA. Therefore, when the overall noise figure uncertainties are calculated, these mismatching uncertainties should be calculated using the uncertainties of the VNA measurements.

3.2 Source Impedance Selection Techniques

Since Lane's proposal of using the least-squares fitting method to find the noise parameters, the source impedance selection has been an important issue. Although using more impedance points can smooth out random errors, the locations of these impedance points also have been shown to play a role in the accuracy of the final result [41]. In Davidson's work, the number of source impedance points and the pattern were investigated. Groups of source impedances were chosen and each was used with a set of known noise parameters of a typical field effect transistor to calculate its corresponding noise figure. Random errors were then artificially added to these calculated noise figures to simulated experimental results. These simulated noise figures then were used to calculate the noise parameters. By evaluating the differences between these calculated noise parameters and the original noise parameters, the goodness of each group of impedances can be shown.

In the simulation, each group consisted nine impedance points whose reflection coefficients form a cross on the Smith chart with one point sitting at the centre. The difference between groups is the orientation on the Smith chart and the maximum magnitude of the outer-most reflection coefficient of the nine. The inner impedances were placed in a "well-spread" manner. The study concludes that the orientation of the cross does not influence the errors in the calculated noise parameters. However, a larger

coverage on the Smith chart yields smaller errors in the noise parameters. Another claim made was that increasing the number of impedances on a particular cross pattern did not improve the overall errors.

Schmatz took a similar approach to evaluate the quality of groups of nine source impedances in the pattern of a cross with different orientations and coverage areas on the Smith chart as shown in Figure 3-2 [62].

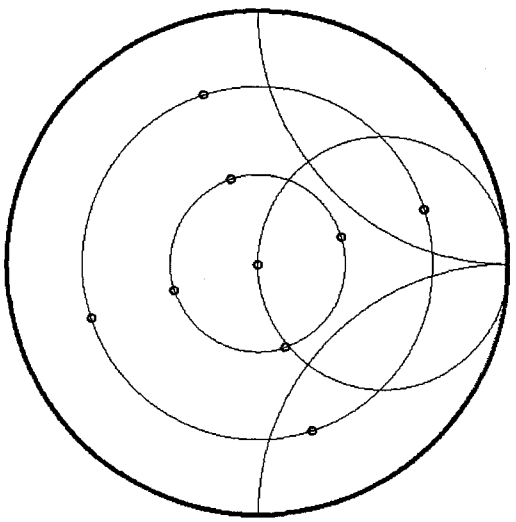

Figure 3-2 - Crossed-shaped source reflection coefficient pattern.

For each group, a noise figure was calculated. Random errors were added to these noise figures. These modified noise figures were treated as measurement values and then use to calculate the noise parameters. The criterion used to evaluate a set of source impedances is the difference between the original F_o and the calculated F_o and is defined as

$$\varepsilon_{RMS} = \sqrt{\frac{1}{N}\sum_{i=1}^{N}\left(\frac{F_{o,original} - F_{o,calculated}}{F_{o,original}}\right)^2}, \tag{3.13}$$

where N is the number of source impedance groups. Figure 3-3 shows the error plotted with respect to $|\Gamma_{o,original}|$ as the X-axis and $|\Gamma_{high}|$, which is the magnitude of the outer circle of the cross pattern, as the Y-axis.

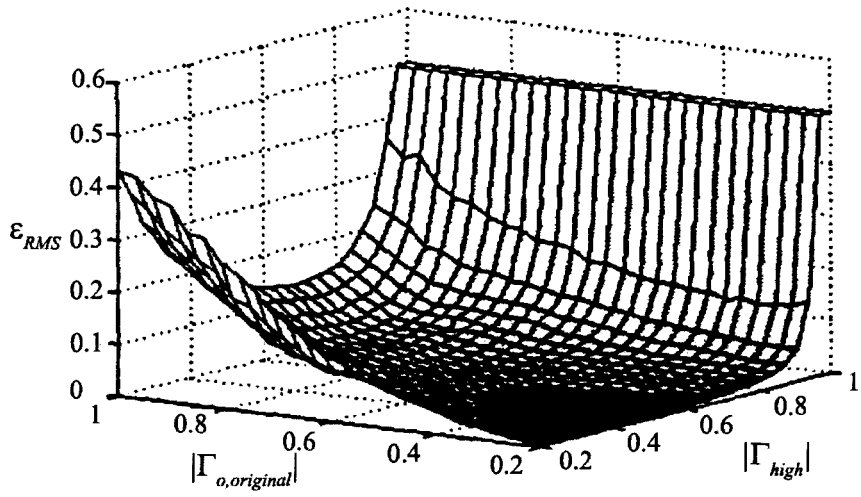

Figure 3-3 - RMS error with respect of $|\Gamma_{o,original}|$ and $|\Gamma_{high}|$ [62].

Figure 3-3 shows that the error generally increases with $|\Gamma_{high}|$. Therefore, it was concluded that the chosen source impedances for noise figure measurements should have magnitudes smaller than 0.8 and greater than 0.4.

Different from the studies that propose desired source reflection coefficient patterns, Caruso suggested a different criterion involving the concept of singular loci to be taken into account when selecting source points [28]. In his study, it was suggested that the error in the computation of noise parameters comes from certain bad source impedances called singular loci. These points create an ill-conditioned coefficient matrix when solving the linearized noise figure equation. The version of the linearized equation is written in terms of noise temperatures as

$$T_e = a + b\frac{1}{1-|\Gamma_S|^2} + c\frac{|\Gamma_S|}{1-|\Gamma_S|^2}\cos(\arg(\Gamma_S)) + d\frac{|\Gamma_S|}{1-|\Gamma_S|^2}\sin(\arg(\Gamma_S)), \qquad (3.14)$$

where

T_e = the effective noise temperature of the DUT,

Γ_s = the source reflection coefficient,

$$a = T_{\min} - 4T_o N\frac{1}{1-|\Gamma_o|^2},$$

$$b = 4T_o N\frac{1+|\Gamma_o|^2}{1-|\Gamma_o|^2},$$

$$c = -8T_o N \frac{|\Gamma_o|}{1-|\Gamma_o|^2}\cos(\arg(\Gamma_o)),$$

$$d = -8T_o N \frac{|\Gamma_o|}{1-|\Gamma_o|^2}\sin(\arg(\Gamma_o)),$$

$$N = Re(Y_s)\cdot R_n.$$

Defining the error criterion as

$$\varepsilon = \frac{1}{2}\sum_{i=1}^{n}(T_{ei} - T_{esi})^2 = \frac{1}{2}\sum_{i=1}^{n} P_i^2 , \tag{3.15}$$

where T_{esi} and T_{ei} are the measured noise temperature and the fitted noise temperature of the i^{th} source impedance, the system of linear equations can be represented as

$$\frac{\partial \varepsilon}{\partial a} = \sum_{i=1}^{n} P_i = 0,$$

$$\frac{\partial \varepsilon}{\partial b} = \sum_{i=1}^{n} \frac{P_i}{1-|\Gamma_{si}|^2} = 0,$$

$$\frac{\partial \varepsilon}{\partial c} = \sum_{i=1}^{n} \frac{P_i}{1-|\Gamma_{si}|^2}|\Gamma_{si}|\cos(\arg(\Gamma_{si})) = 0,$$

$$\frac{\partial \varepsilon}{\partial d} = \sum_{i=1}^{n} \frac{P_i}{1-|\Gamma_{si}|^2}|\Gamma_{si}|\sin(\arg(\Gamma_{si})) = 0, \tag{3.16}$$

Using the conventional approach, more than four source impedances would be used for the noise figure measurement. The results are then used in the system (3.16) for the least squares fitting step to solve for a, b, c, and d. Let the system of equations be written as $Ax = B$ where $x = [a \quad b \quad c \quad d]^T$, $B = [T_{e1} \quad T_{e2} \quad \cdots \quad T_{en}]^T$, and

$$A = \begin{bmatrix} 1 & \frac{1}{|\Gamma_{s1}|} & \frac{|\Gamma_{s1}|}{1-|\Gamma_{s1}|^2}\cos(\arg(\Gamma_{s1})) & \frac{|\Gamma_{s1}|}{1-|\Gamma_{s1}|^2}\sin(\arg(\Gamma_{s1})) \\ 1 & \frac{1}{|\Gamma_{s2}|} & \frac{|\Gamma_{s2}|}{1-|\Gamma_{s2}|^2}\cos(\arg(\Gamma_{s2})) & \frac{|\Gamma_{s2}|}{1-|\Gamma_{s2}|^2}\sin(\arg(\Gamma_{s2})) \\ \vdots & \vdots & \vdots & \vdots \\ 1 & \frac{1}{|\Gamma_{sn}|} & \frac{|\Gamma_{sn}|}{1-|\Gamma_{sn}|^2}\cos(\arg(\Gamma_{sn})) & \frac{|\Gamma_{sn}|}{1-|\Gamma_{sn}|^2}\sin(\arg(\Gamma_{sn})) \end{bmatrix},$$

the solution for x then can be written as $x = (A^T A)^{-1} A^T b$. The 4×4 matrix $A^T A$ is written as

$$A^T A(1,1) = n,\ A^T A(2,1) = \sum_{i=1}^{n} \frac{1}{1-|\Gamma_{si}|^2},\ A^T A(3,1) = \sum_{i=1}^{n} \frac{|\Gamma_{si}|\cos(\arg(\Gamma_{si}))}{1-|\Gamma_{si}|^2},$$

$$A^T A(4,1) = \sum_{i=1}^{n} \frac{|\Gamma_{si}|\sin(\arg(\Gamma_{si}))}{1-|\Gamma_{si}|^2},\ A^T A(2,2) = \sum_{i=1}^{n} \frac{1}{\left(1-|\Gamma_{si}|^2\right)^2},\ A^T A(3,2) = \sum_{i=1}^{n} \frac{|\Gamma_{si}|}{\left(1-|\Gamma_{si}|^2\right)^2},$$

$$A^T A(4,2) = \sum_{i=1}^{n} \frac{|\Gamma_{si}|\sin(\arg(\Gamma_{si}))}{\left(1-|\Gamma_{si}|^2\right)^2},\ A^T A(3,3) = \sum_{i=1}^{n} \frac{|\Gamma_{si}|^2\cos^2(\arg(\Gamma_{si}))}{\left(1-|\Gamma_{si}|^2\right)^2},$$

$$A^T A(4,3) = \sum_{i=1}^{n} \frac{|\Gamma_{si}|^2\cos(\arg(\Gamma_{si}))\sin(\arg(\Gamma_{si}))}{\left(1-|\Gamma_{si}|^2\right)^2},\ A^T A(4,4) = \sum_{i=1}^{n} \frac{|\Gamma_{si}|^2\sin^2(\arg(\Gamma_{si}))}{\left(1-|\Gamma_{si}|^2\right)^2}, \text{ and}$$

$$A^T A(j,k) = A^T A(k,j). \tag{3.17}$$

Caruso reasoned that certain source impedances might make the matrix (3.17) singular or nearly singular, which poses as a problem when solving x. These singular loci are the source reflection coefficients that make (3.17) having equivalent rows or columns and thus satisfy the following conditions:

$$|\Gamma_s| = \text{constant},\ |\Gamma_s|\cos(\arg(\Gamma_s)) = \text{constant},\ |\Gamma_s|\sin(\arg(\Gamma_s)) = \text{constant},$$

$$\tan(\arg(\Gamma_s)) = \text{constant, and } \frac{|\Gamma_s|\sin(\arg(\Gamma_s))}{1-|\Gamma_s|^2} = \text{constant}. \tag{3.18}$$

To avoid an ill-conditioned matrix, Caruso suggested that the source reflection coefficients should be chosen around two different singular curves so that (3.14) is completely defined.

The concept of singular loci was adapted into a more specific source impedance selection strategy by Bosch [63]. In this study, various source reflection coefficients were again used in a simulation along with a set of noise parameters. Noise figures were calculated for each source reflection coefficient. Random errors were added to the calculated noise figures to simulated experimental results. These simulated noise figures then were used to compute the noise parameters supposedly defined by each set of source reflection coefficient pattern. The criterion used to evaluate the various patterns is the error of each calculated noise parameter compared to its original counterpart.

The study concluded from the simulation that the noise parameter F_o's error depends on how close the source reflection coefficient is to Γ_o. Also it was found that R_n's error was not affected much by the pattern used but on the points around Γ_o. Finally it was determined that the errors of G_o and B_o depended on the number of chosen reflection coefficients with real part or imaginary part greater than those of Γ_o. The quantitative relationships between the calculated noise parameters and Γ_o are obtained by calculating their correlations, which can be represented as

$$corr\left(\sum_i \exp\left(\mathrm{sgn}\left(real\left(\mu_{\Gamma_o}\right)\right)\right)\cdot\left(real\left(\Gamma_{si}\right)-real\left(\mu_{\Gamma_o}\right)\right), \sigma_{G_o}\right) = -0.602, \qquad (3.19)$$

$$corr\left(\sum_i \exp\left(\mathrm{sgn}\left(imag\left(\mu_{\Gamma_o}\right)\right)\right)\cdot\left(imag\left(\Gamma_{si}\right)-imag\left(\mu_{\Gamma_o}\right)\right), \sigma_{B_o}\right) = -0.660, \qquad (3.20)$$

$$\text{and } corr\left(\sum_i \exp\left(-\left|\Gamma_{si}-\mu_{\Gamma_o}\right|\right), \sigma_{F_{\min}}\right) = -0.660. \qquad (3.21)$$

Using these results, the authors proposed a two-step method to select the source impedance pattern. The first step is to select, again, a cross-shaped pattern of five impedance points with one at the centre of the Smith chart and the magnitude of the rest to be the maximum value possible. The measurement results of the five points are then used in Lane's method to calculate a set of noise parameters. The Γ_o found is then used to select four other points. The first two points are chosen to be $R_o + j\cdot X_{\max}$ and $R_{\max} + j\cdot X_o$. These two points are chosen according to (3.19) and (3.20) and the observation that the accuracies of G_o and B_o depend on the number of reflection coefficients with real part or imaginary part greater than those of Γ_o. The last two points to chosen, according to (3.21), to be close but not too close to Γ_o.

These selection techniques were designed to satisfy the criteria observed through the simulation described above. The authors claimed these seemingly arbitrary decisions ultimately yield smaller errors in the noise parameters derived compared to random patterns and the cross-shaped pattern proposed by Davidson.

Based on the singular loci concept proposed by Caruso, O'Callaghan developed a more general version of source impedance selection criteria [32]. In this study, Lane's method was again used in solving the noise parameters. The noise factor equation (2.3) was linearized into

$$F=(F_o-2R_nG_o)+R_n\frac{G_s^2+B_s^2}{G_s}-2R_nB_o\left(\frac{B_s}{G_s}\right)+\left[R_n(G_o^2+B_o^2)\right]\frac{1}{G_s}, \qquad (3.22)$$

where the parameters have the usual meanings. Written in matrix form, the system of linear equations becomes $Ax = B$, where

$$A=\left[\overline{V_1}\quad \overline{V_2}\quad \overline{V_3}\quad \overline{V_4}\right],$$

$$x=\left[c_1\quad c_2\quad c_3\quad c_4\right]^T,$$

$$B=\left[F_{M1}\quad F_{M2}\quad \cdots\quad F_{Mn}\right],$$

$$\overline{V_1}=\left[1\quad 1\quad \cdots\quad 1\right]^T,$$

$$\overline{V_2}=\left[\frac{G_{s1}^2+B_{s1}^2}{G_{s1}}\quad \frac{G_{s2}^2+B_{s2}^2}{G_{s2}}\quad \cdots\quad \frac{G_{sn}^2+B_{sn}^2}{G_{sn}}\right]^T,$$

$$\overline{V_3}=\left[\frac{B_{s1}}{G_{s1}}\quad \frac{B_{s2}}{G_{s2}}\quad \cdots\quad \frac{B_{sn}}{G_{sn}}\right]^T,$$

$$\overline{V_4}=\left[\frac{1}{G_{s1}}\quad \frac{1}{G_{s2}}\quad \cdots\quad \frac{1}{G_{sn}}\right]^T,$$

$$c_1=F_{\min}-2R_nG_o,\ c_2=R_n,\ c_3=-2R_nB_o,\ c_4=R_n(G_o^2+B_o^2).$$

So far the formulation of the problem is similar to that used in Lane's method. The coefficient matrix A would be ill-conditioned if some of its four vectors are not linearly independent. The conditions that result in an ill-conditioned are thus

$$\overline{V_1}=\alpha_1\overline{V_2},\ \overline{V_1}=\alpha_2\overline{V_3},\ \overline{V_1}=\alpha_3\overline{V_4},\ \overline{V_2}=\alpha_4\overline{V_3},\ \overline{V_2}=\alpha_5\overline{V_4},\ \overline{V_3}=\alpha_6\overline{V_4},$$

$$\overline{V_1}=\alpha_7\overline{V_2}+\beta_7\overline{V_3},\ \overline{V_1}=\alpha_8\overline{V_2}+\beta_8\overline{V_4},\ \overline{V_1}=\alpha_9\overline{V_3}+\beta_9\overline{V_4},\ \overline{V_2}=\alpha_{10}\overline{V_3}+\beta_{10}\overline{V_4},$$

$$\overline{V_1}=\alpha_{11}\overline{V_2}+\beta_{11}\overline{V_3}+\gamma_{11}\overline{V_4}, \qquad (3.23)$$

where α_i, β_i, and γ_i are constants. The vector equations in (3.23) represent eleven families of singular loci on the source admittances plane. Therefore, if the selected source admittances lie on or close to one of these singular loci, large error would arise.

O'Callaghan pointed out in this study that the original source impedance selection criterion provided by Caruso, as described previously in this section, only avoids one of these eleven conditions. To ensure that A would not be ill-conditioned, all equations in (3.23) must be checked. For $\overline{V_i}$ and $\overline{V_j}$ to be linearly independent, they should by

orthogonal. However, it is impossible to achieve in real measurement. Therefore, the source admittances should be chosen to ensure the greatest orthogonality, which is calculated as

$$\cos\left(\overline{V_i},\overline{V_j}\right)=\frac{\left\langle \overline{V_i},\overline{V_j}\right\rangle}{\left|\overline{V_i}\right|\cdot\left|\overline{V_j}\right|}, \tag{3.24}$$

where $\left\langle \overline{V_i},\overline{V_j}\right\rangle$ is the inner product of the two vectors. The ideal selection of source admittances should minimize the degree of orthogonality for all six combinations of the vectors. O'Callaghan suggested that this criterion would decrease the accuracy of the resultant noise parameters on the accuracies of the source admittances and the measured noise figures. To satisfy all the conditions, the author selected seven source impedances for a particular device at a specific band. The author acknowledged that the seven impedances may have to be re-selected for other devices because the device might not be stable, or the measured noise figure was considered too high. Another reason would be that some of those impedances may simply be unachievable. Therefore, the selection of the seven source impedance points require human judgment for every DUT, and is not suitable for an automatic set-up.

Using a similar formulation of creating a system of four linear equations as in (3.14), Hu attempted an analytical analysis to demonstrate the relationship between the variances of the extracted noise parameters and the error in the measured noise figure or noise temperature [64]. Assuming the measured noise temperatures have normally distributed uncertainty stemmed from measurement inaccuracy, three equations were derived as

$$\mathrm{var}[a]=\sigma_1^2\left(\frac{1-\left|\Gamma_s\right|^2}{\left|\Gamma_s\right|^2}T_{\min}+4T_oN\right)^2+\sigma_2^2\left(\frac{1}{\left|\Gamma_s\right|^2}T_{\min}\right)^2, \tag{3.25}$$

$$\mathrm{var}[b]=\sigma_1^2\left(\frac{1-\left|\Gamma_s\right|^2}{\left|\Gamma_s\right|^2}T_{\min}+4T_oN\right)^2+\sigma_2^2\left(\frac{1-\left|\Gamma_s\right|^2}{\left|\Gamma_s\right|^2}T_{\min}\right)^2, \tag{3.26}$$

$$\mathrm{var}[c]=\mathrm{var}[d]=2\sigma_1^2\left(\frac{1-\left|\Gamma_s\right|^2}{\left|\Gamma_s\right|^2}T_{\min}\right)^2+\sigma_2^2\left(\frac{1-\left|\Gamma_s\right|^2}{\left|\Gamma_s\right|^2}T_{\min}\right)^2, \tag{3.27}$$

where a, b, c, and d are the same as the coefficients in (3.14), and σ_1 and σ_2 are the statistical variations of the uncertainties for the mismatched and matched noise temperature measurements. (3.25) to (3.27) show how the errors of the coefficient matrix depend on the source reflection coefficient Γ_s. With this result, the study concluded that the magnitudes of the selected source reflection coefficients for noise figure measurement should be large to decrease the errors in a, b, and c.

Taking a similar analytical approach, Banerjree also investigated how the error in the measured noise figure affects the uncertainties of the four derived noise parameters [65]. The analysis started by differentiate the noise factor F in (2.3) by each of the four noise parameters F_o, R_n, G_o, and B_o. The resultant four equations were then rewritten so that the differentials of the four noise parameters were in terms of the error parts of the noise figure:

$$\Delta F_o = \Delta F_1, \tag{3.28}$$

$$\Delta R_n = \frac{G_s}{(G_s - G_o)^2 + (B_s - B_o)^2} \times \Delta F_2, \tag{3.29}$$

$$\Delta G_o = \left[-\frac{G_s}{2(G_s - G_o)} \cdot \frac{1}{R_n} \right] \times \Delta F_3, \text{ and} \tag{3.30}$$

$$\Delta B_o = \left[-\frac{B_s}{2(B_s - B_o)} \cdot \frac{1}{R_n} \right] \times \Delta F_4, \tag{3.31}$$

where ΔF_1 to ΔF_4 made up the overall noise factor error Δ_F for a specific source admittance. Based on the derivation, it was concluded that a source admittance $G_s + jB_s$ amplifies the noise factor error if it is close to the optimal source admittance $G_o + jB_o$, and thus should be avoided. Also, it was observed that a small R_n of the DUT would also amplify the effect of the measurement error.

The studies discussed so far have all been focusing on the uncertainty in the measured noise figure and the role the source impedance plays in its error. Also the simulations performed accordingly have been general and had little regard in practical situations involving instrumentation setup. As a result, contradicting conclusions regarding the selection of source impedances arise. For example, some study proposed choosing a Γ_s close to Γ_o while some advised against it. Some recommended using large $|\Gamma_s|$ while some provided argument against having $|\Gamma_s|$ greater than 0.8. These various

conclusions, though backed up by their own evidences, could vary wildly depending on the assumptions made on the measurement environment and the exact analytical procedures. In reality, there are many factors and various sources of errors, as discussed in Section 3.1, which could contribute to the final uncertainties. Therefore, an uncertainty analysis conducted without considering these factors might not have much bearing in an actual measurement setup.

Chapter 4: IMPROVMENTS ON NOISE RECEIVER CHARACTERIZATOIN

In this chapter, an improved on-wafer noise receiver characterization procedure is described. The first section provides a detailed description of the measurement system used. The following sections are devoted to the improved noise receiver characterization method.

4.1 Measurement System

The schematic diagram of the measurement system is shown in Figure 4-1.

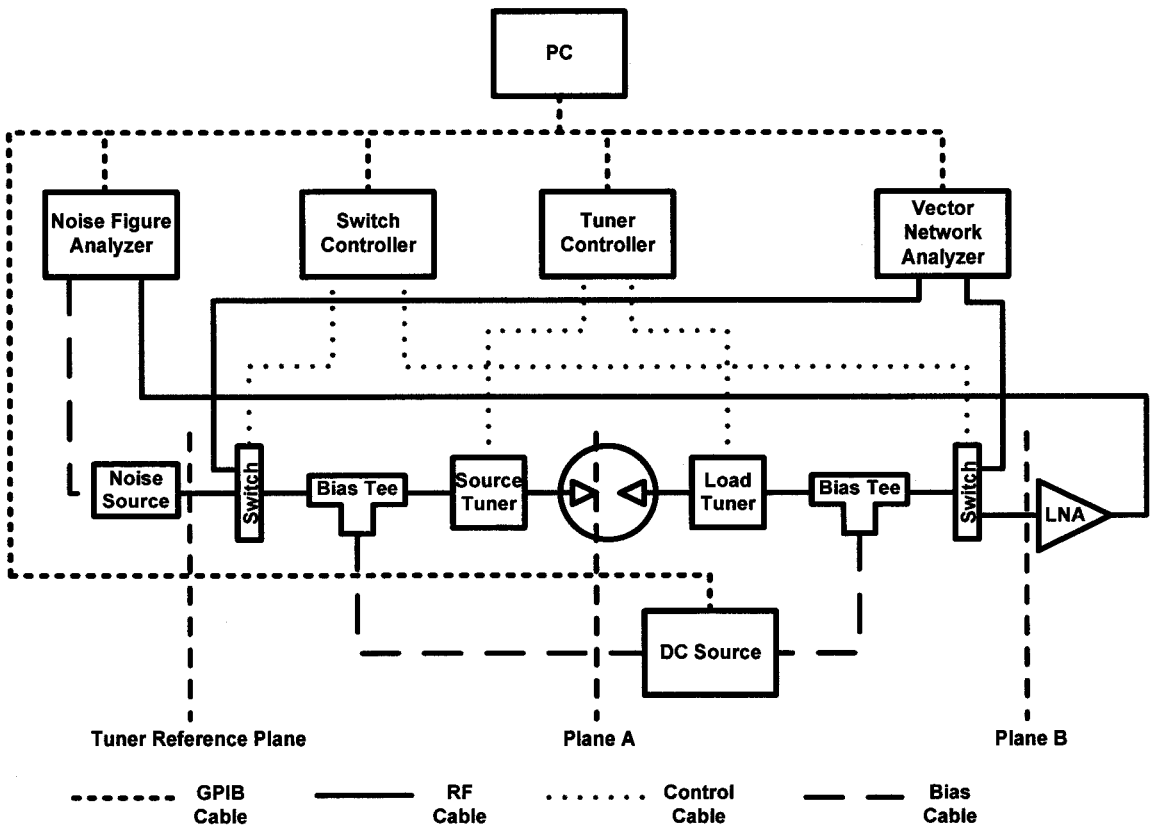

Figure 4-1 - Measurement system setup.

Figure 4-1 contains all the major components of the measurement system used. On the highest level, a computer is used to control the other instruments through a GPIB interface. The noise figure analyzer (NFA) is connected to a noise source which

produces a known amount of noise to the DUT when ON. The noise receiver end of the NFA is connected to the output of the system. It can calculate the noise figure of the system based on the power measurement it makes.

The VNA is responsible for measuring the reflection and transmission characteristics of the system, and can provide the data in *S* parameters. The NFA and the VNA both connected to the measurement platform through two switches, which are also controlled by the computer. The switches would toggle between the VNA and the NFA between different phases of the measurement procedure. The computer also controls the DC source, which is used to bias the DUT as needed through a pair of bias tees. Immediate at the input and the output of the DUT are the source and the load tuner, respectively. They provide different matching conditions as needed for the measurement. However, the load tuner is not used and acts as a THRU during the measurement. The tuners are driven by the tuner controller, which in turn is controlled by the computer. An LNA is placed at the output of the system before the NFA to amplify the noise signal. It is intended to increase the accuracy of the power measurement.

The software on the computer that controls the hardware is Maury Microwave's Automated Tuner System Software (ATSS). At the core of the software is its SNP Dynamic Link Libraries (SNP.dll), which is a software package that provides functions to control the instruments.

Before the measurement can be conducted, the system must first be calibrated. The calibration has two stages. The fist stage is to use the VNA to characterize the system which includes all the components such as cables and probes. The calibration characterizes the system up to the reference plane, which is the plane between the probe tip and the DUT. The calibration uses the SOLT (short-open-load-thru) technique, whose theory is based on the twelve-term error model described in Section 3.1. The reflection properties are measured by connecting the short, open, and load standards to each of the two probes. The transmission property is determined as a THRU standard is placed between the two probes. The calibration determines the twelve error terms and is repeated over the desired frequency range.

The second stage of the calibration procedure is the tuner calibration. In this step, the ATSS moves the tuners so that the reflection coefficients covering as much of the

Smith chart as possible are measured and recorded. At 4 GHz, the calibration could cover around 200 points but the number decreases with increasing frequencies.

While the system calibration is done assisted by the ATSS, the measurement stage is handled by an in-house application that makes use of the SNPDLL. It was written in Visual Basic and has a graphical interface shown below.

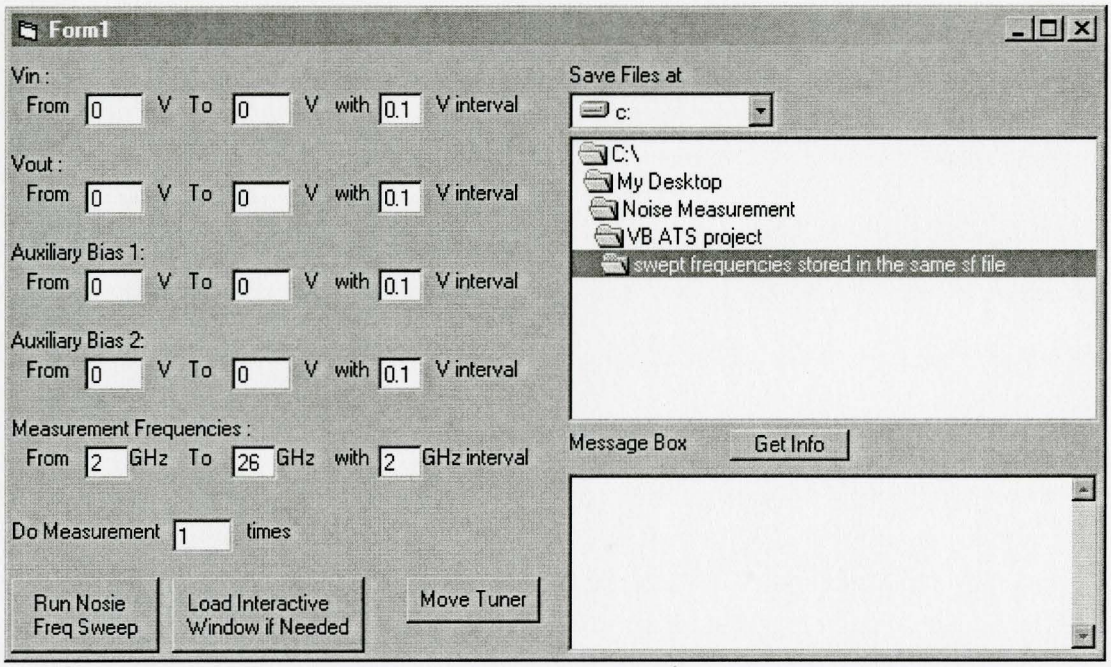

Figure 4-2 - Screenshot of the noise measurement program's user interface

The program allows the user to set the range of the input bias and the output bias for the DUT. The user can also specify the range of frequencies and the number of times the measurement is to be repeated. However, the user cannot select which source impedances to use. The exact impedances to use are picked by Maury's software. The results are stored as text files one frequency at a time.

4.2 Improved Noise Receiver Characterization

As mentioned in Section 2.1, the traditional noise characterization methods based on the Y-factor technique involves placing a known noise source at the DUT's input side. The noise power is then measured for the ON and OFF states of the noise source. These methods usually make the assumption that the source impedance of the noise source the

DUT's input sees stays constant between the ON and OFF states of the noise source. This assumption is false as shown in [66] by Kuhn. This difference ΔZ_{ns} changes the gain of the DUT even though the source impedance of the tuner is the same. Tiemeijer proposed a method to take this error into account by calculating the effective Y-factor and the effective excess noise ratio. However, this method requires the disconnections of the probes and the bias tees. It is also necessary to measure the LNA's S parameters during calibration. This is inconvenient and the disconnections after the calibration is done would introduce extra sources of error.

Another attempt to correct for ΔZ_{ns} makes use of noise equation in terms of power [68]. The method optimizes the noise receiver gain and the noise parameters simultaneously to avoid the effect of ΔZ_{ns}. Such optimization might result in a local minimum. Also, the gain of the noise receiver would be affected by the coherent noise.

In this section, a novel procedure for noise receiver characterization is described. This method uses both the hot (ON) noise source admittance Y_{sh} and the cold (OFF) noise source admittance Y_{sc}, and is able to take care of ΔZ_{ns}. Also, an iterative technique is used to find the receiver gain so the effect of the noise parameters on the receiver gain can be minimized.

The measurement system illustrated in Figure 4-1 can be simplified and modeled as in Figure 4-3.

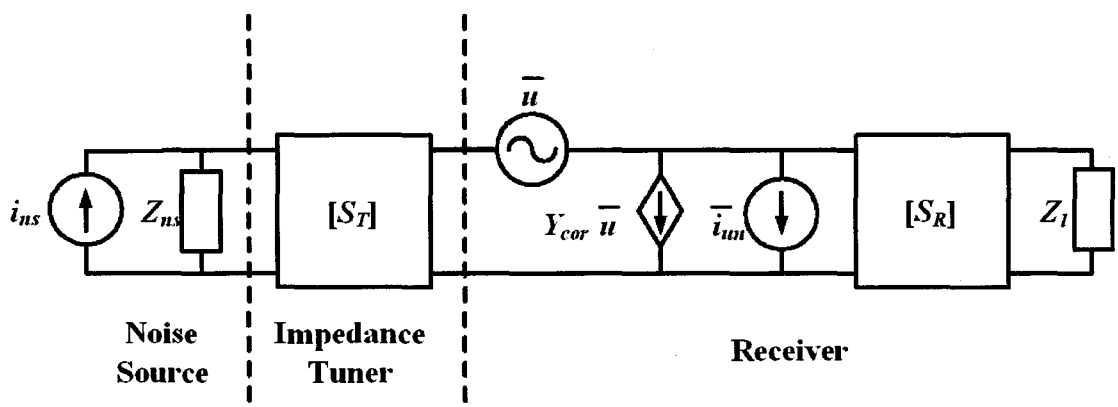

Figure 4-3 - The schematic diagram of the measurement system

In Figure 4-3, the dashed line on the left denotes the tuner reference plane and the one on the right denotes the noise reference plane. The receiver portion includes the LNA, the

NFA, and the cables. During the tuner calibration stage, a THRU standard is in the place of the DUT between the probes. At this stage, the impedance tuner block contains every component after the noise source and before the LNA. During the measurement stage, the DUT is placed between the probes. The noise reference plane then shifts to the input of the DUT, and the receiver now includes every component from the DUT to the NFA. The impedance tuner now consists of everything between the noise source and the DUT.

Using the model in Figure 4-3, the noise power measured by the noise receiver can be written as

$$P_n = \frac{G_{tr}}{4R_s}\left[4kT_{seff}\Delta f R_s + \overline{|i_{un}|^2}|Z_s|^2 + \overline{|u|^2}\left(1+|Y_{cor}|^2|Z_s|^2 + 2G_{cor}R_s - 2B_{cor}X_s\right)\right], \quad (4.1)$$

where

k = the Boltzmann's constant,

Δf = noise bandwidth,

R_s = source resistance,

X_s = source reactance,

$Z_s = R_s + jX_s$ = source impedance at the noise reference plane,

$\overline{u}$ = input referred noise voltage where the overbar indicates time averaging [24],

$\overline{i_{un}}$ = input referred noise current [24],

G_{cor} = correlation conductance,

B_{cor} = correlation susceptance,

$Y_{cor} = G_{cor} + jB_{cor}$ = complex correlation admittance [24],

G_{tr} = noise receiver transducer gain,

T_{seff} = effective source temperature at the noise reference plane.

The transducer gain of the noise receiver G_{tr} can be written as

$$G_{tr} = \frac{\left(1-|\Gamma_s|^2\right)|S_{21r}|^2\left(1-|\Gamma_l|^2\right)}{\left|\left(1-S_{11r}\Gamma_s\right)\left(1-S_{22r}\Gamma_l\right)-S_{12r}S_{21r}\Gamma_s\Gamma_l\right|}$$

$$= \frac{1-|\Gamma_s|^2}{\left|1-\Gamma_{inr}\Gamma_s\right|^2}\cdot G_o, \quad (4.2)$$

where the r in the subscripts indicates receiver, and

$$G_o = \frac{|S_{21r}|^2\left(1-|\Gamma_l|^2\right)}{\left|1-S_{22r}\Gamma_l\right|^2}. \tag{4.3}$$

Γ_{inr} is the reflection coefficient of the noise receiver. G_o as shown in is independent of the source impedance.

T_{seff} in equation (4.1) is calculated as

$$T_{seff} = (T_s - T_c)\cdot G_{avt} + T_c, \tag{4.4}$$

where T_c is the ambient temperature and G_{avt} is the available power gain of the tuner. It can be written as

$$G_{avt} = \frac{\left(1-|\Gamma_{ns}|^2\right)|S_{21t}|^2}{\left|1-S_{11t}\Gamma_{ns}\right|^2\left(1-\left|S_{22t}+\frac{S_{12t}S_{21t}\Gamma_{ns}}{1-S_{11t}\Gamma_{ns}}\right|^2\right)}, \tag{4.5}$$

where the t in the subscripts indicates tuner, and Γ_{ns} is the reflection coefficient of the noise source. The source temperature in (4.4) is the noise temperature of the noise source. Therefore it equals T_h when ON and T_c when OFF. When the noise source is ON, T_h can be calculated using the device's specified *ENR* value as

$$T_h = (ENR+1)T_o. \tag{4.6}$$

Defining three new parameters t_{seff}, R_u, and G_{iun}, such that

$$t_{seff} = \frac{T_{seff}}{T_o},\ R_u = \frac{\overline{|u|^2}}{4kT_o\Delta f},\ G_{iun} = \frac{\overline{|i_{un}|^2}}{4kT_o\Delta f},$$

Equation (4.1) can be rewritten as

$$P_n = \frac{kT_o\Delta f}{G_s}\cdot\frac{1-|\Gamma_s|^2}{\left|1-\Gamma_{inr}\Gamma_s\right|} \times G_o\left[t_{seff}G_s + R_u\left(|Y_s|^2 + |Y_{cor}|^2 + 2G_{cor}G_s + 2B_{cor}B_s\right) + G_{iun}\right], \tag{4.7}$$

where $Y_s = G_s + jB_s$ is the source admittance. Letting $A = R_u$, $B = G_{iun}+|Y_{cor}|^2R_u$, $C = G_{cor}R_u$, and $D = B_{cor}R_u$, the above equation can be put in the form

$$\frac{P_nG_s}{kT_o\Delta f}\frac{\left|1-\Gamma_{inr}\Gamma_s\right|^2}{1-|\Gamma_s|^2} = \left(t_{seff}\cdot G_s + |Y_s|^2\cdot A + B + 2G_s\cdot C + 2B_s\cdot D\right)\cdot G_o. \tag{4.8}$$

The term on the left side of (4.8) consists of only known values obtainable from the measurement. On the right side of the equation, the unknowns are A, B, C, D, and G_o.

In order to solve for G_o, a hot measurement (noise source ON) and four cold measurements (noise source OFF) at four different source impedances are required [43], [44]. The one hot measurement, or any noise temperature different from the other four, is needed to solve for G_o. The original method described in [43] theorized that subtracting the power of a hot measurement by that of a cold measurement while having the source admittance constant, the result obtained using (4.8) can be written as

$$P_h - P_c = \frac{kT_o\Delta f\left(1-|\Gamma_s|^2\right)}{\left|1-\Gamma_{inr}\Gamma_s\right|^2}\cdot G_o\cdot\left(t_h - t_c\right), \tag{4.9}$$

where P_h and P_c are the measured hot and cold powers. Then the only unknown, G_o, can be found. In the proposed method, the source admittances during the hot state and the cold state are denoted as $Y_{sh} = G_{sh} + jB_{sh}$ and $Y_{sc} = G_{sc} + jB_{sc}$, respectively. They are not assumed to be the same. In addition, an iterative procedure is used in the calculation of G_o to reduce the effect of the errors of A, B, C, and D due to ΔY_s on the result. Once G_o is found, A, B, C, and D are then obtained using the cold measurement data.

The proposed method is described in steps as follows:

Step 1: First an initial value of G_o is obtained by letting $A = B = C = D = 0$ while subtracting P_h by P_c using (4.8). This yields, after some rearranging,

$$G_o = \frac{1}{kT_o\Delta f\left(t_{seffh}G_{sh} - t_{seffc}G_{sc}\right)}\cdot\left(P_hG_{sh}\frac{\left|1-\Gamma_{inr}\Gamma_{sh}\right|^2}{1-|\Gamma_{sh}|^2} - P_cG_{sc}\frac{\left|1-\Gamma_{inr}\Gamma_{sc}\right|^2}{1-|\Gamma_{sc}|^2}\right), \tag{4.10}$$

where h and c in the subscripts indicate hot and cold states, respectively.

Step 2: Once an initial G_o is found, (4.8) is rearranged into

$$|Y_s|^2\cdot A + B + 2G_s\cdot C + 2B_s\cdot D + 2B_s\cdot D = G_s\left(\frac{P_n}{kT_o\Delta fG_o}\cdot\frac{\left|1-\Gamma_{inr}\Gamma_s\right|^2}{1-|\Gamma_s|^2} - t_{seff}\right). \tag{4.11}$$

Using the results of the four or more cold measurements, A, B, C, and D can be solved with some sort of fitting procedure.

Step 3: Use the values of A, B, C, and D obtained in the previous step, G_o is calculated again using (4.8) by subtracting P_h by P_c. After some rearranging, this is written as

$$G_o = \left(P_h G_{sh} \frac{\left|1-\Gamma_{inr}\Gamma_s\right|^2}{1-\left|\Gamma_{sh}\right|^2} - P_c G_{sc} \frac{\left|1-\Gamma_{inr}\Gamma_s\right|^2}{1-\left|\Gamma_{sc}\right|^2} \right) \div$$
$$kT_o\Delta f\left[\left(t_{seffh}G_{sh} - t_{seffc}G_{sc}\right) + \left(\left|Y_{sh}\right|^2 - \left|Y_{sc}\right|^2\right)\cdot A + 2\left(G_{sh}-G_{sc}\right)\cdot C + 2\left(B_{sh}-B_{sc}\right)\cdot D\right] \quad . (4.12)$$

Step 4: Step 2 and Step 3 are repeated iteratively until the values of A, B, C, D, and G_o converge.

After A, B, C, and D are found, they can easily be converted to the parameters that defined them in the first place as

$$R_u = A,$$

$$G_{iun} = B - \frac{C^2 + D^2}{A},$$

$$G_{cor} = \frac{C}{A},$$

$$\text{and } B_{cor} = \frac{D}{A}.$$

The conventional noise parameters of the noise receiver then can be found by [25]

$$F_o = 1 + 2R_u G_{cor} + 2\sqrt{R_u G_{iun} + \left(R_u G_{cor}\right)^2},$$

$$R_n = R_u,$$

$$G_o = \sqrt{\frac{G_{iun}}{R_u} + G_{cor}^2},$$

$$\text{and } B_o = -B_{cor}.$$

With this method, the two sets of receiver noise parameters for the two noise reference planes A and B in Figure 4-1 are found, the DUT's noise parameters can be calculated by [48]

$$\left[C_A^{dut}\right] = \left[C_A^A\right] - \left[A^{dut}\right]\left[A^{out}\right]\left[C_A^B\right]\left[A^{out}\right]^T\left[A^{dut}\right]^T - \left[A^{dut}\right]\left[C_A^{out}\right]\left[A^{dut}\right]^T, \quad (4.13)$$

where the superscript T denotes Hermitian conjugation. $\left[C_A^A\right]$ and $\left[C_A^B\right]$ are the noise correlation matrices at plane A and B shown in Figure 4-1. $\left[A^{dut}\right]$ and $\left[A^{out}\right]$ are the chain matrices of the DUT and the output block which includes everything between the DUT's output and the LNA's input. $\left[C_A^{dut}\right]$ and $\left[C_A^{out}\right]$ are the correlation matrices of the DUT

and the output block. Once $\left[C_A^{dut}\right]$ is obtained, the DUT's noise parameters can be found by [19]

$$F_o = 1 + \frac{1}{kT_o}\left(\mathrm{Re}\left(C_A^{dut}(1,2)\right) + \sqrt{C_A^{dut}(1,1)\cdot C_A^{dut}(2,2) - \left(\mathrm{Im}\left(C_A^{dut}(1,2)\right)\right)^2}\right), \quad (4.14)$$

$$Y_o = G_o + jB_o = \frac{\sqrt{C_A^{dut}(1,1)C_A^{dut}(2,2) - \left(\mathrm{Im}\left(C_A^{dut}(1,2)\right)\right)^2} + j\,\mathrm{Im}\left(C_A^{dut}(1,2)\right)}{C_A^{dut}(1,1)}, \quad (4.15)$$

$$R_n = \frac{C_A^{dut}(1,1)}{2kT_o}. \quad (4.16)$$

4.3 Measurement Results and Analyses

In order to demonstrate the difference between the impedances of the noise source in the hot state and the cold state, a measurement was made from 0.5 GHz to 26.5 GHz. The result is recorded in Figure 4-4.

Figure 4-4 shows the real part and the imaginary part of the noise source's impedance across the interested frequency range. For all frequencies used, the impedances are roughly 50 Ω with little fluctuations. For the same frequency, the impedances are slightly different in the hot state and the cold state. Another plot showing the normalized difference is in Figure 4-5. The figure shows that the normalized difference decreases as the frequency increases with the maximum value being 18.4% and the minimum being around 5%.

This difference in the noise source impedance results in a difference in the reflection coefficients the noise receiver sees. The effect is demonstrated in Figure 4-6. The result plotted in Figure 4-6 was measured by placing a THRU between the probes and varying the source tuner's impedance across the Smith chart while taking hot and cold measurements. The figure shows that for the same tuner impedance (same positions for the tuner's motors) the resultant reflection coefficients are different between the hot and the cold states. It also can be seen that the difference is larger for the reflection coefficients near the centre of the Smith chart.

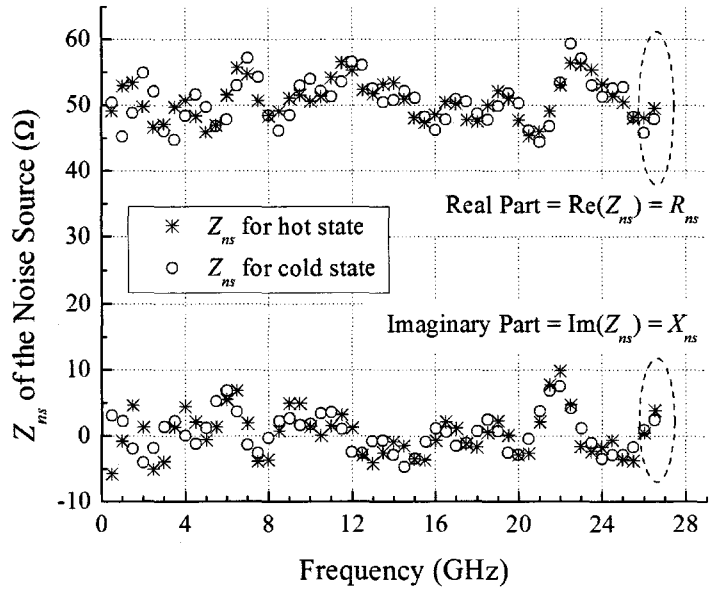

Figure 4-4 - Impedances of the HP 346C noise source in hot and cold states [67].

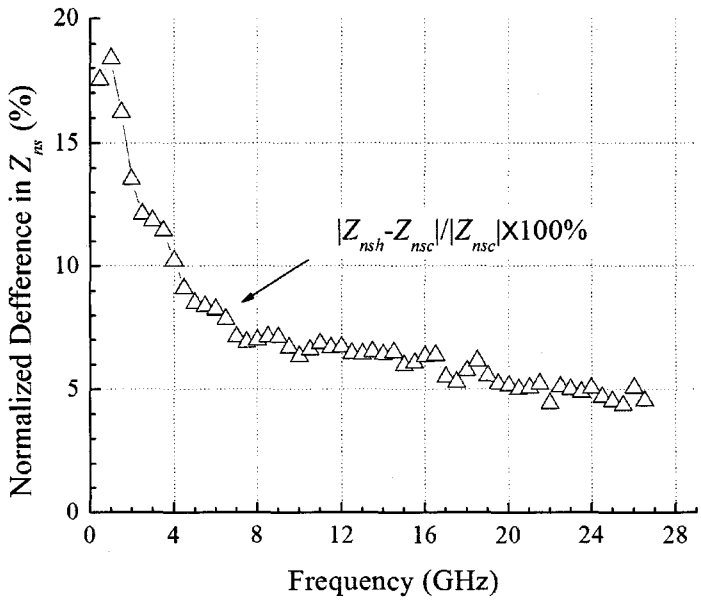

Figure 4-5 - The difference between the noise source impedances in the hot state and the cold state [67].

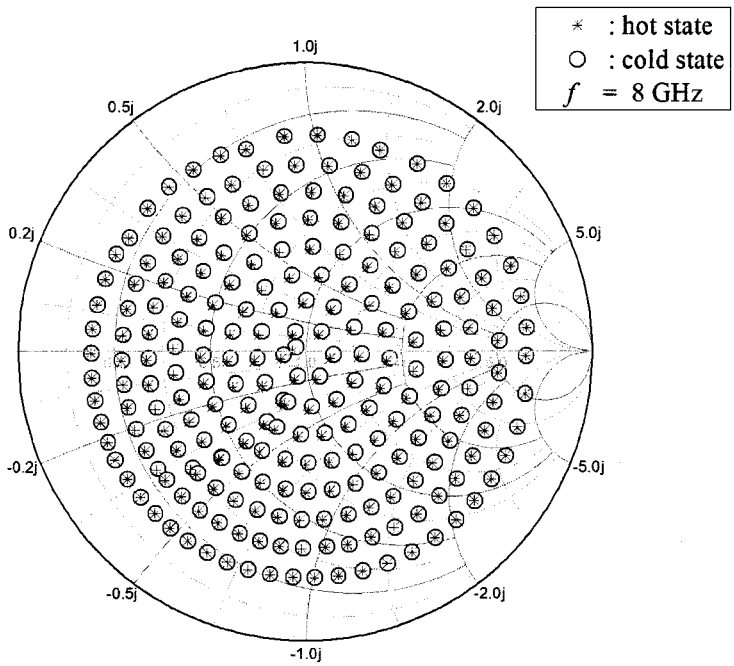

Figure 4-6 - The reflection coefficients seen by the LNA when the DUT is a THRU at 8 GHz [67].

Based on the observation made on Figure 4-6, it can be deduced that a classical method that assumes constant noise source impedance between the hot and the cold states would yield more accurate G_o if the reflection coefficients near the edge of the Smith chart are selected for measurements.

In order to demonstrate the differences between the results obtained from the proposed method and the classical method such as that in [43] and [44], a THRU measurement was made with all the available source tuner positions. The measurement results were used to compute G_o with both methods. Specifically, one G_o was calculated for each source tuner impedance. The order the measurement software followed through all the tuner reflection coefficients is shown in Figure 4-7 - The order of source tuner reflection coefficients the measurement followed through for 8 GHz [67].

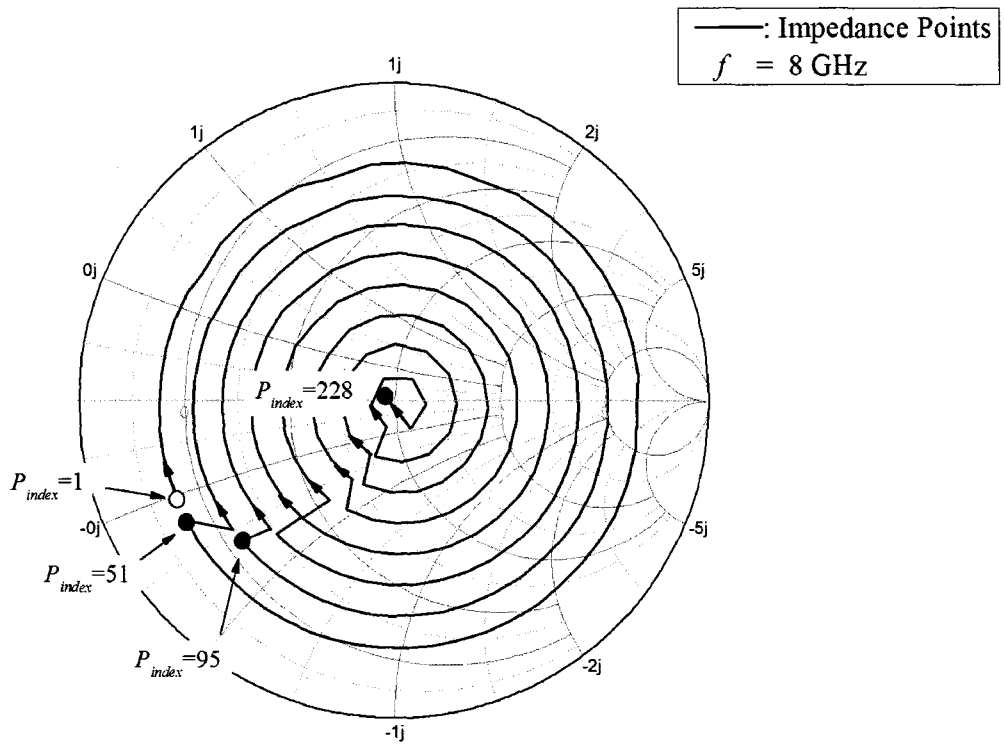

Figure 4-7 - The order of source tuner reflection coefficients the measurement followed through for 8 GHz [67].

The measurement software always starts with a point on the outermost circle and worked its way toward the innermost point. In the case of 8 GHz, 228 tuner positions are available. At other frequencies, the number of terminations used might vary to avoid those that might cause instability. Also the coverage are on the Smith chart might vary at different frequencies for the same source impedances.

The resultant G_o obtained using both methods following this order is plotted in Figure 4-8. The horizontal axis in Figure 4-8 follows the order illustrated in Figure 4-7. The plot shows that there is a systematic fluctuation in the calculated G_o as the reflection coefficient moves toward the centre. The trend is the same for both methods except that the fluctuation is smaller in the proposed method.

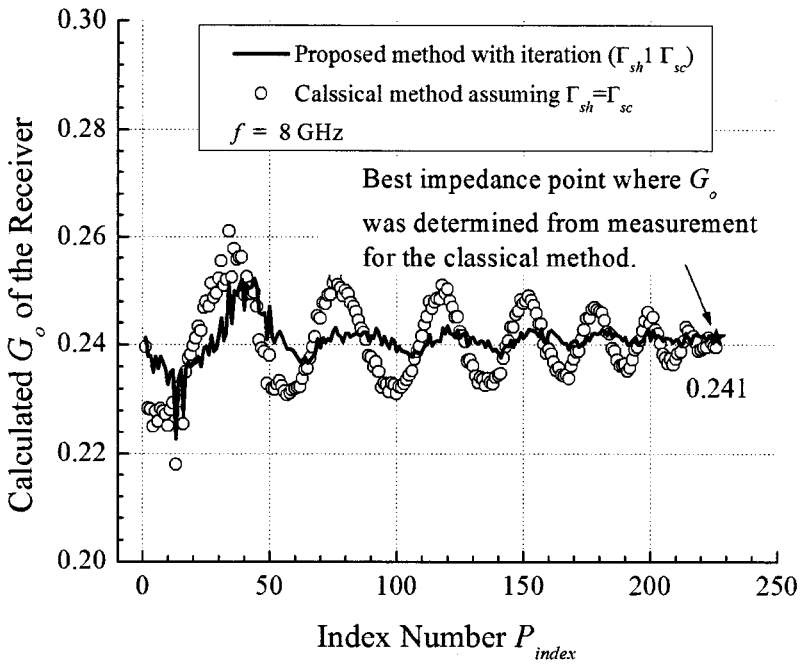

Figure 4-8 - The G_o obtained for all available tuner positions at 8 GHz using the classical method such as that in [43] and [44] and proposed method [67].

However, the proposed method has a smaller error of 2.45% compared to the 8.98% of the classical method. Such improvement can be attributed to the algorithm which takes into account of the different noise source reflection coefficients at different states.

As the tuner reflection coefficient moves toward the centre of the Smith chart, the reflection coefficient of the source tuner's input also decreases and approaches that of the noise source. As the impedance of the noise source is close to 50 Ω, the decreasing input reflection coefficient of the source tuner would mean a trend toward a conjugate match for maximum power transfer. This means more and more of the noise power from the noise source travels through the tuner and eventually reaches the noise receiver. A plot of the measured hot and cold powers of the THRU measurement at 8 GHz is plotted in Figure 4-9.

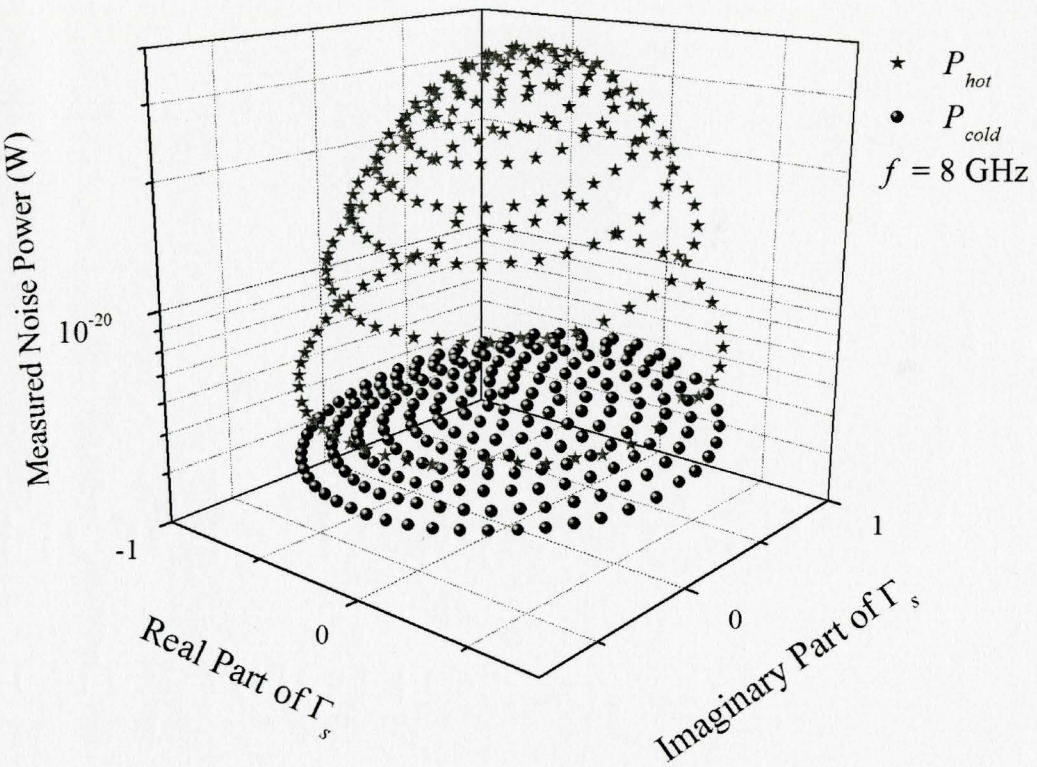

Figure 4-9 - The measured cold and hot powers of a THRU at 8 GHz [67].

As shown in Figure 4-9, the measured hot powers are larger for points near the centre of the Smith chart even though the noise source's power was the same during the measurement. Therefore, the first term in the numerator of equation becomes dominant over the second term, and the terms with t_{seffh} also dominate over the terms with t_{seffc}. This decreases the effect of the difference in the reflection coefficient between the cold and the hot states. Thus it is recommended that these centres points are used for finding G_o of the noise receiver.

Since the proposed method uses an iterative technique to solve for G_o, its efficiency is of interest. A plot showing the value of calculated Go for a tuner point versus the number of iterations is in Figure 4-10.

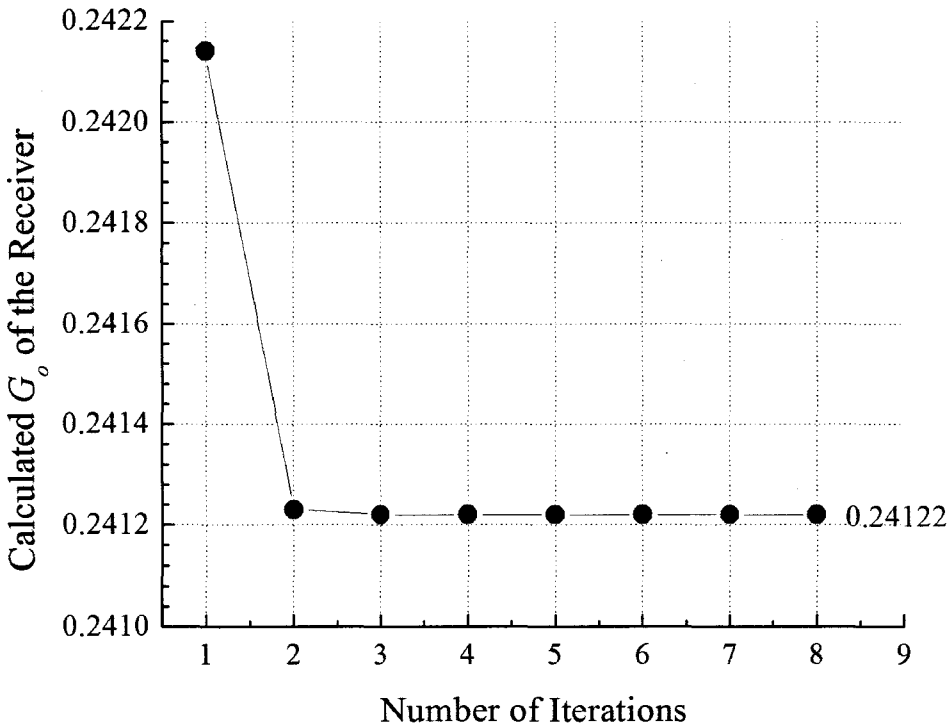

Figure 4-10 - The calculated G_o over iterations using the proposed method [67].

As shown in Figure 4-10, the value of G_o quickly converts after three iterations. This is typical for all frequencies and is, therefore, useful in practice. Also, the high t_{seffh}/t_{seffc} ratio due to the choice of using the centre points for the measurement and computation means the effects of A, B, C, and D in the denominator of equation (4.10) are minimized. This would further contribute to a faster convergence of the iteration procedure.

Once the G_o is obtained, the noise parameters of the noise receiver can be calculated. The extracted noise parameters for 8 GHz were found as F_o = 3.81 dB, R_n = 20.9 Ω, Γ_o = $0.276\angle 117^\circ$, and G_o = -6.18 dB. Using this set of results, the cold and hot power were simulated and plotted with the measured powers in Figure 4-11 and Figure 4-12. The two figures show a good match between the simulated noise power and the measured noise power at 8 GHz.

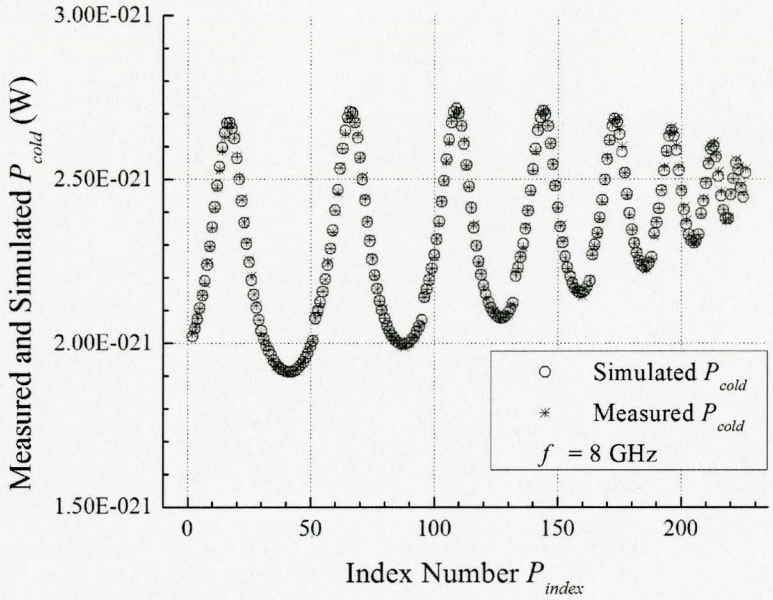

Figure 4-11 - The measured and simulated cold power of the THRU measurement at 8 GHz [67].

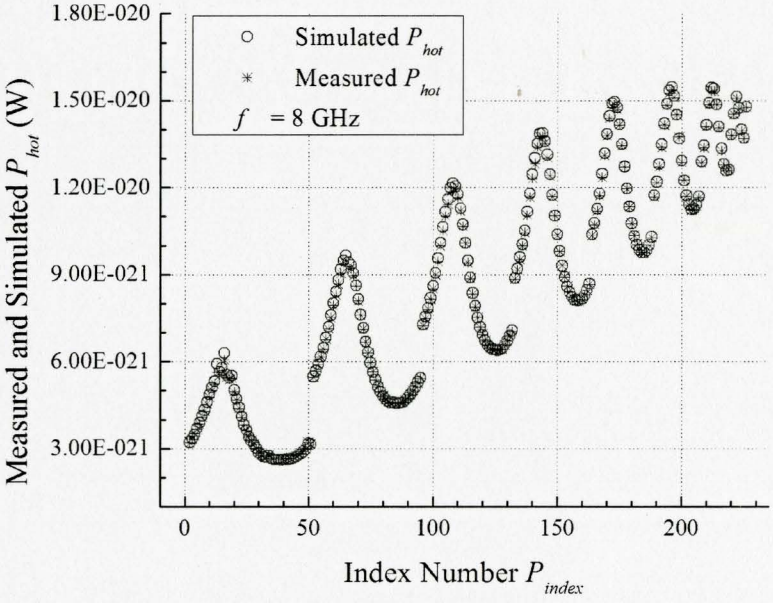

Figure 4-12 - The measured and simulated hot power of the THRU measurement at 8 GHz [67].

For completeness, the receiver noise parameters and the G_o calculated using both the classical method and the proposed method over the frequency range of interest are listed in Table 4.1.

Table 4.1 – The receiver noise parameters and G_o of the measurement system calculated using the proposed method and the classical method at 8 GHz [67].

f (GHz)	F_o (dB)	R_n (Ω)	$\lvert\Gamma_o\rvert$	$\angle\Gamma_o$ (°)	G_o (dB)
4	3.7 (3.69)	22.6 (22.6)	0.111 (0.111)	90.8 (90.8)	-3.95 (-3.93)
6	4.07 (4.12)	35.6 (36.0)	0.189 (0.189)	-33.9 (-33.9)	-5.16 (-5.21)
8	3.81 (3.84)	20.9 (21.0)	0.276 (0.276)	117 (117)	-6.18 (-6.21)
10	3.64 (3.60)	31.8 (31.5)	0.370 (0.370)	-80.9 (-80.9)	-8.00 (-7.96)
12	3.61 (3.56)	27.6 (27.2)	0.297 (0.297)	85.3 (85.3)	-9.11 (-9.05)
14	3.66 (3.67)	23.6 (23.6)	0.202 (0.202)	-93.4 (-93.4)	-10.1 (-10.1)
16	3.59 (3.56)	24.1 (23.9)	0.093 (0.093)	65.5 (65.5)	-10.4 (-10.4)
18	3.66 (3.67)	22.5 (22.5)	0.038 (0.038)	92.7 (92.7)	-10.5 (-10.5)
20	3.78 (3.81)	22.6 (22.7)	0.178 (0.178)	-107 (107)	-12.7 (-12.7)
22	3.69 (3.69)	37.9 (37.8)	0.347 (0.347)	61.4 (61.4)	-13.9 (-13.9)
24	3.77 (3.76)	20.9 (20.8)	0.419 (0.419)	-124 (-124)	-12.7 (-12.7)
26	4.25 (4.25)	43.8 (43.7)	0.307 (0.307)	57.0 (57.0)	-13.2 (-13.2)

In Table 4.1, the values in brackets are those obtained using the classical method. The noise parameter extractions were done for the frequencies listed in the table. As suggested previously, the measurements for tuner reflection coefficients near the centre of the Smith chart were used for the extraction calculation. As implied in Figure 4-8,

using the tuner points near the centre ultimately yields very similar results for both the proposed method and the classical method because the G_o's were similar. It should be noted that all G_o's are less than 0 dB. Such a result can be attributed to the loss in the cables and the other components in the path between the noise source and the NFA.

Once the system calibration is finished, the THRU is replaced by the DUT for measurements. The DUT used was an n-type MOSFET with a geometry of W/L = 128x1μm / 90 nm terminated with probe pads. It was fabricated with a standard 90 nm CMOS technology. The bias was set to V_{GS} = 1.0 V and V_{DS} = 0.8 V. Now the noise reference plane was moved to the input of the DUT, or plane A in Figure 4-1, the new noise correlation matrix $[C_A^A]$ was calculated using the same procedure described previously for each frequency. Finally, the correlation matrix of the DUT and thus its noise parameters were calculated using equations (4.13) to (4.16).

The resultant noise parameters of the DUT with pads versus frequencies are plotted in Figure 4-13 to Figure 4-16.

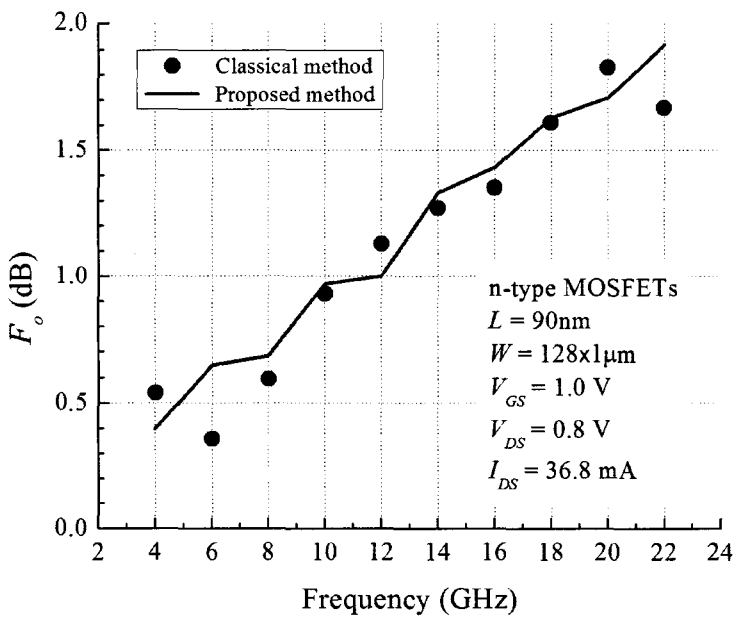

Figure 4-13 - The extracted F_o of the DUT over the frequency range of interest [67].

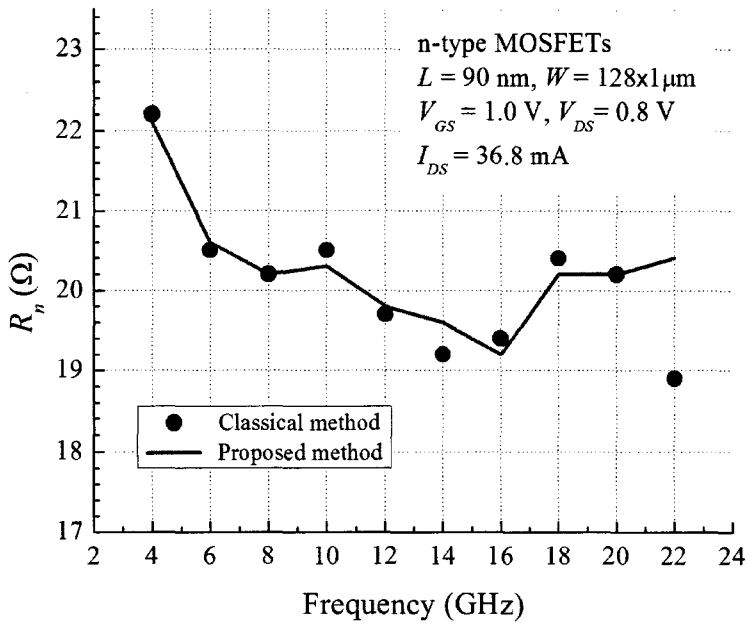

Figure 4-14 - The extracted R_n of the DUT over the frequency range of interest [67].

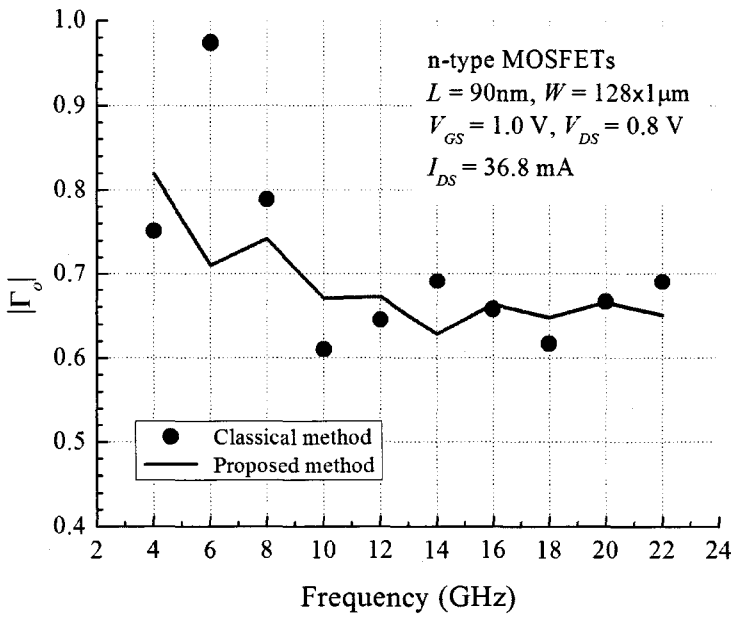

Figure 4-15 - The extracted Γ_o's magnitude of the DUT over the frequency range of interest [67].

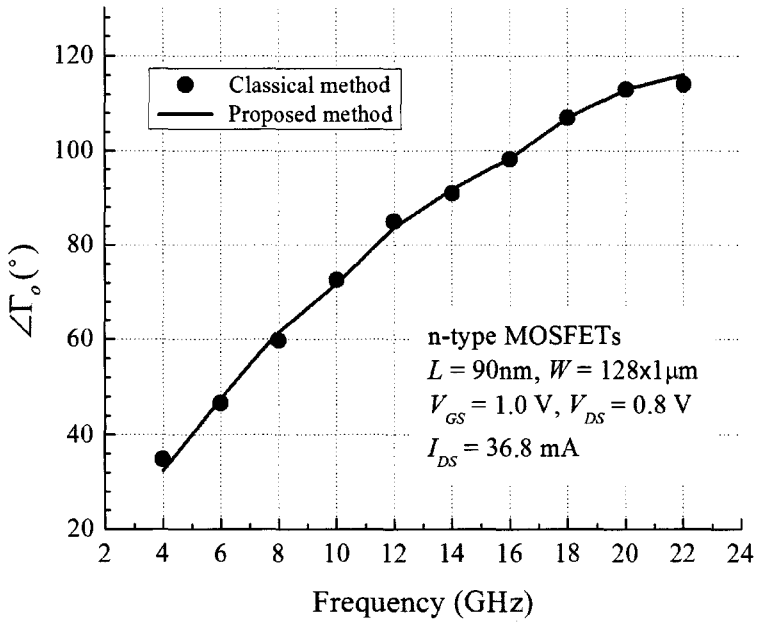

Figure 4-16 - The extracted Γ_o's angle of the DUT over the frequency range of interest [67].

In Figure 4-13, it can be seen that the result obtained using the proposed method exhibits a smoother trend as F_o increases with frequencies, as is what is known to happen for a MOSFET. Less erratic trends are also found in R_n and $|\Gamma_o|$ for the proposed method. The less smooth trend of the classical method can be explained in the difference in G_o between the calibration stage and the measurement stage. At 6 GHz, the G_o of the receiver during the calibration stage is -5.16 dB while the G_o during the measurement stage is 6.05 dB. The larger gain results from the inclusion of the active DUT in the noise receiver during the measurement stage. Therefore, without taking into account of the difference in the noise source impedance, the large G_o would help produce less accurate result.

In summary, the proposed noise receiver characterization method could take into account of the impedance difference of the noise source between its hot and cold states. The method has been applied to extract the noise parameters of the noise receiver of the measurement system and those of a DUT. The results show nicer trends over those obtained using the classical method.

Chapter 5: IMPROVEMENTS ON SOURCE IMPEDANCE SELECTION TECHNIQUE AND UNCERTAINTY ANALYSES

In Chapter 3, several different source impedance selection criteria were described. Depending on the formulation of the noise parameter extraction techniques, different and even contradicting conclusions were drawn as to where the best candidates of source impedances are. In this chapter, a different approach is proposed to evaluate the available source impedances for noise measurement. In particular, a Monte Carlo simulation, which previously was primarily used to simulate a measurement to provide uncertainty data, is used to determine the goodness of a source impedance from the VNA's perspective.

Once the noise parameters have been extracted, a Monte Carlo simulation is again used to calculate the uncertainties associated with each extracted noise parameter. The simulation also takes into account of the VNA's source- and frequency-dependent uncertainties and provides the uncertainty of the extracted noise parameters.

To implement and demonstrate the proposed improvements, Engen's noise measurement and noise parameter extraction technique described in Section 2.4.3 is used. The method was originally intended to be used to characterize packaged devices that have matched terminal impedances. Therefore, the method does not take into consideration the mismatches at the input and output in the case of an on-wafer DUT. In this study, the method is adapted for on-wafer measurements. The modified Engen's method incorporated with the proposed improvements are described and the measurement results are analyzed in this chapter.

5.1 Improved Noise Receiver Characterization by Γ_s Optimization

The first step of the measurement is always the system calibration. Different from the original method, the proposed noise receiver characterization method described in the

last chapter is used. In Figure 4-8, the G_o's obtained using both the classical method and the proposed iterative method have been plotted in the order in which the source reflection coefficients were used. The plot showed that by taking into account the difference in the noise source impedance between its hot and cold states, more accurate G_o could be obtained. However, since G_o is supposed to be a constant and source-independent value intrinsic to the noise receiver at a certain frequency, the systematic ripples seen in the figure need to be addressed.

In Figure 5-1, the fluctuations in the G_o is again demonstrated at 6 GHz.

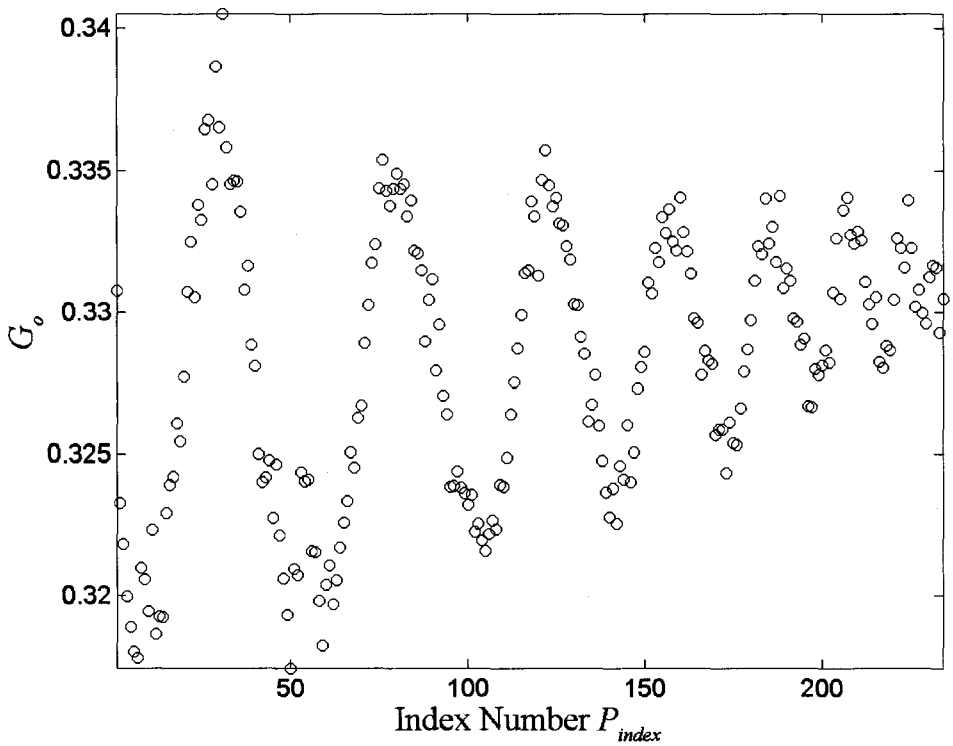

Figure 5-1 - The G_o obtained using the proposed method before the iteration for 6 GHz.

The G_o's in the figure are calculated using (4.10) and have not gone through the iteration step. It has been found that the error in G_o is primarily caused by the inaccuracy in the measured noise source reflection coefficients. To illustrate this observation, a meshgrid of Γ_{sh} around the measured Γ_{sh} of the noise source is created and equation (4.10) is used to calculate the G_o for the 234 source tuner impedances available for the measurement at

6 GHz. The calculation provides 234 roughly-calculated G_o for every Γ_{sh} on the meshgrid. As G_o is a constant, the criterion to evaluate Γ_{sh} is the standard deviation of its 234 G_o. The standard deviation σ is then calculated for each Γ_{sh} and plotted over the Smith chart. The result for 6 GHz is plotted in Figure 5-2 and Figure 5-3. In Figure 5-2, a small area of the meshgrid of Γ_{sh} was chosen to be around the measured Γ_{sh}. It can be seen that σ of the 234 G_o's obtained using the measured Γ_{sh} is not the minimum value. Using a meshgrid of Γ_{sh} that covers the entire Smith chart, σ increases quickly as the Γ_{sh} moves further away from the measured Γ_{sh}. Therefore, an optimization algorithm is required to find the optimal Γ_{sh} and thus reduce the fluctuation in Figure 5-1. This optimal value would allow a more accurate determination of the true G_o. Figure 5-3 shows the calculated standard deviations for Γ_{sh}'s covering a larger portion of the Smith chart.

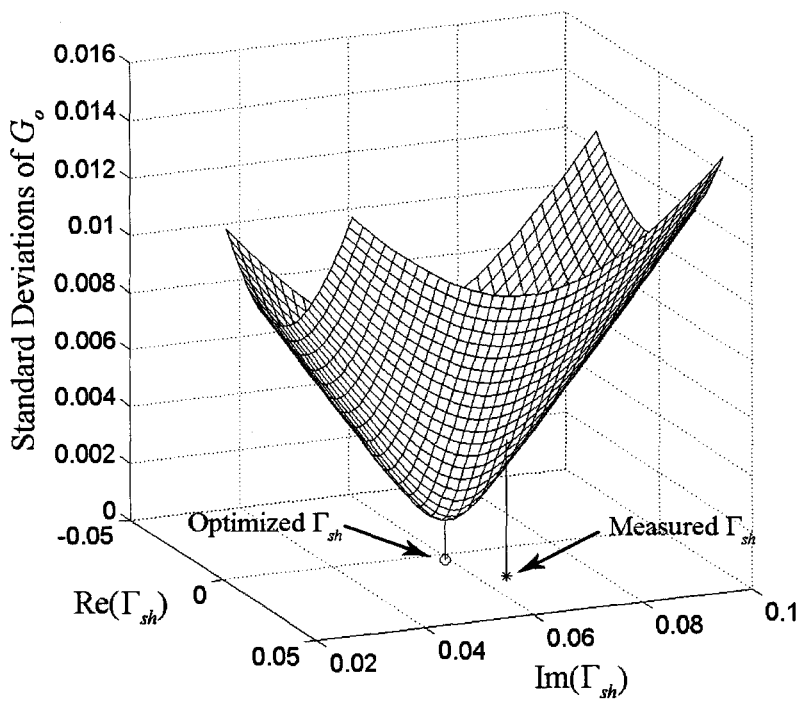

Figure 5-2 - The standard deviations of G_o's obtained using a meshgrid of Γ_{sh}.

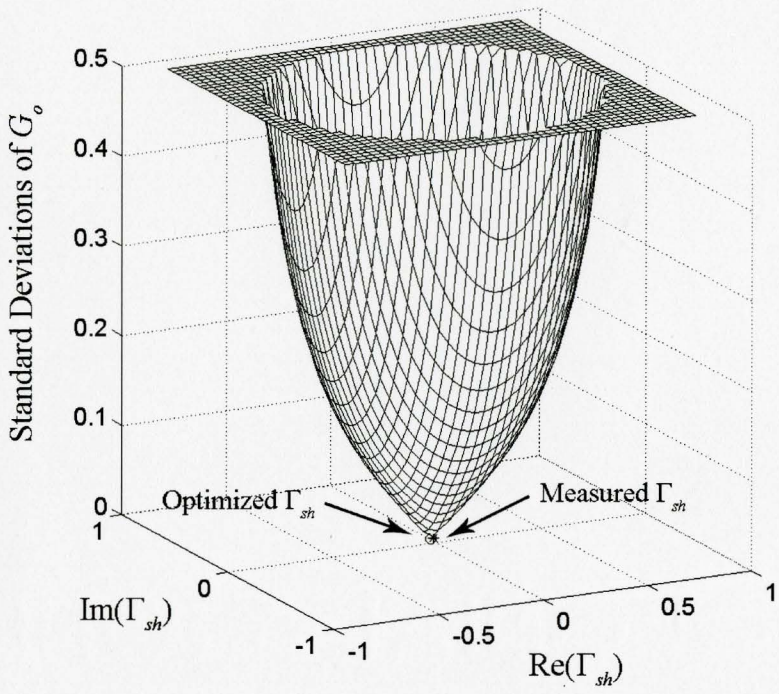

Figure 5-3 - The standard deviations of G_o's obtained using a meshgrid of Γ_{sh} covering a larger area.

To find the optimized Γ_{sh}, the σ's for the measured Γ_{sh} and several Γ's at a certain distance around the measured Γ_{sh} are first calculated. If the minimum σ of the surrounding Γ's is smaller than that of the measured Γ_{sh}, it becomes the new "best σ," and its Γ becomes the best Γ_{sh}. Then the optimization continues in the direction of the best Γ_{sh} and picks one Γ_{sh} along the path. The new Γ_{sh}'s σ is calculated and compared to that of the previously best σ. If the new σ is smaller, the optimization continues along the same direction. Otherwise, several neighbouring Γ_{sh}'s are again chosen for evaluation in order to determine a new optimization path. Finally, when the neighbouring Γ_{sh}'s all yields larger σ's than the σ of the Γ_{sh} in their centre, the centre Γ_{sh} is deemed the optimized Γ_{sh}.

The optimized Γ_{sh} found for the data in Figure 5-1 is labelled in Figure 5-2 along with the Γ_{sh} from the measurement. It can be seen that the optimization found the optimal Γ_{sh}. For comparison, the receiver gain obtained using the optimized Γ_{sh} is plotted with respect to the ordered source impedances in Figure 5-4. Comparing Figure 5-1 and

Figure 5-4, which are plotted using the same scale for the Y-axis, it can be seen that the system ripples present before are no longer apparent. Thus it can be concluded that the error in the measured Γ_{sh} did cause the systematic errors in the calculated G_o.

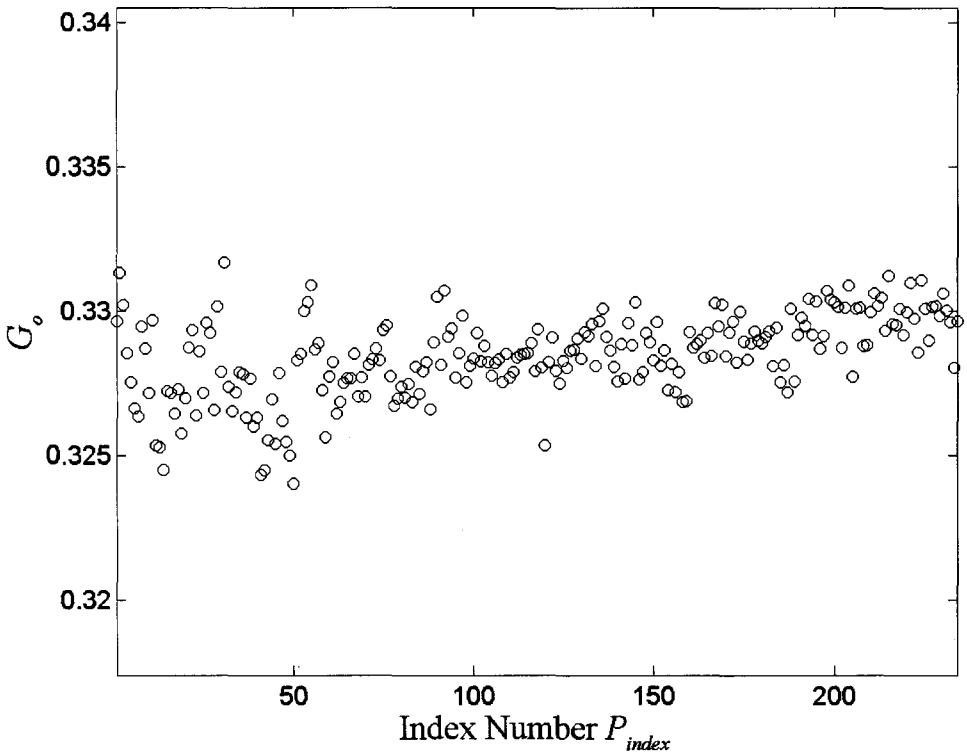

Figure 5-4 - The G_o obtained using the optimized Γ_{sh} before the iteration for 6 GHz.

The 3D plots are shown in Figure 5-5 and Figure 5-6. Figure 5-5 and Figure 5-6 are plotted using the same scale for Z-axis. As can be seen in Figure 5-5, the receiver gain initially exhibits a strong dependence on the source reflection coefficient. With the optimized Γ_{sh}, the receiver gains obtained using different source impedances now look more source-independent over the Smith chart as they should be.

Graphs similar to Figure 5-1 and Figure 5-4 are plotted for the measurement data for 24 GHz.

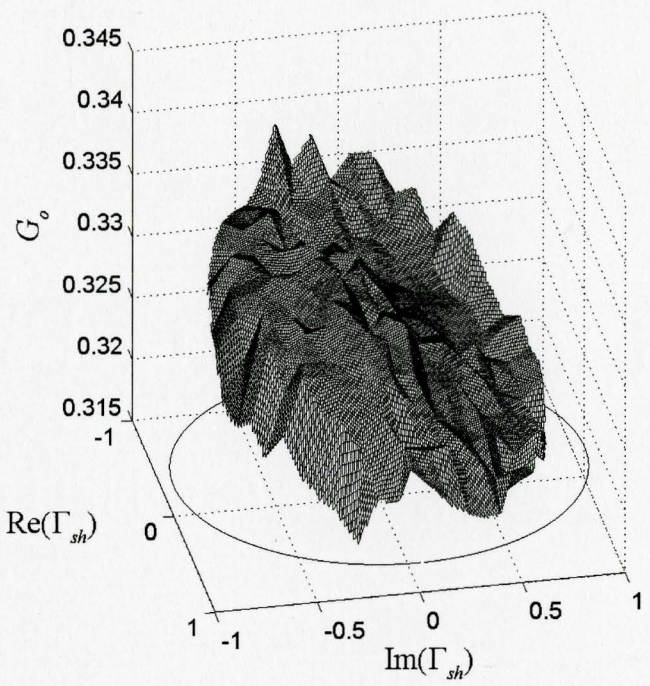

Figure 5-5 - 3D plot of the G_o obtained using the measured Γ_{sh} before the iteration for 6 GHz

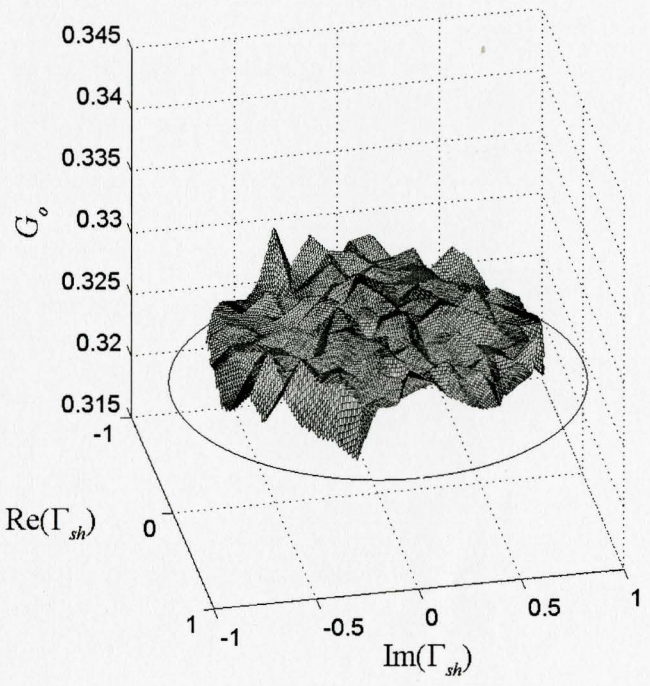

Figure 5-6 - 3D plot of the G_o obtained using the optimized Γ_{sh} before the iteration for 6 GHz.

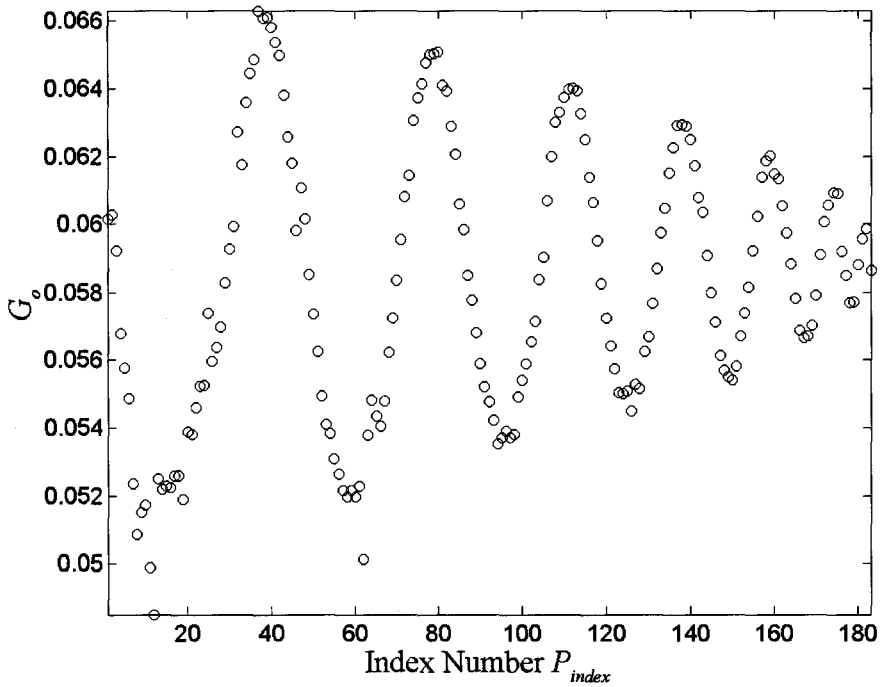

Figure 5-7 - G_o obtained using the measured Γ_{sh} before the iteration for 24 GHz.

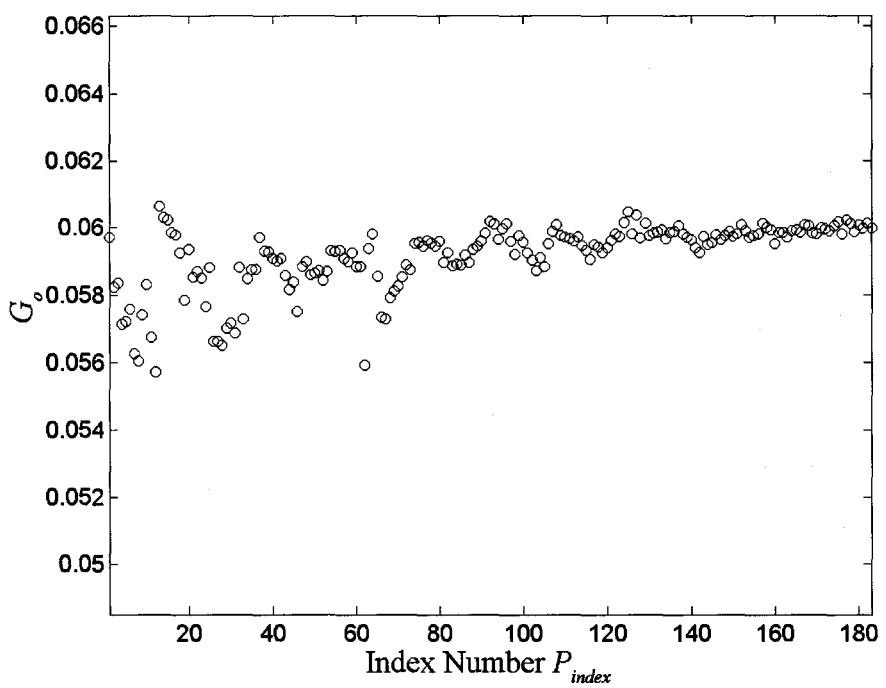

Figure 5-8 - The G_o obtained using the optimized Γ_{sh} before the iteration for 24 GHz.

It should be noted that in Figure 5-8 that, unlike Figure 5-4, there is obvious rippling again even after the optimized Γ_{sh} is used instead of the measured value. This can be explained by examining equation (4.10), which is repeated here.

$$G_o = \frac{1}{kT_o\Delta f\left(t_{seffh}G_{sh} - t_{seffc}G_{sc}\right)} \cdot \left(P_h G_{sh} \frac{\left|1-\Gamma_{inr}\Gamma_{sh}\right|^2}{1-\left|\Gamma_{sh}\right|^2} - P_c G_{sc} \frac{\left|1-\Gamma_{inr}\Gamma_{sc}\right|^2}{1-\left|\Gamma_{sc}\right|^2} \right). \quad (5.1)$$

As the frequency increases, the attenuation of the source tuner gradually increases for all impedances. Its transducer gains' magnitudes at 6 GHz and 24 GHz are plotted in Figure 5-9.

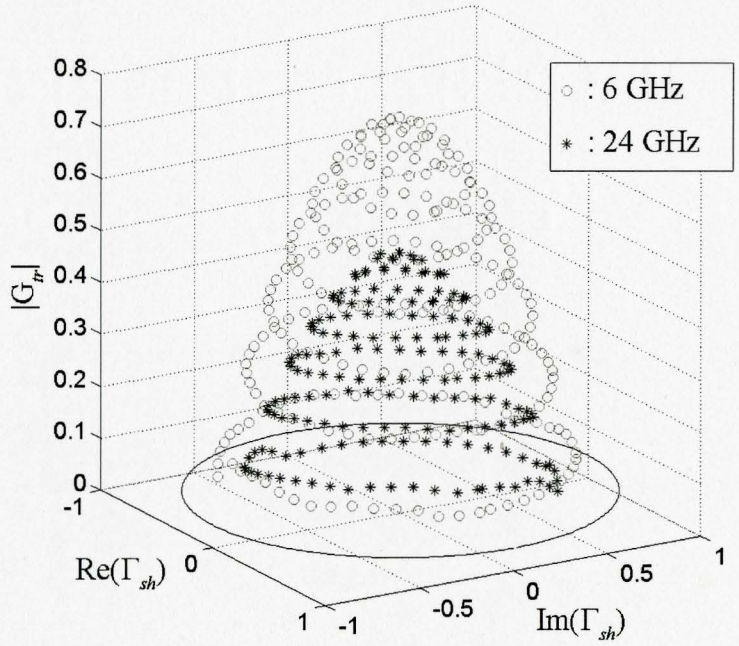

Figure 5-9 - The magnitude of the transducer gain of the source tuner at 6 GHz and 24 GHz.

As shown in Figure 5-9, the transducer gain of the source tuner is generally larger at 6 GHz than that at 24 GHz. As a result, more noise power is transmitted to the noise receiver at 6 GHz than at 24 GHz. This effect in the measured noise powers can be seen in Figure 5-10.

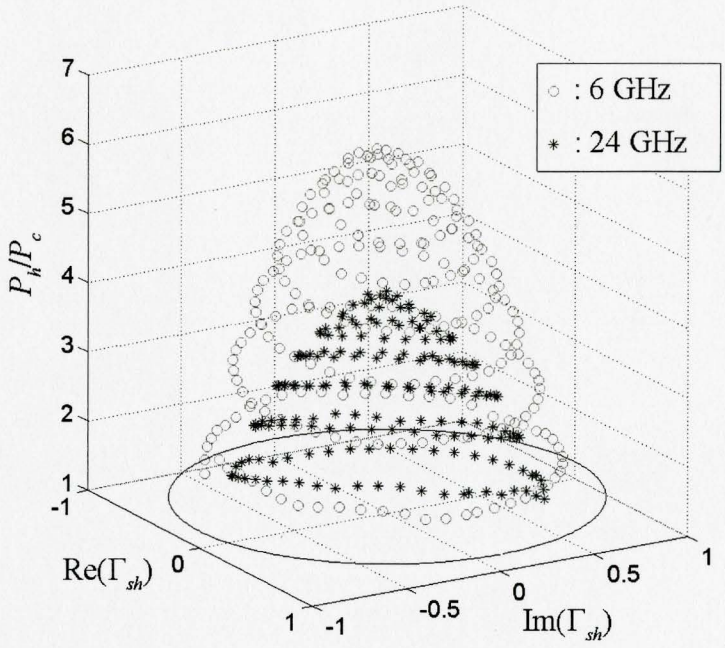

Figure 5-10 - The measured hot power to the cold power ratio at 6 GHz and 24 GHz.

Figure 5-10 shows the ratio of the measured hot noise power to the measured cold noise power. It is clear that at 24 GHz, the measured hot power and the measured cold power are a lot closer and more comparable than in the case of 6 GHz. Therefore, in equation (5.1), while the P_c term in the numerator has little effect on G_o at 6 GHz, it is not the case at 24 GHz. This observation suggests that another optimization to find the ideal Γ_{sc} is necessary to obtain a more constant G_o at higher frequencies.

So far the analyses regarding the accuracy of G_o made use of all the available source tuner impedances for all frequencies of interest. However, it would be impractical to do so many measurements for each frequency as it is very time consuming. In practice, only a handful of source impedances would be used. As described in the previous section, the proposed method only needs a minimum of five impedances. Therefore, it is important to be able to tell which ones are likely to yield the most accurate result. According to the evidences so far, once the optimized reflection coefficients of the noise source are obtained, the G_o's obtained for the various source impedances eventually converge to the values obtained using the few centre points as

shown in Figure 5-1, Figure 5-4, Figure 5-7, and Figure 5-8. Thus it would seem reasonable to use the few centre reflection coefficients for the G_o measurement and find the optimized Γ_{sh}, Γ_{sc}, and G_o.

It should be noted that the conclusion reached in this section does not take into account the uncertainties from other sources such as the measurement instruments. In the next section, these uncertainties' effect on the measurement result is examined.

5.2 Improved Source Impedance Selection Technique

Once the noise receiver, which includes the LNA and every component behind it, has been characterized using the technique described in the previous section, the transducer gain of the noise receiver, G_{tr}, can be found using equation (4.2). Knowing the transducer gain, the available noise power of the rest of the system at the input plane of the LNA can be calculated from the measured noise power. This is required for the following steps to find the reverse noise temperature, T_{rev}, and β of the DUT as defined in Section 2.4.3.

The DUT used is a 65 nm n-type MOSFET. In order to find T_{rev}, and β, a reverse DUT measurement and a forward measurement are necessary. For each measurement, a group of source impedances need to be selected. The studies on impedance selection criteria described so far in Section 3.2 provided different suggestions derived based on different assumptions. Their conclusions were supported by general simulations loosely based on a real measurement setup. In this section, a different impedance selection technique is proposed. The proposed technique applies a Monte Carlo simulation on the reflection coefficient seen by the input of the DUT. More specifically, the uncertainties associated with the VNA discussed in Section 3.1 are calculated and applied to all the transmission and reflection measurements of the VNA. These uncertainties depend on the specific VNA used, the measurement frequency, the calibration method, the calibration standards used, the actual measurement values of the transmission or the reflection coefficient property, and other factors specific to the particular instrument setup that are provided by the manufacturer of the device. The connector repeatability and the cable stability stay the same throughout a measurement and are difficult to quantify, and thus are neglected. The uncertainty in the noise figure metre measurement

is also neglected because the noise parameter extraction method used here does not require noise figure measurements but only the measured noise powers provided by the NFA. Unfortunately, the manufacturer could not provide any information on the uncertainty of the NFA's power measurement.

The uncertainties associated with the VNA can be easily calculated using Agilent's Vector Network Analyzer Uncertainty Calculator [69], which accounts for the residual errors of the system calibration. The uncertainties it provides are 3-sigma values, which cover 99.7 % of the cases, and are listed in Appendix A. Normally distributed random errors are then generated using these values for all measurement quantities including all the *S* parameters and reflection coefficients. The simulated errors are added to the measurement quantities, which are treated as the "true values". A large number of samples are created and treated as sets of measurement values. In the end Γ_s's, the corresponding reflection coefficients looking into the source tuner's output, are calculated using the generated measurement data. The deviation of each of the 1000 generated Γ_s's from their corresponding "true" Γ_s is then calculated and averaged. The averages for all the source impedances are compared. The source impedances with the smallest deviations in the generated Γ_s's would be the most suitable ones for measurements as they produce the least uncertainties in their VNA measurements.

Using the Monte Carlo simulation technique described here, the averaged error of each 1000 sets of generated Γ_s's from their corresponding true Γ_s is plotted with respect to all "true Γ_s's" using a THRU measurement data in Figure 5-11. The data used to plot the figure were obtained at 6 GHz. As can be observed in Appendix A, the lower the frequency, the smaller the uncertainty. In the figure, the circles mark actual data points the Monte Carlo simulation yielded. The surface is an extrapolation of the data points and roughly forms a bowl except for the bottom portion, which is more irregular.

Figure 5-11 suggests that the source reflection coefficients around the edge of the Smith chart would produce relatively more error if used for measurements. This observation agrees with the observation made in the previous section that the receiver gains resulted from the centre source reflection coefficients are where the rest of G_o's converge to after the optimization. This now can be explained in part by the smaller uncertainties the VNA experiences with these centre reflection coefficients.

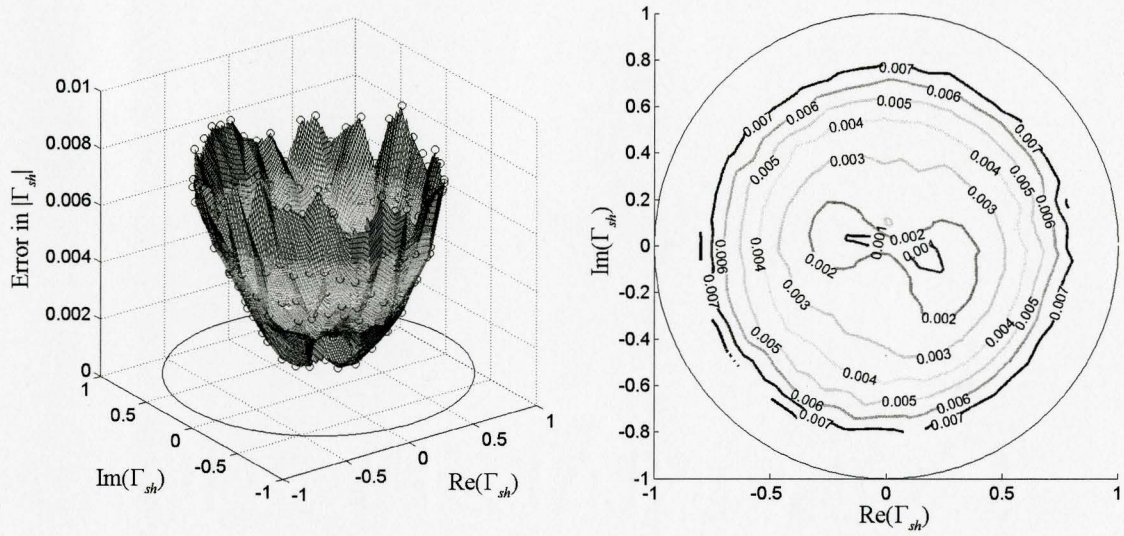

a) b)

Figure 5-11 - Averaged errors in $|\Gamma_{sh}|$ at 6 GHz obtained through a Monte Carlo simulation shown in a) 3D and as b) contours.

With the simulation result, the source impedances can be ranked according to the degree of uncertainty a particular impedance exhibits. Using the ranking, the available source impedances are divided into groups of five in the ranked order. Each group of five impedances are then used to calculate G_o. The results for 4 GHz and 24 GHz are plotted in Figure 5-12. In the figure, the X-axis is the group numbers ranked according to the selection criterion described above with Group 1 being the best source impedances.

As can be observed in the figure, as the source impedances used to calculate G_o become worse according to the selection criterion, it becomes easier to obtained erratic results. The calculated G_o values exhibit such a trend throughout the range of measurement frequencies. This indicates that the calculation results for those impedances likely have greater errors because of less accurate de-embedding caused by input terminations with greater uncertainties.

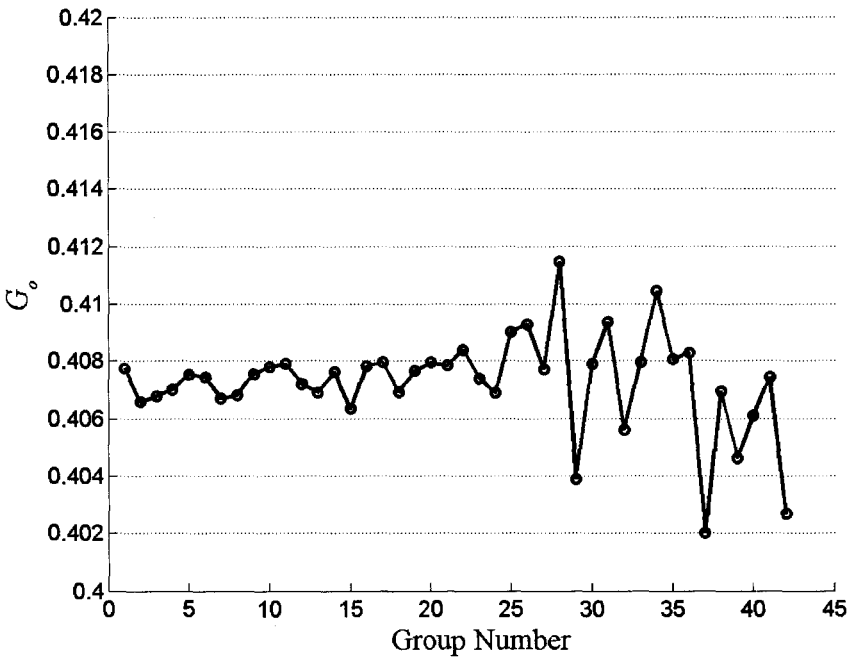

a)

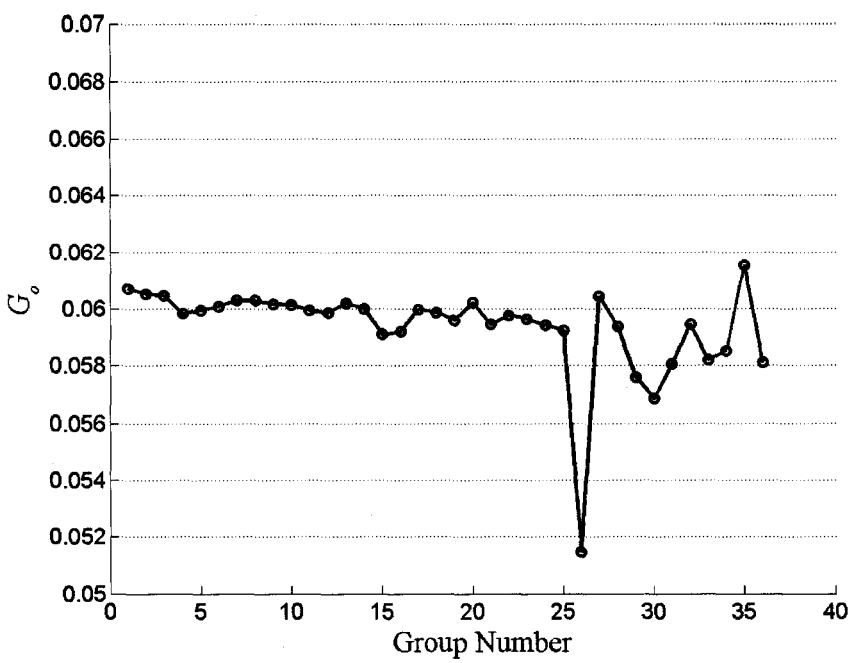

b)

Figure 5-12 – The G_o values calculated using different groups source terminations ranked according to the proposed selection criterion at a) 4 GHz and b) 24 GHz.

The next step in the extraction procedure is finding T_{rev}. T_{rev} is the reverse noise temperature defined as

$$T_{rev} = \frac{\overline{|c_1|^2}}{1-|S_{11}|^2}, \tag{5.2}$$

where c_1 again is the internal noise source of the input port of the DUT. A cold reverse measurement of the DUT is required by Engen's method to extract T_{rev}. In this configuration, the available noise temperature at Port 2 (the DUT's input) is written as

$$T_{out,2} = T_{rev} + A_{21}T_c, \tag{5.3}$$

where A_{21} is the reverse available power gain of the DUT and T_c is the noise temperature of the network connected to the DUT at Port 1.

The method assumes that the DUT is a very unilateral amplifier so that A_{21} is very small, which in turn makes T_c negligible. Thus T_{rev} would approximately equal $T_{out,2}$, which can be derived from the measurement data. Also, a small A_{21} means that little of whatever noise reflected back from the source termination would travel back through the DUT to Port 2.

To determine if the assumption is true for the DUT, its S_{21} is plotted over the measurement frequencies in Figure 5-13. As shown in the figure, the magnitudes of S_{21} at the measurement frequencies are all less than 0.1. This means the reverse transmission of the DUT is weak. The available power gain of the reversed DUT, which is also source-dependent, can be calculated as

$$A_{21} = \frac{1-|\Gamma_s|^2}{|1-S_{11}\Gamma_s|^2}|S_{21}|\frac{1}{1-|\Gamma_{out}|^2}, \tag{5.4}$$

where Γ_{out} is the reflection coefficient of the output of the reverse DUT. The calculated available power gains for all available Γ_s's at 6 GHz and 24 GHz are plotted in Figure 5-14.

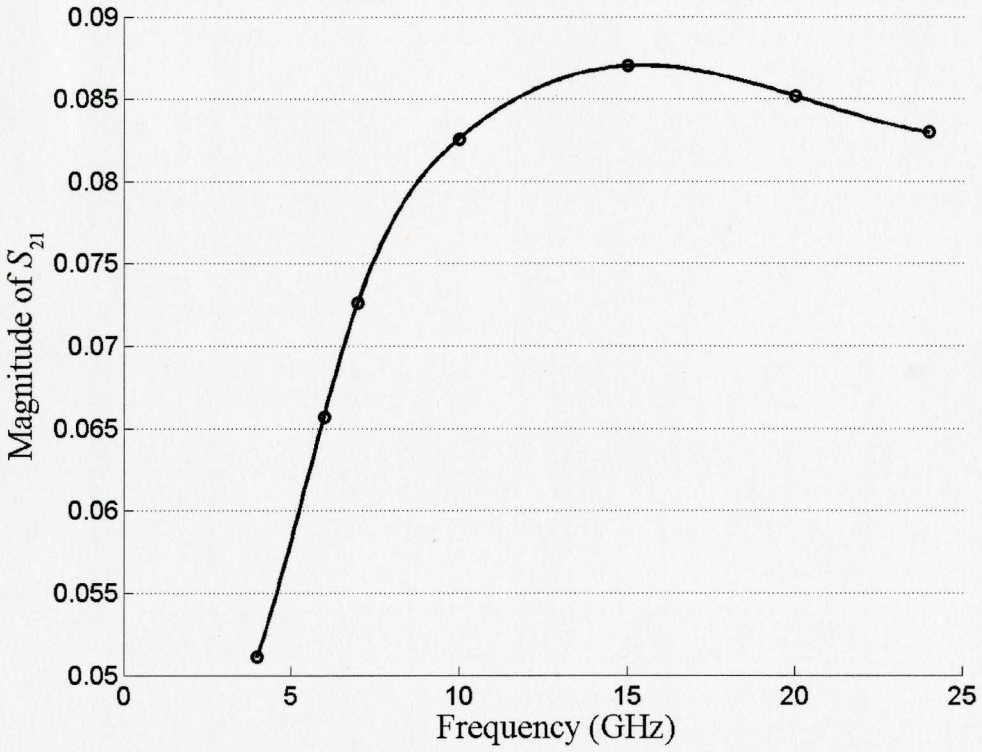

Figure 5-13 – The $|S_{21}|$ of the reversed DUT.

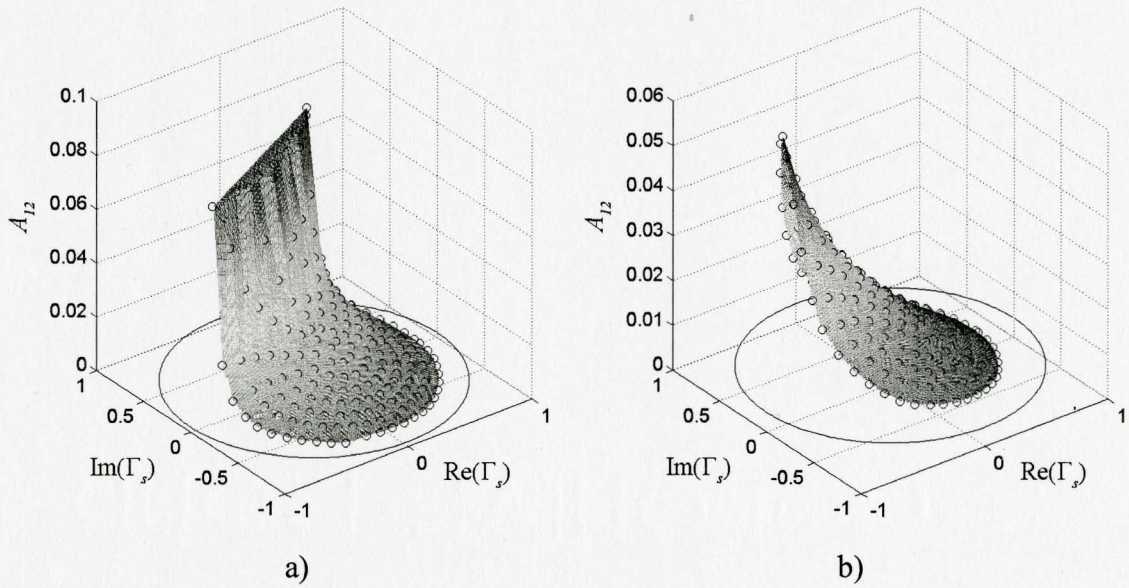

a) b)

Figure 5-14 - The reverse available power gains of the DUT at a) 6 GHz and b) 24 GHz.

In Figure 5-14, the circles mark the available power gains of the source reflection coefficients used on the Smith chart. As shown in the figure, other than the few points near the top left portion for 6 GHz and the left part for 24 GHz, most points yield fairly small available power gains. These points with high A_{12} are the ones near the input stability circle, on which a Γ_s would yield a $|\Gamma_{out}| = 1$. In this case, a Γ_s falling inside the circle would result in a $|\Gamma_{out}| > 1$ and thus creates oscillations. For this reason, the unstable points are not used in measurements.

The other requirement of Engen's method is that the source reflection coefficient is minimal, so the reflection back to the DUT at Port 1 is ideally zero. This means using Γ_s's near the centre of the Smith chart to satisfy the requirement. With the two requirements satisfied, Engen argued that the T_{rev} is approximately equal to $T_{av,2}$, which can be calculated from the measured noise power using the previously obtained transducer power gain of the noise receiver. Using (4.2) and (4.4), T_{rev} can be calculated as

$$T_{rev} = \left(\frac{P_n - P_{rec}}{k \cdot G_{tr}} - T_c \right) / G_{av,tun2} + T_c , \tag{5.5}$$

where

P_n = the measured noise power,

P_{rec} = is the noise power contributed by the noise receiver,

k = the Boltzmann's constant,

$G_{av,tun2}$ = the available power gain of the load tuner as a THRU, and

T_c = the ambient temperature.

Particularly, P_{rec} can be calculated using (4.7) with the noise receiver's transducer gain as

$$P_{rec} = \frac{kT_o \Delta f}{G_s} \cdot \frac{1 - |\Gamma_s|^2}{|1 - \Gamma_{inr}\Gamma_s|} \cdot G_o \left[R_u \left(|Y_s|^2 + |Y_{cor}|^2 + 2G_{cor}G_s + 2B_{cor}B_s \right) + G_{iun} \right], \tag{5.6}$$

where the term with the effective noise temperature contributed by the noise source has been removed. In words, (5.5) yields T_{rev} by first removing the noise power of the receiver from the measured noise power before referring the resulting power back to the reversed DUT's output plane.

The calculations above yield one T_{rev} value for every source termination. The results are plotted in Figure 5-15.

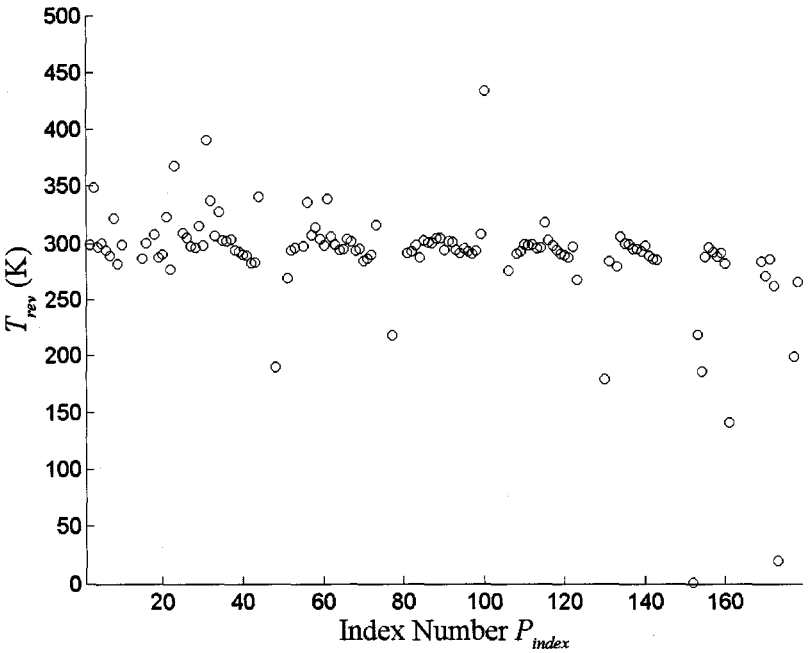
500
450
400
350
300
250
200
150
100
50
0
T_{rev} (K)
20
40
60
80
100
120
140
160
Index Number P_{index}

a)

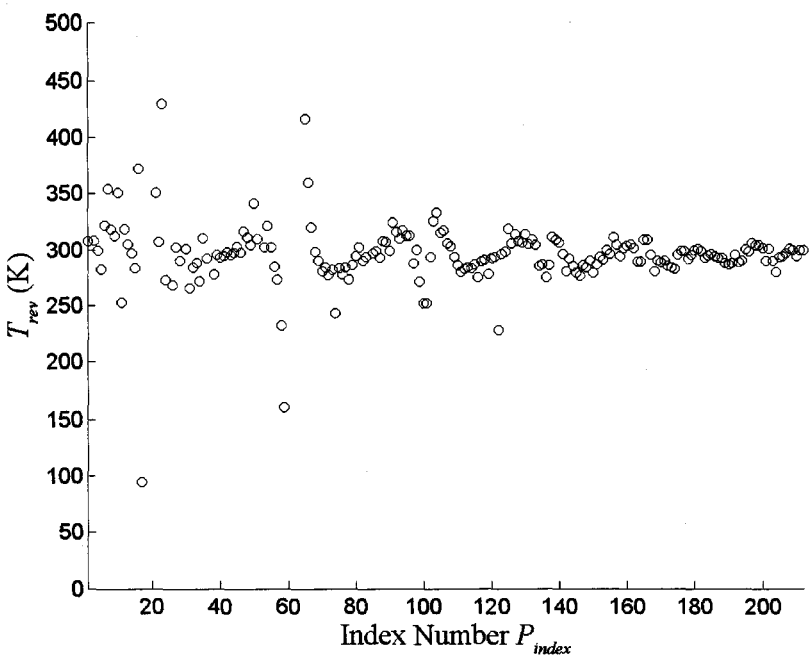
500
450
400
350
300
250
200
150
100
50
0
T_{rev} (K)
20
40
60
80
100
120
140
160
180
200
Index Number P_{index}

b)

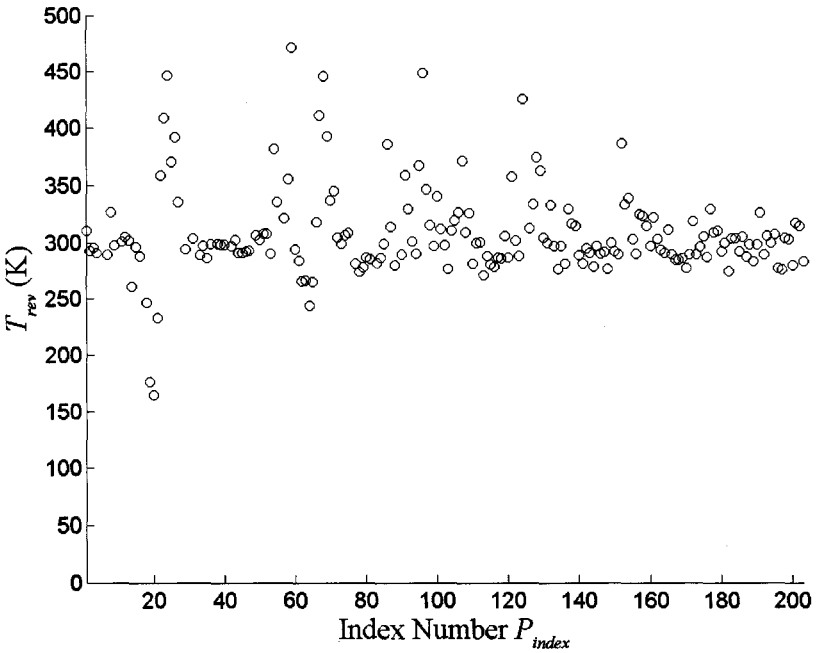

c)

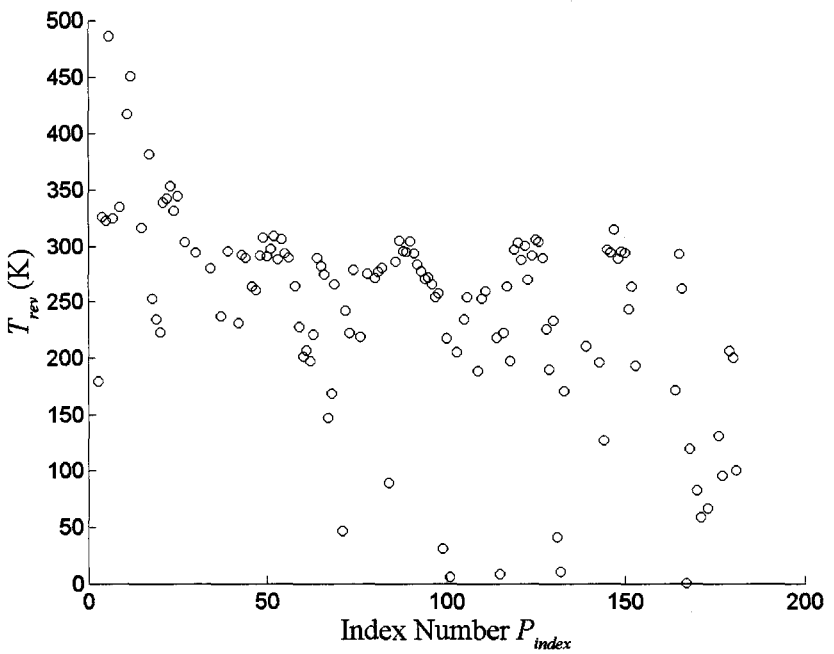

d)

Figure 5-15 - The T_{rev}'s calculated for all available source terminations at a) 6 GHz, b) 15 GHz, c) 20 GHz, d) 24 GHz.

The circles in the figure mark the T_{rev} values calculated. Only results between 0 K and 500 K are plotted while the rest are neglected. As can be seen in Figure 5-15 a), most of the resultant T_{rev} values are around the ambient temperature, which is approximately 295 K for this measurement. This is to be expected because the reverse noise temperature of the device is known to be very low due to the good isolation between the gate and the channel. However, there are also many outlying values that are obviously unphysical and wrong. As the measurement frequency increases, more outlying points can be seen, as shown in b), c), and d). The gradual deterioration of the calculation results could be explained by the general decrease of the measured power combined with the increased uncertainty of the NFA as the frequency increases.

In spite of the deteriorating results shown in Figure 5-15, the validity of the proposed source termination selection criterion still needs to be investigated. According to the criterion, the Γ_s's best suited for noise measurements are roughly the ones around the centre of the Smitch chart. As Figure 5-15 are plotted in the order similar to that shown in Figure 4-7, the centre Γ_s's would correspond to those on the right end of the figure. By observing the plots one can tell that the scattering of the T_{rev} values away from the ambient temperature tends to be worse for Γ_s's further from the centre of the Smith chart and gradually becomes better for centre points. However, this trend is not obvious at 24 GHz as shown in d). The observation suggests that the criterion is only relatively effective at lower frequencies up to 20 GHz in this case. By plotting the calculated T_{rev} values in the order of the source terminations ranked by the criterion as shown in Figure 5-16. As shown in Figure 5-16 a), b), and c), the more lowly-ranked source terminations do tend to yield unrealistic results. However, at 24 GHz, the T_{rev} values are generally bad and the effectiveness of the criterion is no longer apparent.

Once T_{rev} is determined, the next noise parameter to be found is β. To find β, the data obtained from a forward measurement of the DUT are used in (2.142) and (2.143), which are repeated here:

$$\begin{aligned} \beta_r\left(x_1 - x_{ref}\right) + \beta_i\left(y_1 - y_{ref}\right) &= \kappa_1, \\ \beta_r\left(x_2 - x_{ref}\right) + \beta_i\left(y_2 - y_{ref}\right) &= \kappa_2, \end{aligned} \tag{5.7}$$

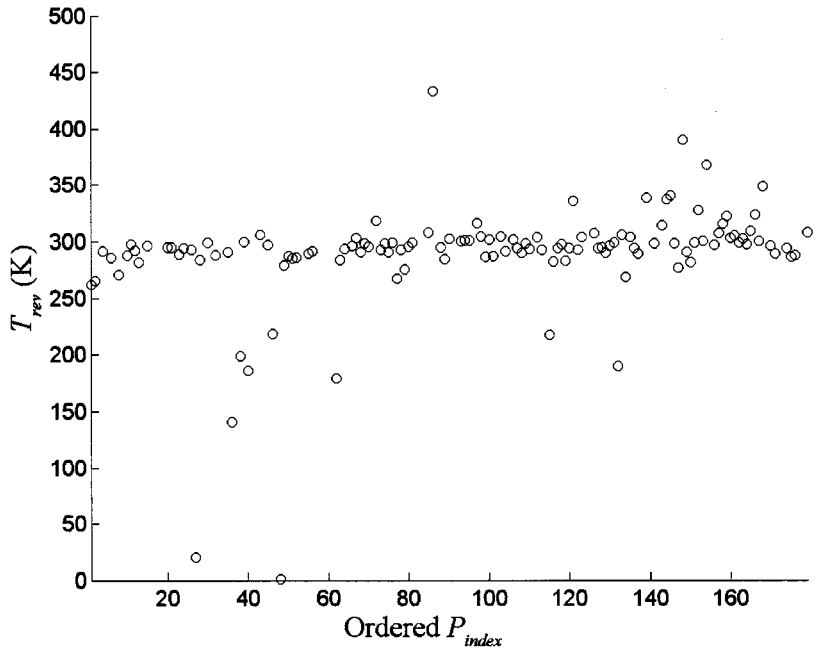
500
450
400
350
300
250
200
150
100
50
0
T_{rev} (K)
20
40
60
80
100
120
140
160
Ordered P_{index}

a)

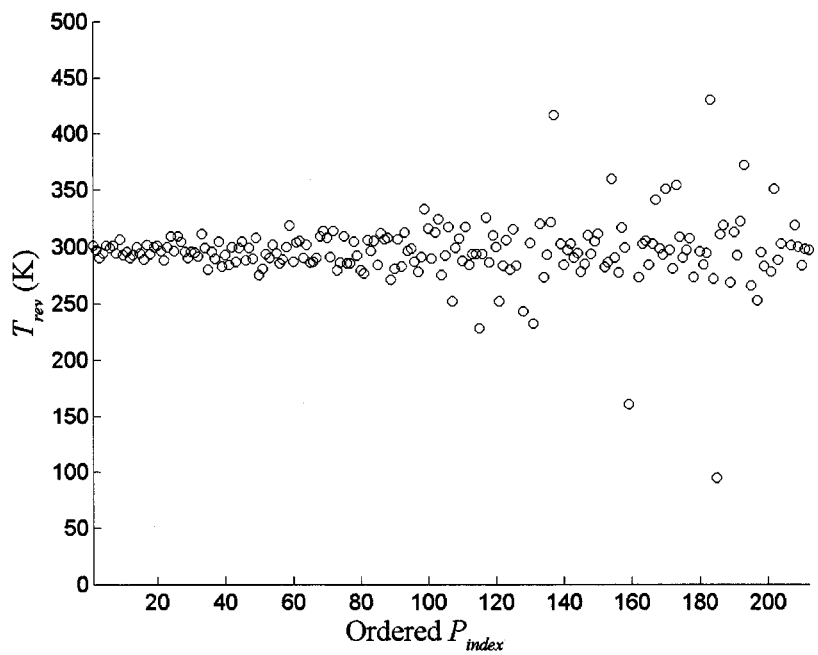
500
450
400
350
300
250
200
150
100
50
0
T_{rev} (K)
20
40
60
80
100
120
140
160
180
200
Ordered P_{index}

b)

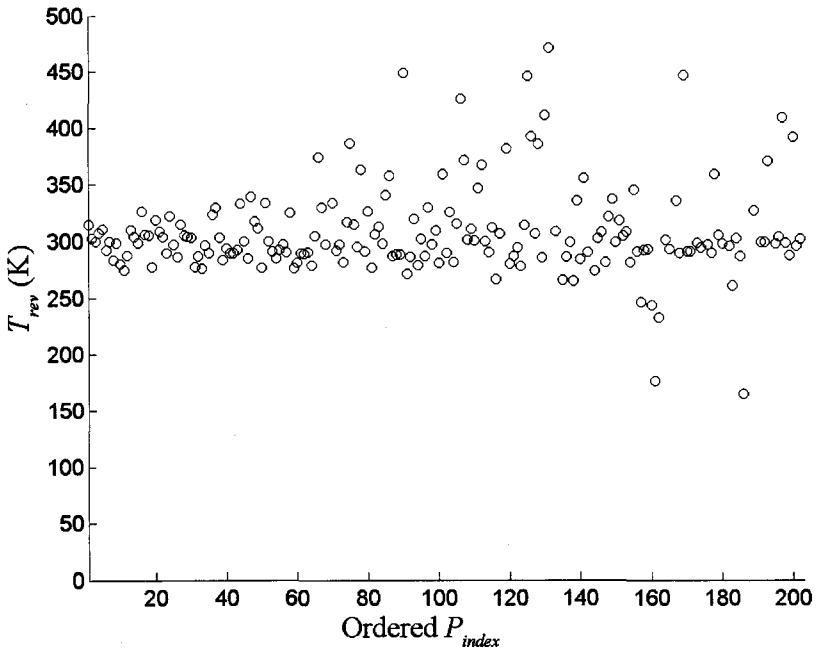

c)

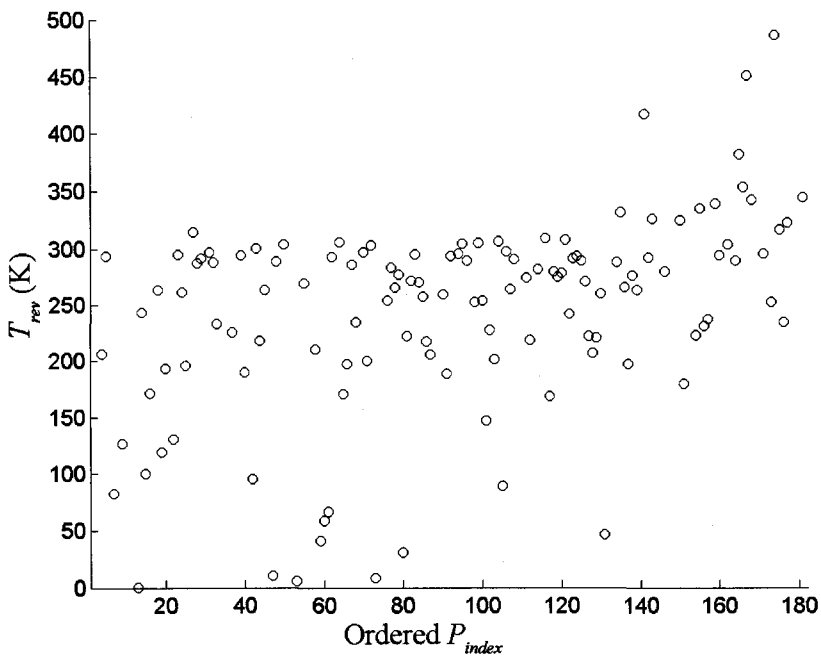

d)

Figure 5-16 - The T_{rev}'s calculated with respect to all source terminations ranked according to the selection criterion at a) 6 GHz, b) 15 GHz, c) 20 GHz, d) 24 GHz

where

$$\beta = \beta_r + j\beta_i,$$

$$\Gamma_S^{'} = x + jy,$$

$$\kappa_x = \frac{\left(1-\left|\Gamma_{2,ref}\right|^2\right)T_{out,2,ref} - \left(1-\left|\Gamma_{2,x}\right|^2\right)T_{out,2,x}}{2GT_{rev}} + \left(1-\frac{T_s}{T_{rev}}\right)\frac{\left|\Gamma_x^{'}\right|^2 - \left|\Gamma_{ref}^{'}\right|^2}{2}, \tag{5.8}$$

Ideally, (5.7) requires the measurement results using three source terminations to solve. Due to inevitable errors in the measurement results, however, it is likely that more than three measurements are needed to perform a fitting in order to solve for β_r and β_i. The measured noise power is again referred back to Port 2 of the DUT using (5.5) to find the $T_{out,2}$ for each source termination.

Using the robust regression algorithm provided in MATLAB's statistic toolbox, the β values obtained are plotted in Figure 5-17 and Figure 5-18. Each β was calculated using the measurement results of five source terminations. The group of five points were ranked according to the source termination selection criterion with Group 1 consisting of source impedances yielding the least errors.

The plots were made for 4 GHz, 15 GHz, and 24 GHz. As can be observed, the magnitudes and angles of calculated β values tend to scatter more as the group number increases. This suggests that the source terminations ranked lower by the selection criterion are more likely to yield erratic results.

Finally, with T_{rev} and β found, T_a can be found with the Y-factor method using again the forward measurement data as shown in (2.144). However, the equation presented by Engen assumes the hot and the cold reflection coefficients of the noise source are the same. Therefore, (2.144) should be corrected to take into account both reflection coefficients and be rewritten as

$$Y = \frac{T_{S,hot}\left(1-\left|\Gamma_{S,hot}^{'}\right|^2\right) + T_a + T_{rev}\left|\Gamma_{S,hot}^{'} - \beta\right|^2}{T_{S,cold}\left(1-\left|\Gamma_{S,cold}^{'}\right|^2\right) + T_a + T_{rev}\left|\Gamma_{S,cold}^{'} - \beta\right|^2} \times \frac{1-\left|\Gamma_{2,cold}\right|^2}{1-\left|\Gamma_{2,hot}\right|^2}, \tag{5.9}$$

where $\Gamma_{2,cold}$ and $\Gamma_{2,hot}$ are the cold and hot reflection coefficients at the output of the DUT.

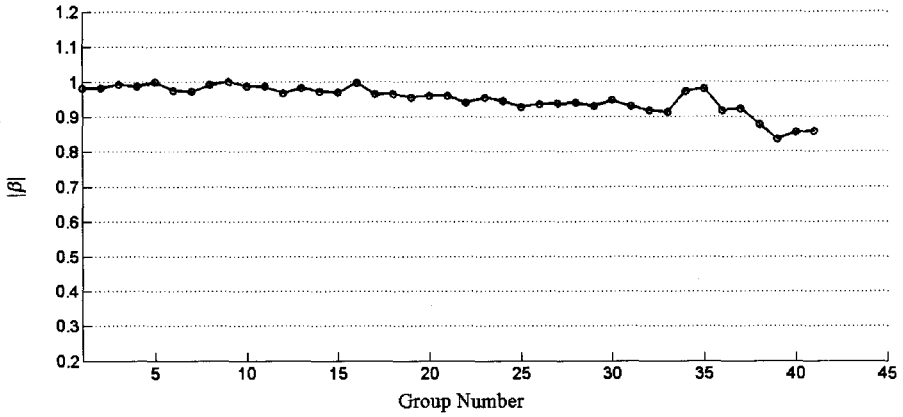

a)

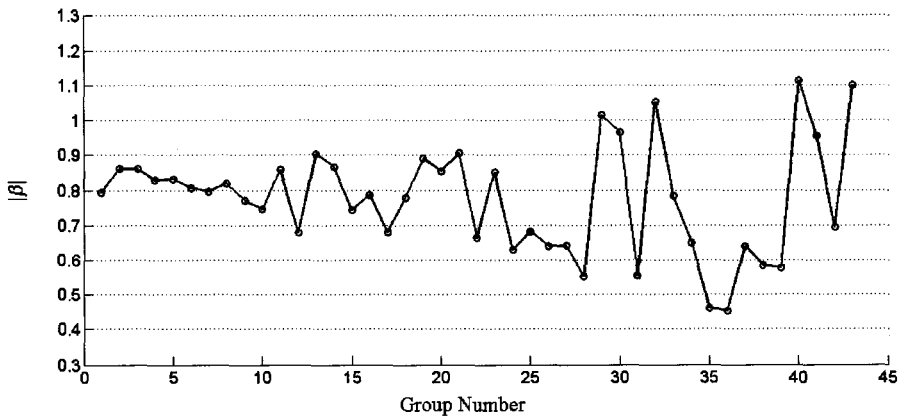

b)

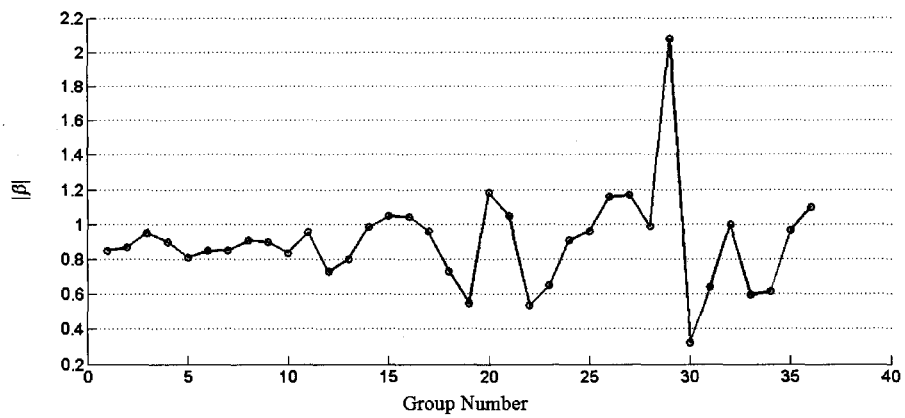

c)

Figure 5-17 - The $|\beta|$'s obtained using different groups of source terminations in the order ranked according to the proposed selection criterion at a) 4 GHz, b) 15 GHz, and c) 24 GHz.

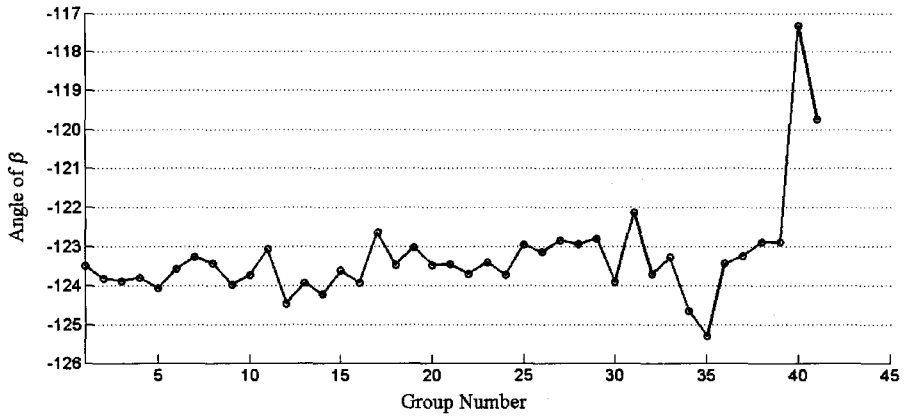

a)

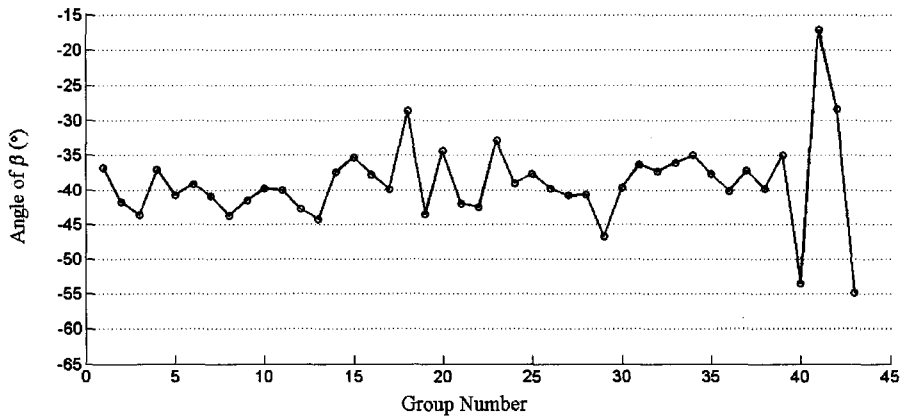

b)

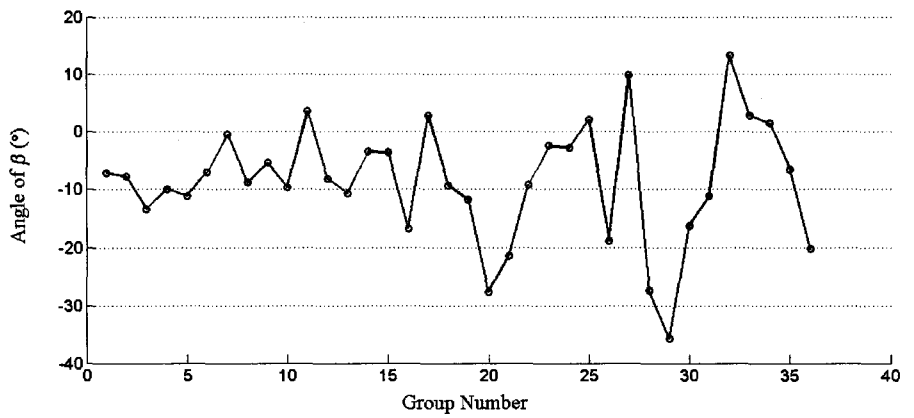

c)

Figure 5-18 - The angles of β obtained using different groups of source terminations in the order ranked according to the proposed selection criterion at a) 4 GHz, b) 15 GHz, and c) 24 GHz.

Equation (5.9) is then rearranged into

$$T_a = \frac{T_{hot} - M \cdot Y \cdot T_{cold}}{M \cdot T_{cold} - 1}, \tag{5.10}$$

where

$$M = \frac{1 - \left|\Gamma_{2,cold}\right|^2}{1 - \left|\Gamma_{2,hot}\right|^2},$$

$$T_{hot} = T_{S,hot}\left(1 - \left|\Gamma'_{S,hot}\right|^2\right) + T_{rev}\left|\Gamma'_{S,hot} - \beta\right|^2, \text{ and}$$

$$T_{cold} = T_{S,cold}\left(1 - \left|\Gamma'_{S,cold}\right|^2\right) + T_{rev}\left|\Gamma'_{S,cold} - \beta\right|^2.$$

Using (5.10), source terminations grouped according to the proposed selection criterion are again used to compute the T_a values. The results are plotted in Figure 5-19. Each T_a was the averaged results of five source terminations chosen according to the ranking yielded by the criterion. The plots again exhibit a trend that grows more erratic as more lowly-ranked source terminations are used.

Since T_a is defined as the portion of the output noise wave that is not correlated to the input noise wave, as shown in (2.128), it might be less or greater than the ambient temperature. Nevertheless, it should be a positive number. Observing Figure 5-19 one can see that as the scattering worsens, more and more results are negative, and thus unphysical.

It should be emphasized that only five source terminations are used to extract β and T_a in the analyses above. In practical situations, more points are usually used to improve the accuracy of the result [41], [62]-[64], [70]. On the other hand, although it is common knowledge that using more points would help reduce uncertainty, it is found that using all the available points often yield erroneous results.

Thus far, the analyses have demonstrated that the proposed source termination selection technique is able to provide a hint on which points to use for noise measurements for better uncertainty. The result contradicts those that suggest the source terminations should be well-spread [41], [63], [70], or within a certain range [62], or simply having a large magnitude [64].

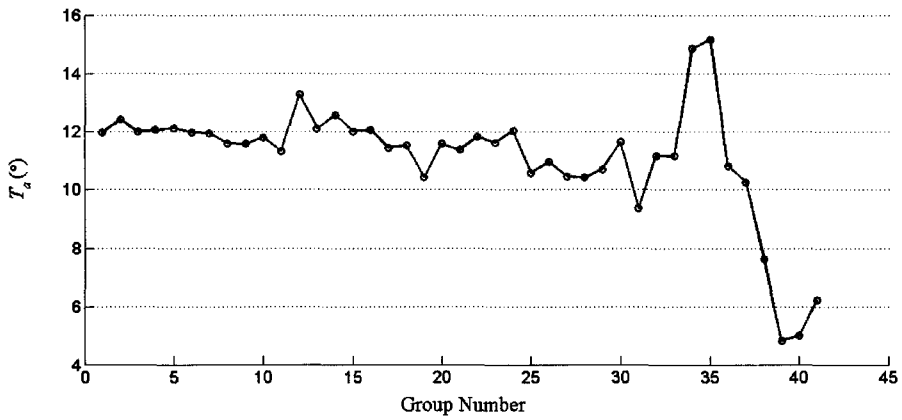

a)

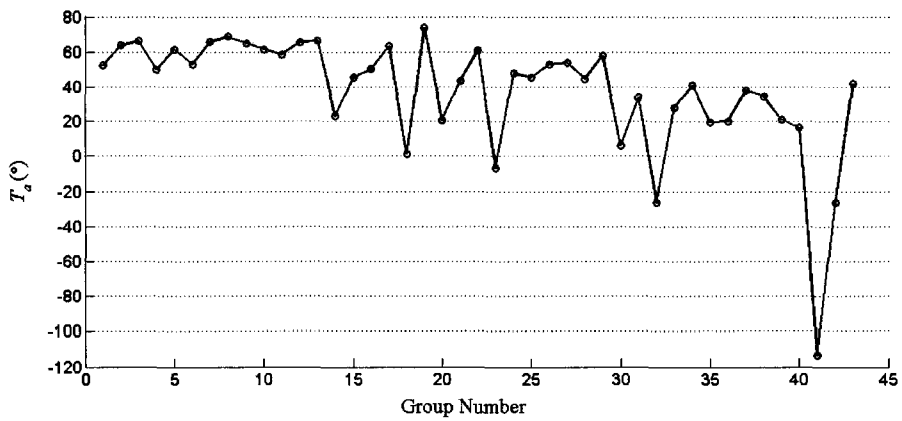

b)

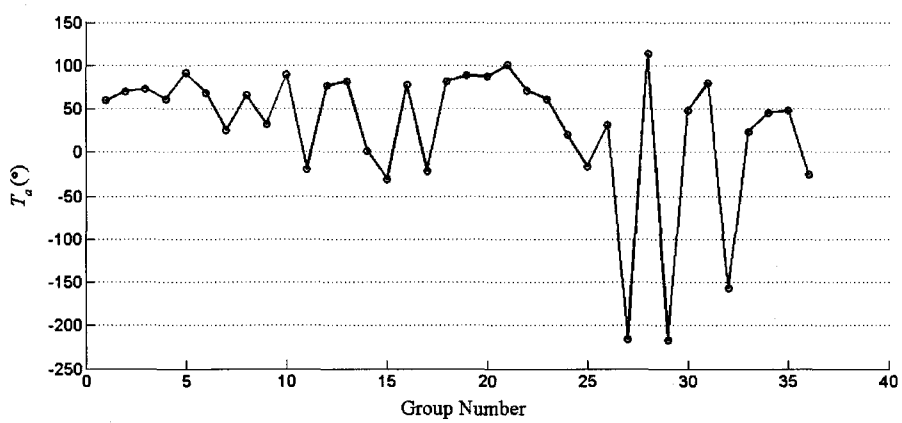

c)

Figure 5-19 - The T_a's obtained using different groups of source terminations in the order ranked according to the proposed selection criterion at a) 4 GHz, b) 15 GHz, and c) 24 GHz.

5.3 Uncertainties of Extracted Noise Parameters

Since the conventional noise parameters $F_{\min}$, Γ_o, and R_n are more widely used, the final resultant are converted to them using (2.131), (2.133), (2.134), and (2.140). The results are plotted in Figure 5-20. The error bars in the figure are the result of Monte Carlo simulations done using the extracted noise parameters. In the simulations, these extracted parameters are treated as true values. Other true values include all the S parameters and reflection coefficients measured by the VNA, the ambient temperature, and the stated *ENR*'s of the noise source. To generate simulated measurement data, normally distributed random error are generated and then added to the true values. The errors of the S parameters are generated the same way as that used in the source termination selection technique. The errors associated with the noise source are also generated according to the manufacturer's specification. The standard deviation of the ambient temperature is assumed to be 1 degree. These true values combined with simulated errors become the simulated measurement values. Using the true noise parameters and the simulated measurement values, 1000 sets of simulated power measurements are created for each frequency. For each set of data, the noise parameter extraction procedure is applied to yield a set of noise parameters. The standard deviation of the 1000 results for each noise parameter is then plotted as the uncertainty of the final result in the figure.

It should be noted that the resultant uncertainties plotted in the figure are not always the standard deviation of exactly 1000 sets of simulated results. It is noticed that with the setup used for generating the simulated measurement data, some results turned out to be unphysical. These data, therefore, have been excluded from the standard deviation calculation, as would have been with real measurement data. However, one important point is that, compared to actual measurement data, the simulated measurement data seem to be more prone to yield unphysical results. This observation hints that the assumption that the uncertainties of the various sources of errors are normally distributed might not be accurate.

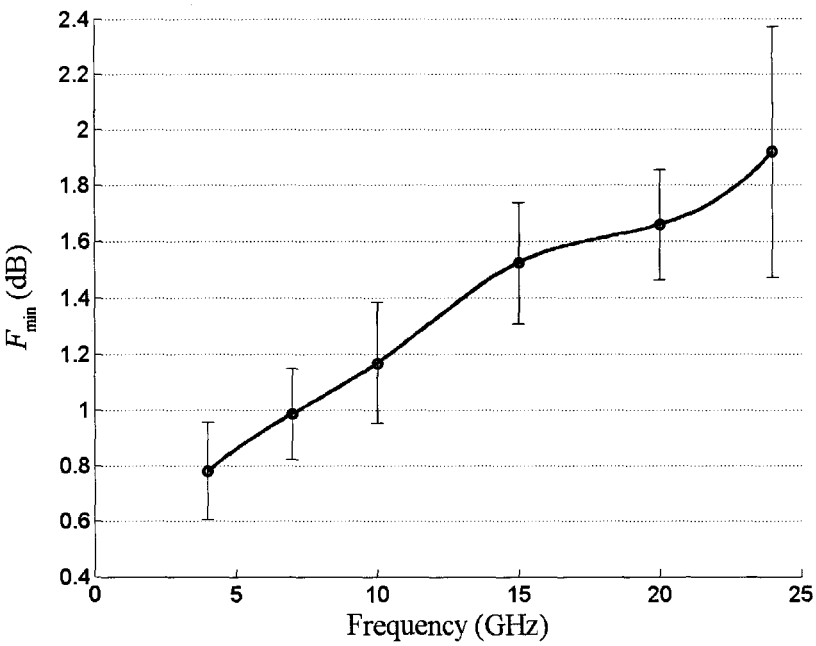
2.4
2.2
2
1.8
1.6
1.4
1.2
1
0.8
0.6
0.4
F_{min} (dB)
0
5
10
15
20
25
Frequency (GHz)

a)

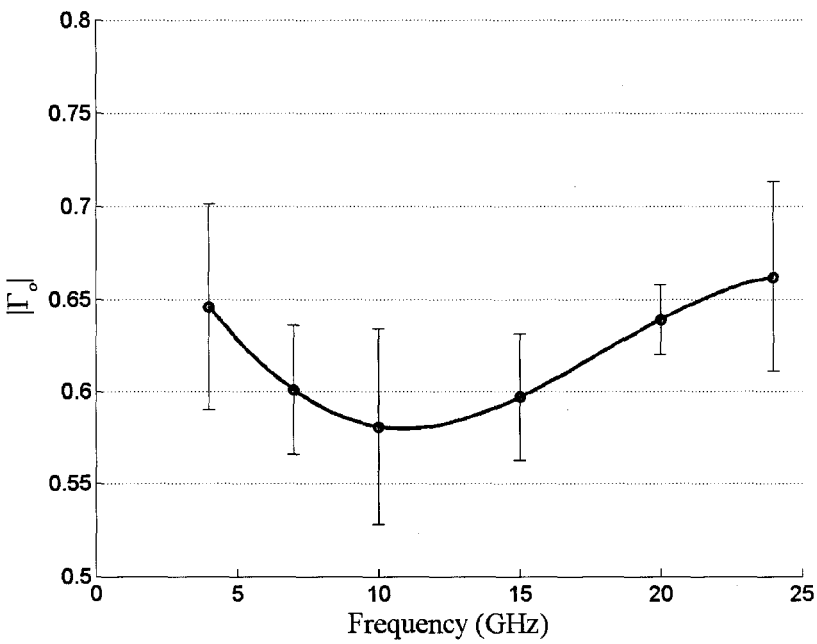
0.8
0.75
0.7
0.65
0.6
0.55
0.5
$|\Gamma_o|$
0
5
10
15
20
25
Frequency (GHz)

b)

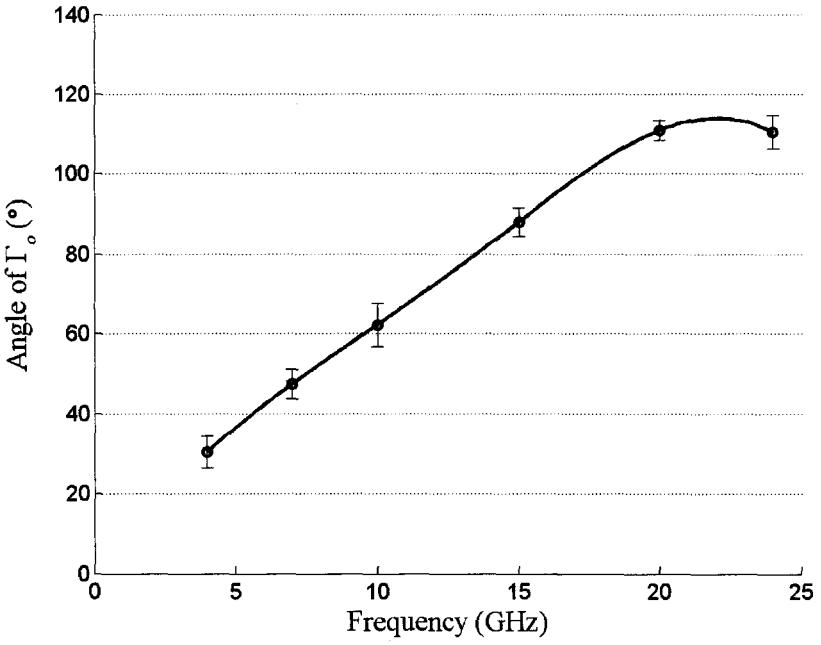

c)

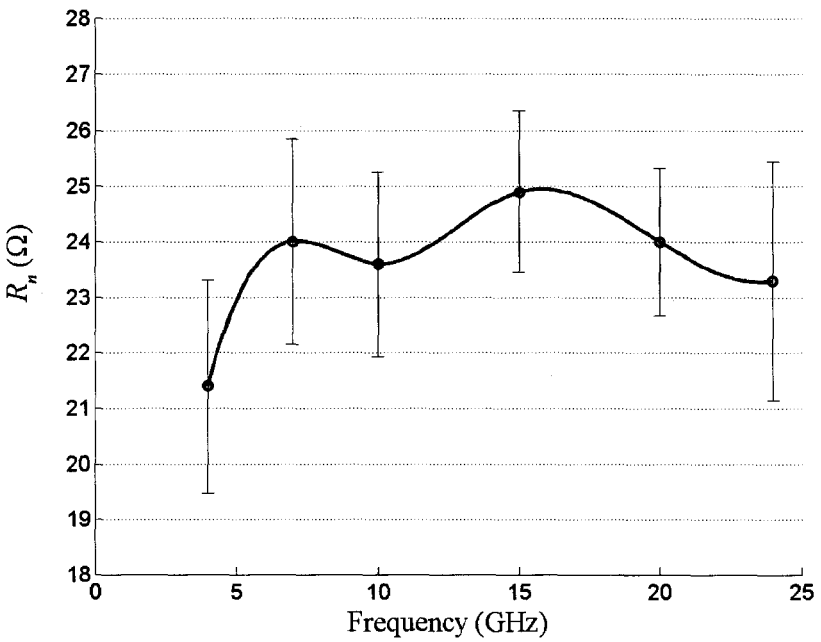

d)

Figure 5-20 - Results for the conventional noise parameters a) F_{min}, b) $|\Gamma_o|$, c) $\angle\Gamma_o$, and d) R_n.

The normally distributed errors simulated in the Monte Carlo simulation might have been exaggerated compared to those of a real measurement. Thus future investigation on the probability distribution of the measurement errors is warranted.

Another point that requires clarification is that the extracted noise parameters presented in Figure 5-20 are not strictly those of the MOSFET, but those of the MOSFET plus the pads where the probes made contacts for the measurement. In order to extract strictly the noise parameters of the device itself, further de-embedding is required.

Chapter 6: CONCLUSIONS

6.1 Summary

In this thesis, the theories behind the noise characterization of a linear two-port has been thoroughly reviewed. The review started with the physical mechanisms of various noise types followed by the specific noise sources present in a high-frequency MOSFET device. Next the concept of noise parameters established by the IRE was introduced. Over the years, many studies have provided ways to extract these noise parameters and their variations. These measurement and extraction techniques have been covered to pave way for the introduction of the proposed improvements upon noise receiver characterization and source termination selection of microwave-frequency noise measurements.

The novel noise receiver characterization method improved upon existing methods by taking into account of the difference in the reflection coefficient of the noise source between its hot and cold states. This allows the resultant receiver gains yielded from different source terminations to appear more source-dependent. It also makes use of an efficient iterative technique to compute the solution. A further improvement was made to correct the systematic errors apparent in the extracted receiver gains caused by the inaccuracy in the reflection coefficient measurement. An optimization method was used to correct the inaccuracy. The final results of the receiver gain calculation demonstrated the removal of the systematic error and the source dependency of the results.

The proposed source termination selection criterion aims to provide a practical method suitable to be used during a noise measurement. The method makes use of the Monte Carlo simulation technique combined with the VNA's uncertainties to identify the most suitable terminations. The measurement method used to verify the selection criterion was originally developed by Engen for packaged amplifiers. It was modified to work with on-wafer measurements for the 65 nm n-type MOSFET DUT used in the study. The analyses on the measurement results demonstrated the validity of the proposed selection criterion for noise measurements.

6.2 Recommendations for Future Work

In Section 5.1, the optimization used to correct the noise source's reflection coefficient was applied only to those for the hot state. As explained previously, the result was acceptable because the large difference between the measured hot and cold noise powers. However, as the frequency increases and the transmission property of the DUT changes, the measured hot and cold powers become more and more comparable. Therefore, it would be best to perform the optimization procedure to correct the noise source's reflection coefficient for the cold state as well.

Another issue worth investigating is the probability distributions of the various errors of the measurement. This is recommended because the Monte Carlo simulation applied to estimate the uncertainties of the extracted noise parameters generated many data sets yielding unphysical results. The observation suggested that it is possible the quoted uncertainties used in the simulation are exaggerated, or the Gaussian distribution assumed was too conservative. Finding out a more accurate probability distribution would install more confidence to the resultant uncertainties of the extracted noise parameters.

Finally, the extracted noise parameters presented in Section 5.3 are of the MOSFET and its probing pads. To correctly characterize the device itself, an extra measurement of the pads alone is required. Using the additional measurement data, the intrinsic noise parameters of the device can then be de-embedded.

Appendix A – VNA Measurement Uncertainties

	Uncertainty Magnitude		
Reflection Coefficient (Linear)	2 GHz to 8 GHz	8 GHz to 20 GHz	20 GHz to 26.5 GHz
0	0.012909647	0.016415552	0.032627075
0.01	0.013018186	0.016535933	0.032798987
0.02	0.013119585	0.016651114	0.03296889
0.03	0.013221845	0.0167691	0.033144795
0.04	0.013326654	0.016891576	0.03332837
0.05	0.013434804	0.017019333	0.033520389
0.06	0.013546756	0.017152833	0.033721289
0.07	0.013662809	0.017292371	0.033931346
0.08	0.01378317	0.017438157	0.034150747
0.09	0.013907991	0.017590341	0.034379619
0.1	0.014037387	0.017749036	0.034618054
0.11	0.014171446	0.017914329	0.034866117
0.12	0.014310237	0.01808629	0.035123854
0.13	0.014453815	0.018264972	0.035391297
0.14	0.014602225	0.018450419	0.035668468
0.15	0.014755502	0.018642666	0.035955377
0.16	0.014913676	0.018841742	0.036252032
0.17	0.01507677	0.019047668	0.036558433
0.18	0.015244802	0.019260462	0.036874575
0.19	0.015417788	0.01948014	0.03720045
0.2	0.01559574	0.019706713	0.037536046
0.21	0.015778667	0.019940187	0.037881351
0.22	0.015966576	0.020180571	0.038236347
0.23	0.016159471	0.020427867	0.038601016
0.24	0.016357357	0.020682079	0.038975338
0.25	0.016560235	0.020943206	0.039359292
0.26	0.016768104	0.021211249	0.039752854
0.27	0.016980964	0.021486206	0.040156002
0.28	0.017198814	0.021768074	0.040568709
0.29	0.01742165	0.022056849	0.040990949
0.3	0.017649469	0.022352527	0.041422696
0.31	0.017882266	0.022655103	0.041863923
0.32	0.018120035	0.02296457	0.0423146
0.33	0.018362773	0.023280923	0.042774699
0.34	0.018610471	0.023604153	0.043244191
0.35	0.018863123	0.023934254	0.043723045
0.36	0.019120723	0.024271217	0.044211232
0.37	0.019383262	0.024615034	0.04470872
0.38	0.019650732	0.024965695	0.045215479
0.39	0.019923124	0.025323192	0.045731476
0.4	0.020200431	0.025687516	0.046256681

0.41	0.020482642	0.026058655	0.04679106
0.42	0.020769749	0.0264366	0.047334581
0.43	0.021061741	0.02682134	0.047887212
0.44	0.021358609	0.027212865	0.048448919
0.45	0.021660344	0.027611164	0.04901967
0.46	0.021966933	0.028016225	0.049599432
0.47	0.022278368	0.028428038	0.050188169
0.48	0.022594636	0.02884659	0.05078585
0.49	0.022915729	0.02927187	0.051392439
0.5	0.023241633	0.029703867	0.052007904
0.51	0.023572338	0.030142568	0.052632209
0.52	0.023907833	0.03058796	0.05326532
0.53	0.024248107	0.031040032	0.053907203
0.54	0.024593147	0.031498772	0.054557824
0.55	0.024942941	0.031964166	0.055217146
0.56	0.025297479	0.032436202	0.055885137
0.57	0.025656748	0.032914867	0.05656176
0.58	0.026020736	0.033400149	0.057246981
0.59	0.026389431	0.033892035	0.057940765
0.6	0.02676282	0.03439051	0.058643076
0.61	0.027140892	0.034895563	0.059353879
0.62	0.027523633	0.03540718	0.060073139
0.63	0.027911032	0.035925347	0.060800821
0.64	0.028303076	0.036450052	0.061536888
0.65	0.028699752	0.036981281	0.062281306
0.66	0.029101047	0.03751902	0.063034038
0.67	0.029506949	0.038063256	0.063795049
0.68	0.029917445	0.038613974	0.064564303
0.69	0.030332522	0.039171163	0.065341765
0.7	0.030752167	0.039734807	0.066127398
0.71	0.031176368	0.040304893	0.066921167
0.72	0.03160511	0.040881407	0.067723036
0.73	0.032038381	0.041464335	0.068532968
0.74	0.032476167	0.042053663	0.069350928
0.75	0.032918457	0.042649377	0.07017688
0.76	0.033365235	0.043251463	0.071010787
0.77	0.03381649	0.043859908	0.071852614
0.78	0.034272208	0.044474696	0.072702324
0.79	0.034732374	0.045095814	0.07355988
0.8	0.035196977	0.045723248	0.074425248
0.81	0.035666003	0.046356983	0.07529839
0.82	0.036139438	0.046997005	0.076179269
0.83	0.036617268	0.047643299	0.077067851
0.84	0.03709948	0.048295852	0.077964098
0.85	0.037586061	0.04895465	0.078867974
0.86	0.038076997	0.049619676	0.079779443
0.87	0.038572275	0.050290919	0.080698467
0.88	0.03907188	0.050968361	0.081625012

0.89	0.039575799	0.051651991	0.082559039
0.9	0.040084019	0.052341792	0.083500513
0.91	0.040596526	0.053037751	0.084449397
0.92	0.041113305	0.053739852	0.085405655
0.93	0.041634344	0.054448082	0.08636925
0.94	0.042159628	0.055162425	0.087340145
0.95	0.042689144	0.055882867	0.088318305
0.96	0.043222878	0.056609394	0.089303691
0.97	0.043760816	0.057341991	0.090296268
0.98	0.044302944	0.058080643	0.091295998
0.99	0.044849249	0.058825335	0.092302846
1	0.045399715	0.059576053	0.093316775

	Uncertainty Phase		
Reflection Coefficient (Linear)	2 GHz to 8 GHz	8 GHz to 20 GHz	20 GHz to 26.5 GHz
0	180	180	180
0.01	180	180	180
0.02	40.90937462	56.34444983	180
0.03	26.07926661	33.97278284	180
0.04	19.39345618	24.96843881	56.37835625
0.05	15.52057835	19.89008893	42.06029693
0.06	12.98342825	16.60138488	34.16152979
0.07	11.19068022	14.29211906	28.96283031
0.08	9.856639258	12.58042208	25.23901519
0.09	8.825724018	11.26120088	22.4272075
0.1	8.005765614	10.21400391	20.22434556
0.11	7.338614155	9.36327988	18.45043079
0.12	6.785738683	8.659174423	16.99099254
0.13	6.320582677	8.067431665	15.76942129
0.14	5.92424065	7.563721864	14.73235997
0.15	5.582884135	7.130281472	13.84143049
0.16	5.286162493	6.753833867	13.06828371
0.17	5.026172992	6.424254402	12.39150314
0.18	4.796776766	6.133685977	11.79459571
0.19	4.593132203	5.87593698	11.26464652
0.2	4.411369143	5.64606161	10.79139388
0.21	4.248356637	5.440061151	10.36657839
0.22	4.101534341	5.254667361	9.983475354
0.23	3.968788079	5.08718277	9.636552891
0.24	3.848356624	4.93536115	9.321217822
0.25	3.738760935	4.797316854	9.033624046
0.26	3.638749771	4.671455173	8.770526155
0.27	3.54725742	4.556418259	8.529166254
0.28	3.463370515	4.451042679	8.307185505
0.29	3.386301725	4.354325786	8.102554297
0.3	3.315368725	4.265398849	7.913516618

0.31	3.249977235	4.183505393	7.738545355
0.32	3.189607255	4.107983622	7.576306098
0.33	3.133801799	4.038252036	7.425627615
0.34	3.08215762	3.973797607	7.285477606
0.35	3.034317532	3.914165975	7.154942653
0.36	2.989964009	3.858953287	7.033211561
0.37	2.948813823	3.807799364	6.919561422
0.38	2.91061353	3.760381947	6.813345899
0.39	2.875135654	3.716411828	6.713985339
0.4	2.842175438	3.675628715	6.620958372
0.41	2.811548076	3.637797703	6.533794756
0.42	2.783086336	3.602706252	6.452069249
0.43	2.756638519	3.570161579	6.375396346
0.44	2.732066693	3.539988416	6.303425733
0.45	2.709245168	3.512027062	6.235838361
0.46	2.68805916	3.486131691	6.172343023
0.47	2.668403635	3.462168874	6.112673382
0.48	2.650182296	3.440016287	6.056585367
0.49	2.633306687	3.419561582	6.003854887
0.5	2.617695414	3.400701385	5.954275831
0.51	2.603273451	3.383340416	5.907658291
0.52	2.58997153	3.367390716	5.863827004
0.53	2.577725596	3.352770951	5.822619959
0.54	2.566476328	3.339405801	5.783887173
0.55	2.556168704	3.327225414	5.747489588
0.56	2.546751625	3.316164917	5.713298093
0.57	2.538177564	3.30616398	5.681192652
0.58	2.530402264	3.297166424	5.651061519
0.59	2.523384457	3.289119872	5.622800527
0.6	2.517085619	3.281975427	5.596312466
0.61	2.511469743	3.275687392	5.571506501
0.62	2.506503138	3.270213012	5.548297662
0.63	2.502154242	3.265512237	5.526606376
0.64	2.498393461	3.261547514	5.506358046
0.65	2.495193015	3.258283593	5.487482666
0.66	2.4925268	3.255687356	5.469914471
0.67	2.490370265	3.253727654	5.453591625
0.68	2.488700298	3.252375166	5.438455924
0.69	2.487495121	3.251602264	5.424452541
0.7	2.486734194	3.251382892	5.411529778
0.71	2.486398131	3.251692461	5.399638848
0.72	2.486468617	3.252507738	5.388733671
0.73	2.486928337	3.253806762	5.378770692
0.74	2.487760906	3.255568753	5.369708705
0.75	2.488950811	3.257774034	5.361508701
0.76	2.490483351	3.26040396	5.354133719
0.77	2.492344582	3.263440852	5.347548717
0.78	2.494521276	3.266867933	5.341720447

0.79	2.497000868	3.270669269	5.33661734
0.8	2.499771419	3.274829722	5.332209403
0.81	2.502821578	3.279334898	5.328468122
0.82	2.506140542	3.284171101	5.325366369
0.83	2.509718026	3.289325291	5.322878321
0.84	2.513544236	3.294785047	5.320979383
0.85	2.51760983	3.30053853	5.319646112
0.86	2.521905903	3.306574447	5.318856153
0.87	2.526423955	3.312882023	5.318588177
0.88	2.531155869	3.319450969	5.31882182
0.89	2.536093893	3.326271456	5.31953763
0.9	2.541230615	3.333334091	5.320717019
0.91	2.546558949	3.340629888	5.32234221
0.92	2.552072112	3.348150252	5.324396198
0.93	2.557763614	3.355886956	5.326862705
0.94	2.563627237	3.363832118	5.329726146
0.95	2.569657025	3.371978188	5.332971585
0.96	2.575847266	3.380317927	5.336584709
0.97	2.582192484	3.388844395	5.340551792
0.98	2.588687423	3.39755093	5.344859663
0.99	2.59532704	3.406431139	5.349495685
1	2.60210649	3.415478884	5.354447719

	Uncertainty Magnitude		
Transmission Coefficient (dB)	2 GHz to 8 GHz	8 GHz to 20 GHz	20 GHz to 26.5 GHz
-90	1.964342772	2.920747899	4.702911576
-89	1.795348502	2.666515518	4.332854179
-88	1.641611308	2.433501253	3.989030136
-87	1.501958815	2.220455439	3.670512327
-86	1.375266527	2.026117225	3.376265311
-85	1.260464017	1.849231236	3.105166952
-84	1.156539215	1.688561948	2.856030178
-83	1.062541011	1.542905676	2.627624109
-82	0.97758042	1.411100208	2.418693919
-81	0.900830546	1.292032177	2.22797894
-80	0.831525591	1.184642387	2.054228664
-79	0.768959096	1.087929295	1.896216473
-78	0.712481623	1.000950933	1.752751022
-77	0.661498022	0.922825512	1.622685337
-76	0.615464439	0.852730997	1.504923755
-75	0.57388516	0.789903868	1.398426911
-74	0.536309396	0.733637312	1.302214971
-73	0.502328076	0.683279011	1.215369395
-72	0.471570699	0.638228697	1.13703343
-71	0.44370229	0.597935575	1.066411596
-70	0.418420491	0.561895706	1.002768368

-69	0.395452793	0.529649401	0.94542623
-68	0.374553937	0.500778639	0.893763274
-67	0.355503473	0.474904539	0.847210484
-66	0.338103492	0.451684865	0.805248792
-65	0.322176519	0.430811567	0.767406027
-64	0.307563569	0.412008356	0.733253797
-63	0.294122351	0.395028306	0.702404387
-62	0.281725629	0.379651498	0.674507695
-61	0.270259716	0.36568271	0.649248258
-60	0.259623099	0.352949181	0.626342376
-59	0.249725195	0.341298455	0.605535378
-58	0.240485214	0.330596335	0.586599016
-57	0.231831132	0.32072495	0.569329023
-56	0.22369877	0.311580962	0.553542831
-55	0.21603095	0.303073907	0.539077441
-54	0.208776751	0.295124685	0.525787474
-53	0.20189083	0.287664185	0.513543362
-52	0.195332817	0.280632061	0.502229711
-51	0.190869261	0.275086541	0.492709206
-50	0.187828468	0.271686342	0.485834356
-49	0.185021084	0.268581716	0.479619328
-48	0.182421388	0.26573612	0.473990892
-47	0.180006509	0.263117743	0.468883993
-46	0.177756106	0.260698871	0.464240834
-45	0.175652092	0.258455342	0.460010072
-44	0.173678376	0.256366065	0.456146089
-43	0.171820645	0.254412612	0.452608352
-42	0.170066161	0.252578862	0.449360834
-41	0.16840359	0.250850697	0.446371513
-40	0.166822841	0.249215734	0.443611915
-39	0.165314928	0.247663099	0.441056711
-38	0.163871845	0.246183232	0.438683367
-37	0.162486457	0.244767712	0.436471818
-36	0.161152399	0.243409113	0.434404195
-35	0.15986399	0.242100877	0.432464565
-34	0.158616151	0.240837196	0.430638711
-33	0.157404335	0.23961292	0.42891393
-32	0.156224462	0.238423468	0.427278851
-31	0.15507286	0.237264749	0.425723267
-30	0.153946208	0.236133099	0.424237993
-29	0.152841487	0.235025211	0.422814715
-28	0.151755932	0.233938083	0.421445872
-27	0.150686981	0.232868958	0.420124522
-26	0.149632231	0.231815277	0.418844226
-25	0.148589388	0.23077462	0.417598927
-24	0.147556215	0.229744658	0.416382821
-23	0.146530478	0.22872309	0.415190228
-22	0.145509883	0.227707585	0.414015446

-21	0.144492004	0.226695706	0.412852591
-20	0.1434742	0.225684834	0.411695406
-19	0.142453514	0.224672066	0.410537047
-18	0.141426555	0.223654105	0.409369816
-17	0.14038935	0.222627114	0.408184849
-16	0.139337162	0.221586548	0.406971723
-15	0.138264267	0.220526939	0.405717986
-14	0.137163675	0.219441635	0.404408558
-13	0.136026784	0.21832247	0.403025
-12	0.134842944	0.217159357	0.401544596
-11	0.133598915	0.215939772	0.399939205
-10	0.132278184	0.214648113	0.39817382
-9	0.13086011	0.213264898	0.39620477
-8	0.129318851	0.211765751	0.39397745
-7	0.127622016	0.210120131	0.391423478
-6	0.125728965	0.208289744	0.388457115
-5	0.123588676	0.20622653	0.384970754
-4	0.121137065	0.203870145	0.380829247
-3	0.118293601	0.201144785	0.375862737
-2	0.114957052	0.197955186	0.369857615
-1	0.111000113	0.194181591	0.362545081
0	0.106262642	0.189673395	0.353586652
1	0.11276549	0.196415453	0.368261743
2	0.120713042	0.204666648	0.386521187
3	0.13047945	0.214818025	0.40930538
4	0.142536844	0.227363149	0.437808186
5	0.15748156	0.24292562	0.473549076
6	0.176067724	0.262294348	0.518468109
7	0.199250473	0.286469003	0.57505234
8	0.228241874	0.316718939	0.646506331
9	0.2645838	0.354660134	0.736985827
10	0.310243729	0.402356607	0.851924287

	Uncertainty Phase		
Transmission Coefficient (dB)	2 GHz to 8 GHz	8 GHz to 20 GHz	20 GHz to 26.5 GHz
-90	14.63808088	23.55286906	45.89205612
-89	13.2118908	21.05222496	40.26708714
-88	11.94536209	18.85872001	35.62208637
-87	10.8191255	16.92802626	31.69792636
-86	9.8165166	15.22428311	28.33418464
-85	8.9230971	13.71789797	25.42214521
-84	8.126286999	12.3840637	22.88334751
-83	7.415075941	11.20172251	20.65849668
-82	6.779792437	10.15281869	18.70119425
-81	6.2119163	9.221744478	16.97414484
-80	5.703923963	8.394918783	15.44673392

-79	5.249159315	7.660459832	14.09341102
-78	4.841724688	7.007925748	12.89256947
-77	4.476388003	6.428105538	11.82574465
-76	4.148503077	5.912848281	10.87702371
-75	3.853940782	5.454921927	10.03259979
-74	3.589029257	5.047895497	9.280427963
-73	3.350501753	4.686040093	8.609954155
-72	3.135450954	4.364245274	8.011897955
-71	2.941288839	4.077948042	7.478075797
-70	2.765711314	3.823072283	7.001255114
-69	2.60666697	3.595976819	6.57503258
-68	2.462329418	3.393410537	6.193731423
-67	2.331072745	3.212473304	5.852314015
-66	2.211449701	3.050581549	5.546306857
-65	2.10217229	2.90543761	5.271735721
-64	2.002094463	2.775002126	5.025069204
-63	1.910196689	2.657468905	4.803169307
-62	1.82557218	2.551241879	4.603247929
-61	1.747414582	2.454913853	4.422828398
-60	1.675006991	2.367246875	4.259711329
-59	1.607712138	2.287154121	4.111944223
-58	1.544963622	2.213683211	3.977794356
-57	1.486258085	2.146000938	3.855724546
-56	1.431148239	2.083379338	3.744371507
-55	1.379236634	2.025183091	3.642526484
-54	1.33017012	1.970858172	3.549117963
-53	1.283634906	1.919921712	3.463196221
-52	1.239352162	1.871952971	3.383919562
-51	1.209228507	1.834152104	3.317292644
-50	1.188713491	1.810983998	3.269227531
-49	1.169780742	1.789839015	3.225811034
-48	1.152255127	1.770465965	3.186521457
-47	1.135981075	1.752646404	3.150896509
-46	1.120820371	1.736190214	3.118526448
-45	1.106650201	1.72093177	3.089048022
-44	1.093361417	1.706726632	3.062139103
-43	1.080857001	1.693448688	3.03751394
-42	1.069050694	1.680987696	3.014918977
-41	1.057865792	1.669247166	2.994129143
-40	1.047234074	1.658142534	2.974944579
-39	1.037094845	1.647599597	2.957187752
-38	1.027394094	1.637553151	2.940700889
-37	1.018083744	1.627945827	2.925343715
-36	1.009120986	1.618727076	2.910991445
-35	1.000467681	1.609852292	2.897533003
-34	0.992089837	1.601282048	2.884869435
-33	0.983957133	1.592981429	2.872912495
-32	0.976042497	1.584919446	2.861583378

-31	0.968321726	1.577068519	2.850811581
-30	0.960773139	1.569404013	2.840533868
-29	0.953377271	1.561903823	2.830693322
-28	0.946116575	1.55454799	2.821238466
-27	0.938975163	1.547318345	2.812122438
-26	0.931938547	1.540198167	2.803302191
-25	0.924993395	1.533171847	2.794737706
-24	0.918127283	1.526224545	2.786391191
-23	0.911328451	1.51934183	2.778226242
-22	0.904585536	1.512509289	2.770206931
-21	0.897887288	1.505712081	2.762296786
-20	0.891222246	1.49893443	2.754457621
-19	0.884578366	1.492159018	2.746648151
-18	0.877942586	1.485366248	2.738822327
-17	0.871300291	1.478533348	2.730927308
-16	0.864634674	1.471633259	2.722900948
-15	0.857925929	1.464633239	2.714668663
-14	0.851150261	1.457493119	2.706139506
-13	0.844278629	1.450163092	2.697201213
-12	0.837275175	1.442580928	2.687713938
-11	0.830095229	1.434668432	2.677502319
-10	0.822682784	1.426326954	2.666345394
-9	0.814967295	1.417431682	2.653963792
-8	0.806859606	1.407824387	2.640003439
-7	0.798246778	1.397304184	2.624014816
-6	0.788985506	1.385615792	2.605426562
-5	0.778893746	1.372434575	2.583511844
-4	0.767740055	1.357347504	2.557345548
-3	0.755230022	1.33982893	2.525749735
-2	0.740988991	1.319209719	2.487224177
-1	0.724540068	1.294637978	2.439857887
0	0.705276115	1.265029029	2.381216424
1	0.733372267	1.309918055	2.479423372
2	0.767471939	1.365407604	2.603056101
3	0.809213738	1.434412398	2.759265412
4	0.860689439	1.520665835	2.957312009
5	0.924572494	1.628960163	3.209250567
6	1.00428503	1.765463587	3.530875341
7	1.104216085	1.938142948	3.943052872
8	1.230008881	2.157333772	4.473644509
9	1.38894231	2.436520132	5.160357939
10	1.590443074	2.793420152	6.05511939

References

[1] P. R. Gray *et al.*, "Analysis and design of analog integrated circuits," Fourth edition, *John Wiley & Sons, Inc.*, 2001.

[2] R. Brown, "Mikroskopische Beobachtungen über die in Pollen von Pflanzen enthaltenen Partikeln, und über das allgemeine Vorkommen aktiver Moleküle in organischen und anorganischen Körpern," *Ann, Phys.*, vol. 14, p.294, 1828.

[3] A. Einstein, "Zur Theorie der Brownschen Bewegung," *Ann. Phys.*, vol. 19, pp. 371–381, 1906.

[4] M. von Smoluchovski, "Zur Kinetischen Theorie der Brownschen Molekularbewegung und der Suspensionen," *Ann. Phys.*, vol. 21, pp. 756–780, 1906.

[5] W. Schottky, "Über spontane Stromschwankungen in verschiedenen Elektrizitätsleitern", *Ann. Phys.* Vol. 57, p. 541, 1918.

[6] S. O. Rice, "Mathematical Analysis of Random Noise," *Bell Syst. Tech. J.*, vol. 23, pp. 282–332, 1944.

[7] J. B. Johnson, "Thermal Agitation of Electricity in Conductors," *Phys. Rev.*, vol.32, pp. 97–109, 1928.

[8] H. Nyquist, "Thermal Agitation of Electric Charge in Conductors," *Phys. Rev.*, vol.32. pp. 110–113, 1928.

[9] R. Sarpeshkar, T. Delbruck, and C. A. Mead, "White noise in MOS transistors and resistors," *IEEE Circuits Devices Mag.*, vol. 9, no. 6, pp. 23–29, 1993.

[10] J. B. Johnson, "The Schottky effect in low frequency circuits," *Phys. Rev.*, vol. 26, pp. 71–85, 1925.

[11] W. Schottky, "Small-Shot Effect and Flicker Effect," *Phys. Rev.*, vol. 28, pp. 74–103, 1926.

[12] D. S. Tan, "Current pulses during breakdown in silicon P-N junctions," *Proc. IEEE*, vol. 53, pp. 210–211, 1965.

[13] E. Morifuji et al., "Future perspective and scaling down roadmap for RF CMOS," *VLSI Symp. Tech. Dig.*, pp. 165–166, 1999.

[14] T. C. Holloway et al., "0.18 μm CMOS technology for high-performance, low-power, and RF applications," *VLSI Symp. Tech. Dig.*, p. 13, 1997.

[15] A. van der Ziel, "Gate noise in field effect transistors at moderately high frequencies," *Proc. Inst. Electr. Eng.*, vol. 51, no. 3, pp. 461–467, 1963.

[16] M. Shoji, "Analysis of high-frequency thermal noise of enhancement mode MOS field-effect transistors," IEEE Trans. Electron Devices, vol. ED-13, no. 6, pp. 520–524, 1966.

[17] D. P. Triantis, A. N. Birbas, and S. E. Plevridis, "Induced gate noise in MOSFETs revised: The submicron case," Solid State Electron., vol. 41, no. 12, pp. 1937–1942, 1997.

[18] A. J. Scholten et al., „Noise modeling for RF CMOS circuits simulation," IEEE Trans. Electron Devices, vol. 50, no. 3, pp. 618–632, 2003.

[19] C. H. Chen et al., "Extraction of the induced gate noise, channel noise, and their correlation in submicron MOSFETs from RF noise measurements," *IEEE Trans. Electron Devices*, vol. 38, no. 12, pp. 2884–2892, 2001.

[20] A. A. Abidi, "High-frequency noise measurements on FET's with small dimensions," *IEEE Trans. Electron Devices*, vol. ED-33, pp. 1801–1805, 1986.

[21] A. Litwin, "Overlooked interfacial silicidep-polysilicon gate resistance in MOS transistors," *IEEE Trans. Electron Devices*, vol. 48, no. 9, pp. 2179–2181, 2001.

[22] S. Asgaran, M. J. Deen, and C. H. Chen, "Analytical modeling of MOSFET's channel noise and noise parameters," IEEE Trans. Electron Devices, vol. 51, no. 12, pp. 2109–2114, 2004.

[23] H. T. Friis, "Noise figures of radio receivers," *Proc. Of the IRE*, vol. 32, no. 7, pp. 419–422, 1944.

[24] H. Rothe and W. Dahlke, "Theory of noisy fourpoles," *Proc. Of the IRE*, vol. 44, no. 6, pp. 811–818, 1956.

[25] IRE Subcommittee 7.9 on Noise, "Representation of noise in linear twoports," *Proc. Of the IRE*, vol. 48, no. 1, pp. 69–74, 1960.

[26] R. Q. Lane, "The determination of device noise parameters," *Proc. of the IEEE*, vol. 57, no. 8, pp. 1461–1462, 1969.

[27] M. S. Gupta, "Determination of the noise parameters of a linear 2-port," *Electron. Lett.*, vol. 6, no. 17, pp. 543–544, 1970.

[28] G. Caruso and M. Sannino, "Computer-aided determination of microwave two-port noise parameters," *IEEE Trans. Microwave Theory Tech*, vol. MTT-26, no. 9, pp. 639–642, 1978.

[29] J. Lange, "Noise characterization of linear twoports in terms of invariant parameters," *IEEE J. Solid-State Circuits*, vol. SC-2, no. 2, pp. 37–40, June 1967.

[30] IRE Subcommittee 7.9 on Noise, "Description of the noise performance of amplifiers and receiving systems," *Proc. of the IEEE*, vol. 51, issue 3, pp. 436–442, 1963.

[31] M. Sannino, "On the determination of device noise and gain parameters," *Proc. of the IEEE*, vol. 67, no. 9, pp. 1364–1366, 1979.

[32] J. M. O'Callaghan and J. P. Mondal, "A vector approach for noise parameter fitting and selection of source admittances," *IEEE Trans. Microwave Theory Tech*, vol. 39, no. 8, pp. 1376–1382, 1991.

[33] G. I. Vasilescu *et al.*, "Exact computation of two-port noise parameters," *Electron. Lett.*, vol. 25, no. 4, pp. 292–293, 1988.

[34] M. Mitama and H. Katoh, "An improved computational method for noise parameter measurement," *IEEE Trans. Microwave Theory and Tech.*, vol. MTT-27, no. 6, pp. 612–615, 1979.

[35] A. Boudiaf and M. Laporte, "An accurate and repeatable technique for noise parameter measurements," *IEEE Trans. Instrumentation and Measurement*, vol. 42, no. 2, pp. 532–537, 1993.

[36] W. Wiatr and D. K. Walker, "Systematic errors of noise parameter determination caused by imperfect source impedance measurement," *IEEE Trans. Instrumentation and Measurement*, vol. 54, no. 2, pp. 696–700, 2005.

[37] W. Wiatr, "A method of estimating noise parameters of linear microwave two-ports," Ph.D. dissertation, Warsaw Tech. Univ., Warsaw, Poland, 1908.

[38] M. W. Pospieszalski, "On the measurement of noise parameters of microwave two-ports," *IEEE Trans. Microwave Theory Tech*, vol. 34, no. 4, pp. 456–458, 1986.

[39] M. W. Pospieszalski and W. Wiatr, "Comment on design of microwave GaAs MESFETs for broad-band, low-noise amplifiers," *IEEE Trans. Microwave Theory Tech*, vol. 34, no. 1, p. 194, 1986.

[40] J. W. Archer and R. A. Batchelor, "Fully automated on-wafer noise characterization of GaAs MESFET's and HEMT's," *IEEE Trans. Microwave Theory Tech*, vol. 40, no. 2, pp. 209-216, 1992.

[41] A. C. Davidson *et al.*, "Accuracy improvements in microwave noise parameter measurements," *IEEE Trans. Microwave Theory Tech*, vol. 37, no. 12, pp. 1973–1978, 1989.

[42] L. F. Tiemeijer *et al.*, "Improved Y-factor method for wide-band on-wafer noise parameter measurements," *IEEE Trans. Microwave Theory Tech.*, vol. 53, no. 9, pp. 2917–2925, 2005.

[43] V. Adamian and A. Uhlir, "A novel procedure for receiver noise characterization," *IEEE Trans. Instrumentation and Measurement*, vol. IM-22, no. 2, pp. 181–182, 1973.

[44] Marcel N. Tutt, "Low and high frequency noise properties of heterojunction transistors," Ph.D. thesis, EE&CS, The University of Michigan, Ann Arbor, MI, 1994.

[45] R. Meierer and C. Tsironis, "An on-wafer noise parameter measurement technique with automatic receiver calibration," *Microwave J.*, vol. 38, no. 3, pp. 22–37, 1995.

[46] M. Kantanen *et al.*, "A wide-band on-wafer noise parameter measurement system at 50-75 GHz," *IEEE Trans. Microwave Theory Tech*, vol. 51, no. 5, pp. 1489–1495, 2003.

[47] P. Penfield, "Wave representation of amplifier noise," *IRE Trans. Circuit Theory*, vol. CT–9, pp.84–86, 1962.

[48] H. Hillbrand and P. H. Russer, "An efficient method for computer aided noise analysis of linear amplifier networks," *IEEE Trans. Circuits Syst.*, vol. 23, no. 4, pp. 235–238, 1976.

[49] R. P. Meys, "A wave approach to the noise properties of linear microwave devices," *IEEE Trans. Microwave Theory Tech.*, vol. MTT–26, pp. 34–37, 1978.

[50] E. C. Valk *et al.*, "De-embedding two-port noise parameters using a noise wave model," *IEEE Trans. On Instrum. Meas.*, vol. 37, no. 2, pp. 195–200, 1988.

[51] R. P. Hecken, "Analysis of linear noisy two-ports using scattering waves," *IEEE Trans. Microwave Theory Tech.*, vol. MTT–29, pp. 997–1004, 1981.

[52] S. W. Wedge and D. B. Rutledge, "Noise waves and passive linear multiports," *IEEE Microwave and Guided Wave Lett.*, vol. 1, no. 5, 1991.

[53] S. W. Wedge and D. B. Rutledge, "Wave techniques for noise modeling and measurement," *IEEE Trans. Microwave Theory Tech.*, vol. 40, no. 11, pp. 2004–2012, 1992.

[54] S. Withington, "Scattered noise waves in microwave and mm-wave networks," *Microwave Journal*, vol. 32, pp. 169–178, 1989.

[55] G. F. Engen, "A new method of characterizing amplifier noise performance," *IEEE Trans. Instrum. Meas.*, vol. IM–19, pp. 344–349, 1970.

[56] D. Wait and G. F. Engen, "Application of radiometry to the accurate measurement of amplifier noise," *IEEE Trans. Instrum. Meas.*, vol. 40, no. 2, pp. 433–437, 1991.

[57] J. Randa, "Noise-parameter uncertainties: A Monte Carlo simulation," *J. Res. Nat. Inst. Stand. Tech.*, vol. 107, no. 5, pp. 431–444, 2002.

[58] J. Randa and D. K. Walker, "On-wafer measurement of transistor noise parameters at NIST," *IEEE Trans. Instrum. Meas.*, vol. 56, no. 2, pp. 551–554, 2007.

[59] "Reference Guide – Agilent Technologies 9719ET/20ET/22ET, 8719ES/20ES/22ES Network Analyzers," *Agilent Technologies*, pp. 10-1 – 10.11, 2002.

[60] "De-embedding and Embedding S-Parameter Networks Using a Vector Network Analyzer," *Agilent Technologies*, pp. 14–21, 2001.

[61] D. Boyd, "Calculate The Uncertainty Of NF Measurements," *Microwaves & RF*,. Oct. 1999.

[62] M. L. Schmatz and H. R. Benedickter, "Accuracy Improvements in Microwave Noise Parameter Determination," *51st ARFTG Conference Digest*, pp. 62–64, 1998.

[63] S. Van den Bosch and L. Martens, "Improved impedance-pattern generation for automatic noise-parameter determination," *IEEE Trans. Microwave Theory Tech.*, vol. 46, pp.1673–1678, 1998.

[64] R. Hu and T. H. Sang, "An analytical approach on the determination of generator reflection coefficients used in the noise-parameter measurement," *Int. J. Infrared Millimeter Waves*, vol. 27, no. 1, pp. 151–162, 2006.

[65] G. Banerjee, K. Soumyanath, and D. J. Allstot, "Measurement and modeling errors in noise parameters of scaled-CMOS devices," *IEEE Trans. Microwave Theory Tech.*, vol. 54, no. 6, pp.2335–2345, 2006.

[66] N. J. Kuhn, "Curing a subtle but significant cause of noise figure error," *Microwave J.*, vol. 27, no. 6, pp. 85–98, 1984.

[67] C. H. Chen *et al.*, "Novel noise parameter determination for on-wafer microwave noise measurements," *IEEE Trans. Instrumentation and Measurement*, vol. 57, no. 11, pp. 2462-2471, 2008.

[68] "Theory of Noise Measurement," Application note: 5C-042, *Maury Microwave*, 06 July, 1999.

[69] Vector Network Analyer Uncertainty Calculator, Agilent Technologies, <http://www.home.agilent.com/agilent/editorial.jspx?cc=US&lc=eng&ckey=1000000418:epsg:sud&nid=-35211.426019.02&id=1000000418:epsg:sud&cmpid=93648>.

[70] S. Long *et al.*, "On-wafer noise characterization of low-noise amplifiers in the Ka-band," IEEE Trans. Instrum. Meas., vol. 52, no. 10, pp. 1606-1610, 2003.